Kingston University London

School of Aerospace and Aircraft Engineering

PhD THESIS

Academic Years 2011-2014

Omid Razmkhah

Effect of Sideways Impact Fall on the Osteoporosis Fractures of Proximal Femur

Director of Studies:

Dr Hessam Ghasemnejad

February 2014

This thesis is submitted in partial fulfilment of the requirements for the degree of Doctor of Philosophy

ABSTRACT

Hip fracture is the most common reason for admission to an orthopaedic trauma word. It is usually a 'Fragility' fracture caused by a fall affecting an older person with osteoporosis or osteopenia (a condition in which bones lose calcium and become thinner, but not as much as in osteoporosis). The National Hip Fracture Database worldwide reports the average age of a person with hip fracture is 84 years for men and 83 years for women, 76% of fracture occurs in women. By 2050, the worldwide incidence of hip fracture in men is projected to increase by 24% in women and 31% in men. Hip fractures due to sideways falls are a worldwide health problem, especially amongst elderly people.

The experienced force to the proximal femur during a fall leading to hip fracture is significantly dependent on density, thickness and stiffness of the body during impact. The process of fracture and healing can only be understood in terms of structure and composition of the bone and also its mechanical properties. Bone fracture analysis investigates to predict various failure mechanisms under different loading conditions. In an effort to improve and assist scientists and researchers to predict the impact damage response of bone structures and estimate femoral fracture load in vitro, an accurate explicit finite element (FE) method has been investigated in this study.

In the first part, the main goal is to create a 3D reconstruction and registration of semi-transparent Computed Tomography (CT) scan image data using SIMPLEWARE software. In the second part, effect of cortical thickness and impact velocity on the energy absorption of hip during a fall has been investigated on a 3D model. Additionally composite femora were mechanically tested to failure and regression analyses between measured fracture load and FE-predicted fracture load were performed. The results indicate that this sophisticated technique, which is still early in its development, can achieve precision comparable to that of densitometry and can predict femoral fracture load to within 18% with 95% confidence.

Keywords: Bone; Hip Fracture; Damage; Impact; Osteoporosis; FE; Femur; Fracture load

Table of Contents

List of Figures

List of Tables

MEDICAL TERMINOLOGY

Acetabulum: The cup-shaped cavity at the base of the hipbone into which the ball-shaped head of the femur fits

Adduction: The movement of a limb toward the midline or axis of the body

Antegrade: Performed in the normal direction of flow

Anterior: Pertaining to a surface or part situated toward the front or facing forward

Anterversion: The angulation created in the transverse plane between the neck of the femur and shaft of the femur. The normal angle is between 15 and 20 degrees during stance

Arthritis: Inflammation of a joint, usually accompanied by pain, swelling, and stiffness, resulting from infection, trauma, degenerative changes, metabolic disturbances, or other causes

Articulation: The place of anatomical union, usually movable, between two or more bones

Calcitonin: A hormone produced by the thyroid gland that lowers the levels of calcium and phosphate in the blood and promotes the formation of bone.

Cancellous: Lattice like, porous, spongy. Cancellous tissue is normally present in the interior of many bones, where the spaces are usually filled with marrow

Cartilage: A tough, elastic connective tissue found in the joints, outer ear, nose, larynx, and other parts of the body

Celiac disease: Disease of the digestive system that damages the small intestine and interferes with the absorption of nutrients from food

Condyle: A rounded projection at the end of a bone that anchors muscle ligaments and articulates with adjacent bones

Contralateral: Affecting or originating in the opposite side of a point of reference, such as a point on a body

Cortical: Pertaining to or emanating from a cortex, usually bone

Coxa valga: Deformity of the hip with increase in the angle of inclination between the neck and shaft of the femur

Coxa vara: Deformity of the hip with decrease in the angle of inclination between the neck and shaft of the femur

Diaphysis: The shaft of a long bone

Distal: Away from or the farthest from a point of origin or attachment

Epidemiology: The study of the determinants of disease events in populations

Epiphysis: The expanded articular end of a long bone

Eversion: A turning outward or inside out, such as a turning of the foot outward at the ankle

Extension: The act of straightening or extending a flexed limb

Femur: The long bone of the thigh, and the longest and strongest bone in the human body, situated between the pelvis and the knee and articulating with the hipbone and with the tibia and patella

Flexion: The act of bending or the condition of being bent

Fracture: A break or rupture in a bone

Gait: The manner or style of walking

Greater Trochanter: A strong area at the proximal and lateral part of the shaft of the femur, overhanging the root of the neck; it gives attachment to the gluteus medius and minimus, piriformis, obturator internus and externus, and gemelli muscles

In vitro: A procedure performed not in a living organism but in a controlled environment

In vivo: Experimentation using a whole, living organism

Lateral: Relating to or situated at or on the side

Lunate: Shaped like a crescent xiv

Medial: Pertaining to, situated in, or oriented toward the midline of the body

Morbidity: A diseased condition or state

Mortality: The condition of being subject to death

Musculoskeletal: Relating to or involving the muscles and the skeleton

Osteoporosis: A disease characterized by decrease in bone mass and density

Osteopenia: A condition in which bones lose calcium and become thinner, but not as much as in osteoporosis

Parathyroid hormone: A hormone that is made by the parathyroid gland and that is critical to calcium and phosphorus balance.

Posterior: In the back part of a structure

Proximal: Nearer to a point of reference such as an origin, a point of attachment, or the midline of the body

Retrograde: Moving backward or against the usual direction of flow

Retroversion: A turning or tilting backward

Resorption: Loss of bone mass

Tibia: The inner and larger of the two bones of the lower leg, extending from the knee to the ankle, and articulating with the femur, fibula, and talus

Statement of Originality

This thesis and the work to which it refers are the results of my own efforts. Any ideas, data, images or text resulting from the work of others (whether published or unpublished) are fully identified as such within the work and attributed to their originator in the text, bibliography or in footnotes. This thesis has not been submitted in whole or in part for any other academic degree or professional qualification.

I agree that the University has the right to submit my work to the plagiarism detection service TurnitinUK for originality checks. Whether or not drafts have been so-assessed, the University reserves the right to require an electronic version of the final document (as submitted) for assessment as above.

Omid Razmkhah

LIST OF ABBREVIATIONS

BEM	Boundary Element Method
BMC	Bone Mineral Content
BMD	Bone Mineral Density
BV/TV	Trabecular bone volume per trabecular volume
BW	Body Weight
CAD	Computer Aided Design
CPM	Corpuscular Method
CSA	Bone Cross-Sectional Area
CT	Computed Tomography
Conn. D	Connectivity density
DEXA/DXA	Dual Energy X-ray Absorptiometry
DICOM	Digital Imaging and Communications in Medicine
DoG	Difference of Gaussian
DMA	Dynamic mechanical analyser
FEA	Finite Element Analysis
FEM	Finite Element Model
Kc	Stress intensity factor
MRI	Magnetic Resonance Imaging
STL	Stereo lithography
SD	Standard deviation
Tb.N	Trabecular number
W_f	Critical work to fracture of a specimen
WHO	World Health Organisation

LIST OF NOMENCLATURE

A	Ante version/retroversion angle
C	Damping coefficient
E	Modulus of Elasticity
L	Length
σ_y	Yield stress
α	Ducker-prager yield function alpha
β	Varus/valgus angle
ζ	Damping ratio
ε	Strain
γ	Anterior/posterior angle
ρ	Density
ϑ	Poisson ratio
σ	Stress
u	Displacement
$\dot{u}$	Velocity
$\ddot{u}$	Acceleration
K	Linear stiffness
ω_n	Natural frequency
D_s	Lowest frequency
ω_0	Larmor frequency
B_0	Magnetic field

Acknowledgements

It would not have been possible to write this doctoral thesis without the help and support of the kind people around me, to only some of whom it is possible to give particular mention here. Firstly, I would like to thank my supervisor, Dr Hessam Ghasemnejad for his guidance, encouragement and constant support throughout the course of this project. My sincere thanks must go to my second supervisor, Dr Akbar Aboutorabi for his support and persistent help.

I would also like to say a big thank you to Mr Dean Wells for teaching me laboratory techniques and whose practical help has been invaluable in the completion of this work. Also, I would like to thank all my friends for their kindness, friendship and moral support.

I would like to thank my family, especially my mother and father for always believing in me, for their continuous love and their supports in my decisions. Without whom I could not have made it here.

Finally, a special mention and many thanks to my lovely fiancé, Dr Shadi Bokaee for her support, encouragement, quiet patience and unwavering love.

Chapter 1 - Introduction

1.1 Background

Hip fracture has become a significant health care problem which involves major costs for society, and suffering, morbidity and mortality, for the elderly people. About 70,000 to 75,000 hip fractures (proximal femoral fractures) occur annually in the UK, with a cost amounting to about £2 billion a year including medical and social care. An estimate 1.7 million total hip fractures occurred globally twenty years ago. It seems that by 2050, there will be 6.3 million across the world (Cooper *et al.*, 1992). However, the population of most 'first world' countries are ageing as a result of lower birth rates, low immigration rates and increased longevity. Consequently, projections indicate that the UK annual incidence will rise to 91500 by 2015 and 101000 in 2020, with an associated increase in annual expenditure. The majority of this expenditure will be accounted for by hospital bed days and a further substantial contribution will come from health and social aftercare. At present about a quarter of patients with a hip fracture are admitted from institutional care and about 10–20% of those admitted from home ultimately move to institutional care (British Orthopaedic Association, 2007).

Hip fracture is the most common reason for admission to an orthopaedic trauma ward. It is usually a 'fragility' fracture caused by a fall affecting an older person with osteoporosis or osteopenia (a condition in which bones lose calcium and become thinner, but not as much as in osteoporosis). The National Hip Fracture Database reports the average age of a person with hip fracture is 84 for men and 83 for women, 76% of fracture occurs in women. By 2050, the worldwide incidence of hip fracture in men is projected to increase by 240% in women and 310% in men. The estimated number of hip fractures worldwide will rise from 1.66 million in 1990 to 6.26 million in 2050, even if age-adjusted incidence rates remain stable. Mortality is high – about 10% of people with a hip fracture die within one month and about one third within 12 months.

Most of the deaths are due to associated morbidities and not just to the fracture itself reflecting the high prevalence of comorbidity in people with hip fracture. It is often the occurrence of a fall and fracture that signals underlying ill health.

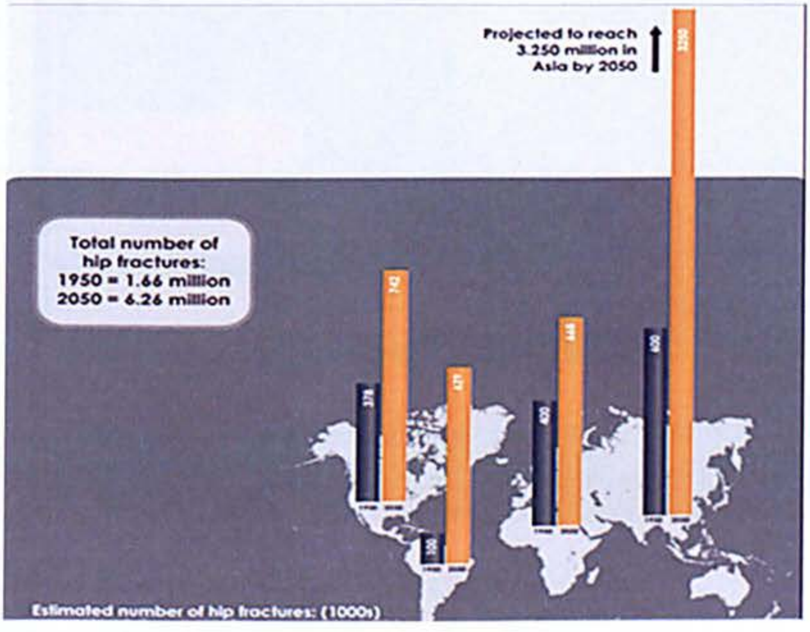

Figure 1.1: Worldwide osteoporotic hip fractures (Cooper *et al.*, 1992).

As a result of the high volume of osteoporotic fractures which occurs each year, health care expenditures to treat these fractures exceed those of many other major disease, including heart disease, stroke and breast cancer.

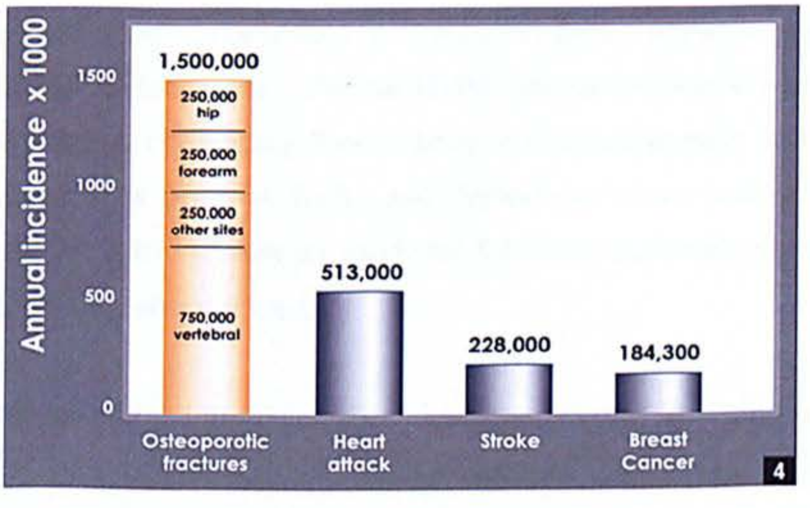

Figure 1.2: Osteoporotic fractures compared with other diseases (American Heart Association, 1996).

Hip fractures have a significant morbidity, with a mortality more than 20% that extends well beyond 12 months following fracture. At first year, a large percentage of patients have residual functional deficits in essential and instrumental activities of daily living.

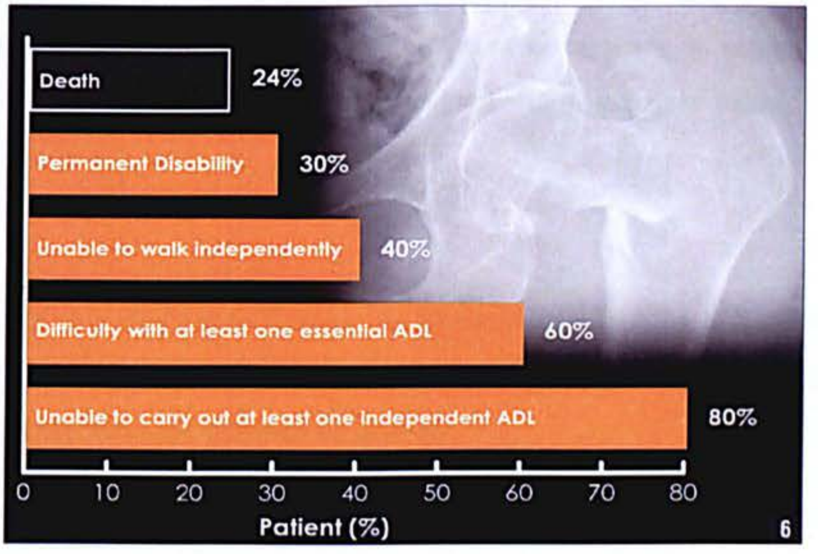

Figure 1.3: One-year hip fracture mortality and morbidity (Lu-Yao *et al.*, 1994).

Thus hip fractures are by no means an exclusively surgical concern. Its effective management requires the co-ordinated application of medical, surgical, anaesthetic and multidisciplinary rehabilitation skills and a comprehensive approach covering the full time course of the condition from presentation to subsequent follow-up, including the transition from the hospital to the community. For the Health Service and social work professionals hip fractures are uniquely challenging. Firstly, because it occurs in older people and is most common with those with previous frailty and dependency issues and with pre-existing medical problems. Secondly, because an accidental fall, most commonly at home, marks the beginning of a complex journey of care.

This takes patients from the emergency department to an operating theatre and for recovery purposes goes to an orthopaedic ward. Sometimes, depending the circumstances of the patient and nature of the services available, the patient goes back home either directly, via more extended inpatient rehabilitation. Occasionally, they have an alternative placement within the private or voluntary sectors, a local authority or NHS care. Many disciplines, specialties and agencies are involved, and a patient undergoing even fairly straightforward management for hip fracture may meet many various professionals in the course of one admission. So hip fractures can be viewed as a tracer condition in systems of care for older patients, testing hospital and community health services and social work provision, and also importantly, testing how these different services are coordinated to provide acute care, rehabilitation and continuing support for a large and vulnerable group of patients.

1.2 Aims and Objectives

The main aim of this study is to develop an advanced method for estimating the load of proximal femoral fracture in the stance load configuration. In order to achieve this overall aim, the following objectives are outlined as follows:

1- To determine the causes of hip fracture.
2- To study the nonlinear FE models in predicting proximal femoral.
3- To compare the existing models and make the nonlinear FE models which would predict a proximal femoral fracture load with much greater precision than previous linear FE models.
4- To determine the importance of development of an automated method of generating CT scan-based nonlinear FE models and then an evaluation is conducted to discover the ability of the models to predict the fracture load of a patient in the stance configuration.
5- After evaluation of FE model, then three composite femora were mechanically tested to failure and regression analyses between measured fracture load and FE-predicted fracture load were performed.

1.3 Structure of the thesis

The thesis is presented in seven chapters. A brief synopsis is given as follows:

Chapter 1: Introduction

In this chapter, the aims and objectives of this project has been mentioned. Also, the increase in the prevalence of hip fracture in elderly as well as other underlying factors have been illustrated which resulted in this project to be carried out.

Chapter 2: Literature review

In this chapter, knowledge of anatomy and physiology of bone are an elementary step towards the understanding of the human body and also provides the motivation behind the need for this study and research goals the thesis sets out to accomplish. A review on bone histology and anatomy of the femur and various effects such as age, gender and anatomical differences on the bone fracture and healing process in elderly people is reviewed in detail. Also in this chapter fracture mechanics and mechanical properties of bone tissues are investigated in terms of failure and fracture mechanisms as well as biomechanical aspects of femur fractures.

Chapter 3: Three Dimensional Proximal Femur Model from CT Scan Data

The first part reviews the principles of various image analysis techniques employed in biomechanics. The second part has the main goal of creating 3D reconstruction and registration of semi-transparent CT scan image data using SIMPLEWARE software.

Chapter 4: Explicit Finite Element Modelling of Hip Bone

This chapter discusses finite element modelling in LS-DYNA and how the theory is implemented in the programme to investigate effect of low velocity impact on the osteoporosis hip in ageing people. Effect of cortical thickness and impact velocity on the energy absorption of hip during a fall will be studied on a 3D model, using latest techniques and also it will be validated using experimental data. The critical impulse loading of hip will create a benchmark to improve the new design of hip protectors and consequently wellbeing of elderly people.

Chapter 5: A Practical Approach to Mechanical Performance of Composite Proximal Femur

The purpose of experimental testing is to create and obtain valuable pre-clinical data to the researcher and clinicians. It provides a benchmark to validate numerical and analytical models as well as enabling engineers and surgeons to improve the design of a potential new implant or surgical technique under controlled laboratory conditions.

Chapter 6: Discussions and Result

This chapter summarises the outcomes of this project and also the advantages of the proposed models in comparison to previous published models. The future work will be also outlined to propose other possible developments in this filed.

Chapter 7: Conclusions and Recommendations of Future Work

This chapter focuses on the overall conclusions of the project and also recommends the possible works to be done in future.

Chapter 2 - Literature Review

2.1 Structure and Physiology of Bone

Three components make up the connective tissue of an organic matrix - the cells, the fibres or collagen, and the ground substance. The fibres and the ground substance are generally predominant. Bone is a type of connective tissue containing an extensive matrix of intercellular materials. Bone tissue's organic matrix, unlike other types of connective tissues, is hardened and comprises 65% of minerals (Jee, 2001). This is what contributes to the hardness of the bone and its good radiopacity with many medical imaging modalities that are based on X-rays. The role of bone in the body is a supportive framework. Hormones remodel the external mechanical environment of the bone structure continuously. The remodelling is a repeating process that replaces old or damaged bone tissue with new bone tissue.

2.2 Types of Cells

Bone tissue comprises four types of cells as osteogenic, osteoblasts, osteocytes and osteoclasts cells. Osteogenic cells, which are found at the endosteum and the inner portion of the periosteum, are capable of mitotic division. The osteoblasts cannot divide mitotically. These are the cells that form bone. Collagen and other organic compounds necessary for the formation of bone matrix are secreted by osteoblasts. They are located at the margins of growing bone and on the surface of bones. The bone matrix that osteocytes form encases them during the process of bone formation. Osteocytes control their own metabolism lie within their own cavity in the bone environment. These lacunae must be within 100-150μm of a blood vessel to prevent necrosis where the osteocyte exchanges nutrients and waste. The osteoclast is a large multi-nucleated cell born of the fusion of up to 50 monocytes, a type of white blood cell (Martin and Burr, 1989).

2.3 Bone Salt

The primary bone salt presented in the bone tissue is calcium hydroxyapatite. It has the unit cell formula of $3Ca_3 (PO_4)_2$ - $Ca (OH)_2$ (Martin and Burr, 1989). A crystal is a few unit cells thick with approximate dimensions of $5 \times 5 \times 40$ nm^3 and its major component is mineral salts. About 99% of calcium in the body is stored in bone which is a vital component of homeostatic mechanisms which are maintained in regulating concentrations of Ca^{2+}, H^{+}, and $(HPO_4)^{2-}$ (Martin and Burr, 1989).

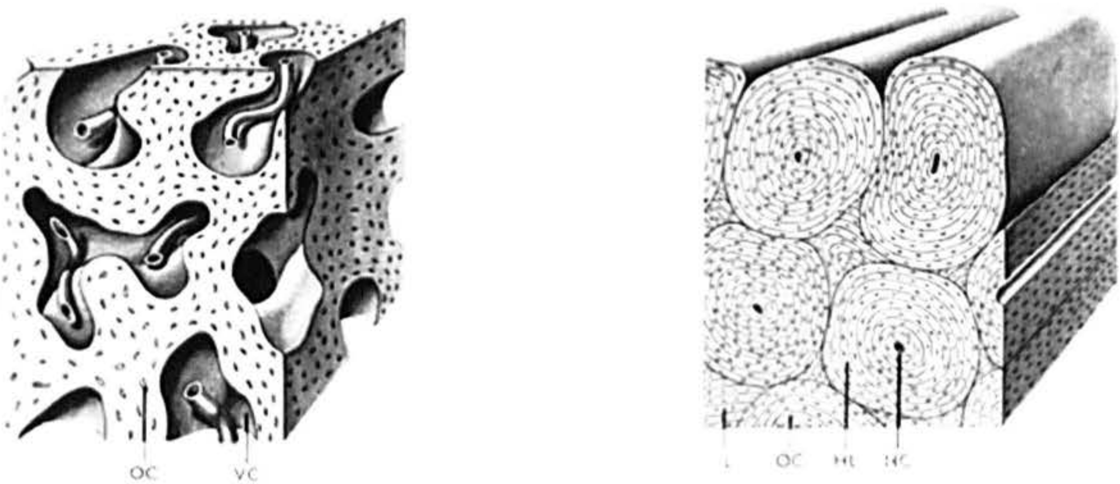

a) Bone is initially deposited as woven bone **b) Lamellar bone.**

Figure 2.1: Woven and lamellar bone. OC: osteocytes. HC: Haversian canal. HL: Lamellae. IL: Interstitial lamellae (Reproduced from Hancox, 1972).

2.4 Woven and Lamellar Bone

Bone is deposited as woven bone which acts as a sort of temporary scaffold (as shown in Figure 2.1 a) eventually it becomes lamellar bone. In woven bone, collagen fibres are oriented in every direction and vascular channels are wide. Thus, the bone in its woven state is weaker. Osteocytes are scattered throughout the bone matrix (see Figure 2.2). Lamellar bone is stronger and consists of fine parallel collagen fibres which are grouped into layers called lamellae. The name for the central canal of each functional unit is Haversian canal, after Havers (1691). When they are grouped with concentric lamellae they are referred to as an osteon or Haversian system. The rate of replacement of lamellar bone in trabecular is about 25% and cortical bone approximately 5% (Martin, 1998). The lamellar bone formation's orientation is affected by external mechanical stimuli. Here the collagen fibres follow the direction of stress (Martin and Burr, 1989).

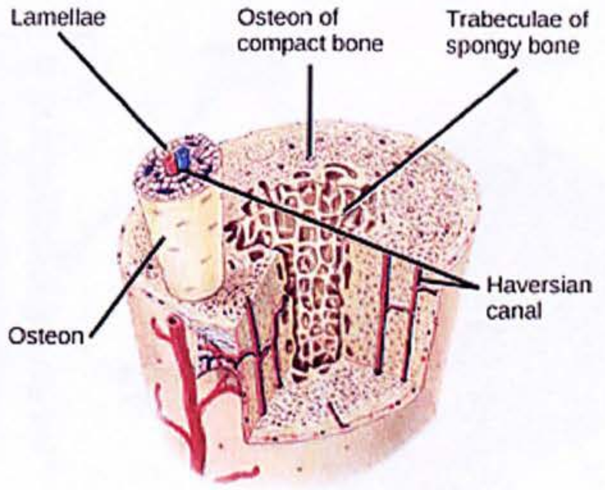

Figure 2.2: Osteons (Haversian systems) in cortical bone. (Reproduced from Taylor *et al.*, 2007; Original images courtesy of Tortora, 2002; Colopy *et al.*, 2004).

2.5 Cortical and Trabecular Bone

Bones in the macroscopic view can be categorised into cortical (compact) and trabecular (cancellous) bone. The compact bone, as the word implies, is dense. It comprises only spare vascular channels. This is described as structure of the external layers of all bones. It is hard material which is necessary as its role of providing protection to organs, and for supporting the skeleton. The cortical bone possesses an extensive network of canals across the width of bone. They are known as the perforating canals or Volkmann's canals. Cortical bone is a concentric ring structure, and blood vessels, lymphatic vessels and perforating canals nerves inter-connect with those in the medullary cavity, periosteum and the Haversian canals (see Figure 2.2).

Trabecular bone is also named cancellous bone or spongy bone. It is the irregular latticework constructed within bone columns called trabecular. The thickness is about 200 μm (see Figure 2.3). Marrow or myeloid tissue fills the space between the trabecular. The majority of the short, flat and irregularly shaped bone in the body is made up of trabecular bone. It is also present in and around the marrow cavity of the diaphysis of long bones. These are areas not subject to enormous mechanical stress. However, trabecular bone usually has a surround of cortical bone which aids strength and rigidity. The types of bone in the body are varied and depend on the need for strength or flexibility.

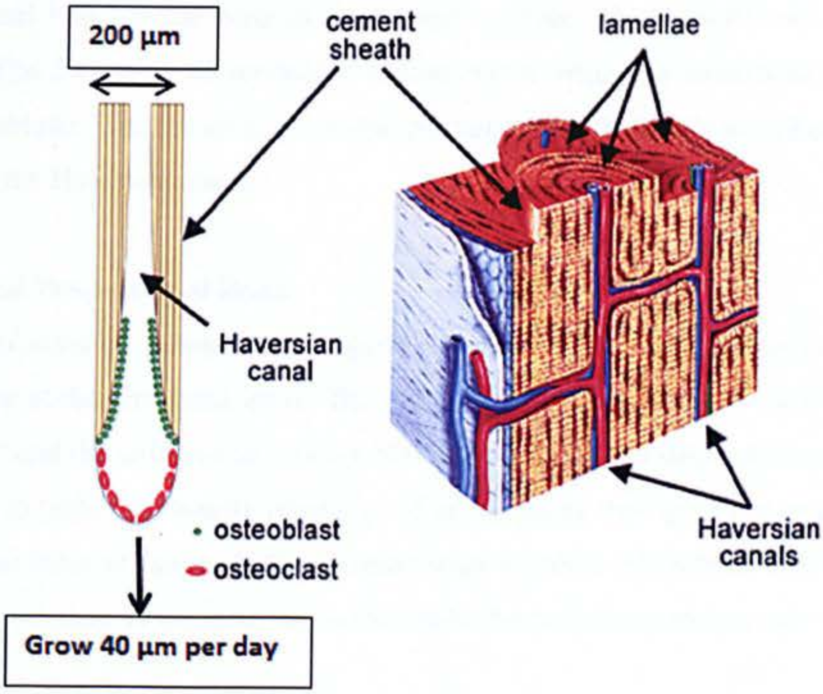

Figure 2.3: A BMU consisting of osteoblasts and osteoclasts in the formation of bone (Taylor *et al.*, 2007).

2.6 Modelling and Remodelling of Bone

Wolff's law offers the classical findings of Wolff (1892) from his seminal which was published in 1892. The document reveals his observation of bone remodelling, where bones become reshaped by stresses that act upon it. Wolff's observations have been widely challenged (Bertram and Swartz, 1991; Cowin, 1997; Taylor and Lee, 2007), but many continue to accept his findings that bone remodelling response to mechanical stresses does produce an optimal structure for coping with the new condition. The remodelling phenomenon has been analysed by Frost (1973). His observations are as follow:

1. 'Flexure' is not principal stress which can cause remodelling.
2. Remodelling is triggered by repetitive dynamic loads.
3. All affected bone surfaces drift towards concavity because of 'dynamic flexure'.

The actions of osteoclasts and osteoblasts cause remodelling. The actions form a basic multi-cellular unit (BMU). It consists of about 10 osteoclasts and hundreds of osteoblasts. The process involves the stages of activation, resorption and formation of bone. In the stage of activation, the fusion of monocytes becomes involved in the formation of osteoclasts. Osteoclasts tunnel into cortical bone in the resorption stage. The tunnels have a diameter of about 200μm. The formation of secondary osteon occurs when the excavated tunnel wall is lined with osteoblasts. But the core, or central portion, of the tunnel is not filled completely, and it is left for the Haversian canal.

2.6.1 Mechanical Properties of Bone

The load-deformation relation (see Figure 2.4) can be determined from the mechanical testing of a bone at the structural level. The elastic deformation is represented by the linear part of the curve and the stiffness or rigidity of the structure by the slope of the elastic region. The bone starts to yield nonlinearly after a yield point, going through the irreversible plastic deformation. The force at failure is the ultimate load which is when bone breaks. The work needed to cause a failure is the area measured under the load-deformation curve (Turner and Burr, 2001).

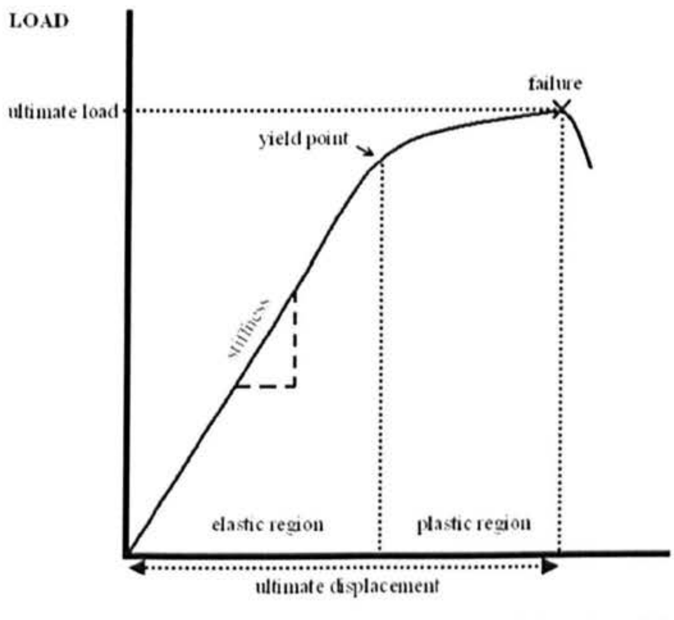

Figure 2.4: Characteristic load-deformation curve from mechanical testing of a bone (Turner and Burr, 2001).

The stress of a normalised load and normalised deformation is described as the force per unit area. The strain is described as the relative change in length. The intrinsic material properties of bone, tensile, compressive, shear, and bending loads, are represented by these measures. Bone material properties at tissue level are commonly characterised by stress-strain curve which is the normalised load deformation relation.

When a load is applied to a bone specimen, the deformation that results is measured. When tensile loads elongate the specimen or compressive loads shorten and widen the specimen, normal stresses occur. It is by measuring the slope of the elastic region, called Young's modulus or Elastic modulus, and the stress and strain values at yield and failure points of bone can be characterised in Table 2.1 (Enoka, 2002).

Table 2.1: Basic parameters of bone mechanical properties (Enoka, 2002).

Parameter	Equation	Unit	Description
Stress	$\sigma = \frac{F}{A}$	[Pa] or [N/M^2]	**F is the applied force and A is the cross sectional area**
Strain	$\varepsilon = \frac{\Delta L}{L}$	% or $\mu\ \varepsilon$	ΔL is the change in length and L is the original length
Young's Modulus	$E = \frac{\sigma}{\varepsilon}$	[Pa] or [N/M2]	***σ*** **is the stress and** ***ε*** **is the strain in elastic region**

Bone as a composite material has a higher fracture load in compression typically than in tension as shown in Figure 2.5. Elastic modulus and yield stress are commonly higher in cortical than in trabecular bone as shown Table 2.2 shows. Material properties measured in the table are represented with different techniques for a typical long bone (femur).

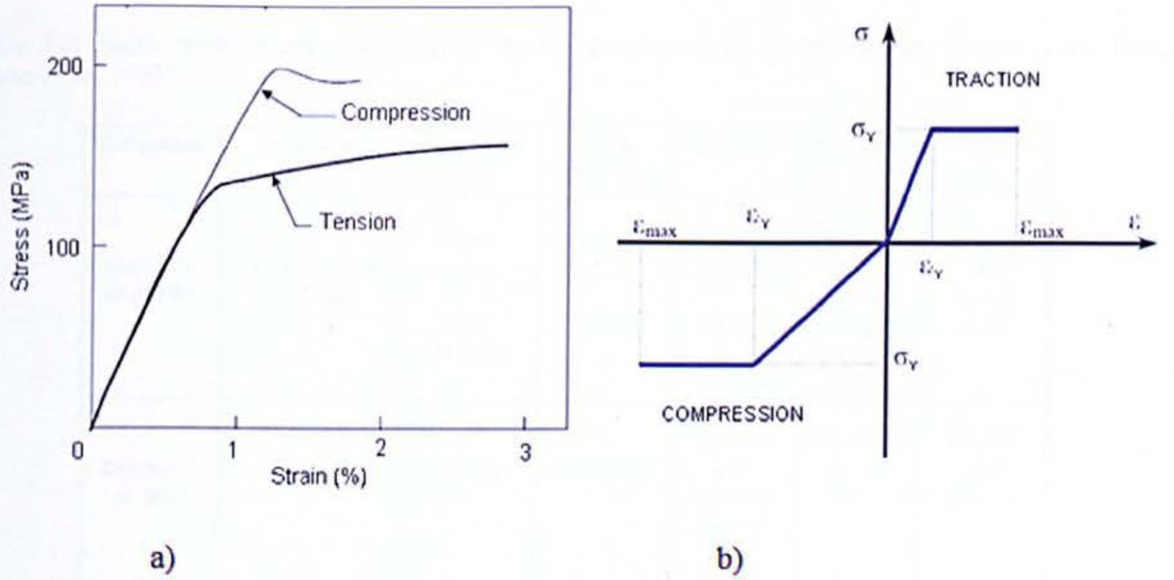

Figure 2.5: a) Schematic of the tensile and compressive stress/strain curves for cortical bone along the axis of a long bone b) Theoretical law of behaviour of compact bone, of tensile and compressive (Charpail, 2006).

Trabecular bone is quite heterogeneous, viscoelastic and anisotropic. The yield point of trabecular bone differs during traction and during compression, and traction stress is about 50% less than compression stress. When compressed, trabecular bone exhibits extensive inelastic deformation (see Figure 2.6), often attaining strains exceeding 60% before failure (Mercer *et al.*, 2006).

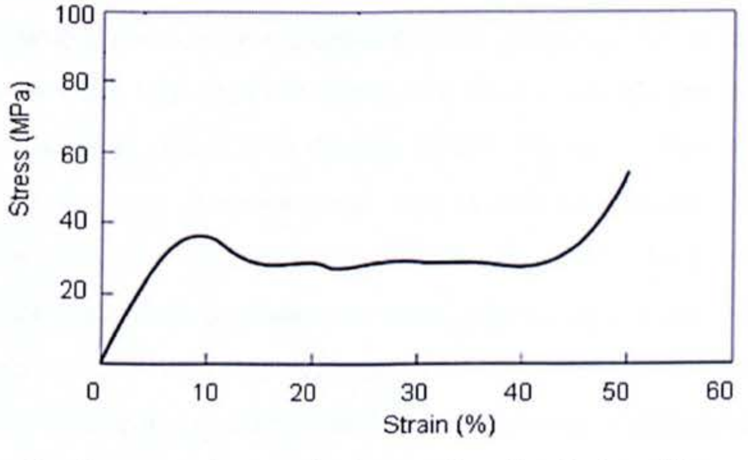

Figure 2.6: Schematic of a compressive stress/strain curve for trabecular bone (Mercer *et al.*, 2006).

Table 2.2: Elastic modulus and yield stress of the femur measured in different studies (Turner *et al.*, 1999; Zysset *et al.*, 1999).

Reference	Method	Anatomic site	Bone Specimen	E [GPa]	σ_{yt} [MPa]	σ_{yc} [MPa]
Bayraktar et al 2004	Experimental and FEA	Neck Mid-diaphysis	Trabecular Cortical	18.0 ± 2.8 (N = 12) 19.9 ± 1.8* (N = 74)	84.9 ± 11.2 (N = 6) 107.9 ± 12.3 (N = 74)	135.3 ± 34.3 (N = 6) N/A
Kaneko et al. 2003	Experimental	Diaphysis	Trabecular	22.7 ± 1.7* (N = 16) 23.0 ± 1.8** (N = 16)	83.9 ± 8.8 (N = 7)	153.0 ± 16.5 (N = 7)
Turner et al. 1999	Nanoindentation	Distal femur Mid-diaphysis	Trabecular Cortical	18.1 ± 1.7 (N =30) 20.0 ± 0.3 (N = 60)	N/A	N/A
Zysset et al.1999	Nanoindentation	Neck	Trabecular Cortical	11.4 ± 5.6 (N = 8) 15.8 5.3 (N = 8)	N/A	N/A
Zysset et al.1999	Nanoindentation	Mid-diaphysis	Cortical	19.1 5.4 (N = 8)	N/A	N/A

2.6.2 Structural Properties of Bone

The structural properties of bone are defined by its geometry. The reason why the femur of an adult can carry more load than the femur of a child is mainly due to the difference in size or bone cross-sectional area (CSA) (Enoka, 2002). The way a bone under considerable stress survives is if its large cross-sectional area is able to withstand the stress. In the proximal femur, for example, where bending stresses are greater, the femoral neck shape is more elliptical at the neck-shaft junction. However, where compressive stresses are greater the shape is more circular near the femoral head (Zebaze *et al.*, 2005). Bone micro architecture refers to the cortical porosity and the characteristics of trabecular, the amount, the orientation and thickness, and the connectivity. Micro architecture also plays a role in the defining of bone mechanical competence (Dempster, 2003).

2.6.3 Cortical bone Material Properties

The human cortical bone has been demonstrated as an anisotropic and heterogeneous material showing that the material properties can be different depending on the anatomic location that the specimen came from (Ashman, *et al.*, 1984). Depending on donor species, test methodology and specimen preparation can cause variations in the material properties obtained when tested upon. To limit the variability of the material properties, only studies using human femoral bone are used. Even within this sub-group, variability is still evident. In a study conducted by Ashman in 1984, it was found that variations in femoral cortical bone elastic modulus with anatomical site and the mid-section of the diaphysis have the greatest elastic modulus. The same study demonstrated that a continuous wave ultrasound and tensile mechanical test could produce the same moduli values. The finding indicates that the variation originates more from varying the properties of the bone than differences in test methodology as summarised in Table 2.3.

The viscoelastic behaviour of the femoral cortical bone has also been demonstrated by being tested by the use of tensile and compressive creep tests to fracture. This was done by applying a constant and instantaneous stress to the specimen and a varying strain over time was measured until the fracture point was reached. The torsional creep test also showed that a varying strain over time with a constant stress applied and differences can have a different result depending on the level of load. The dynamic mechanical analyser which is also referred to as DMA is a test methodology used to determine the viscoelastic behaviour of a material by employing a sinusoidal force or a sinusoidal stress to a material and measuring the sinusoidal strain response.

On a certain phase angle the strain delays by the applied stress. This phase angle is a measure of the mechanical damping of the material. If the material was purely elastic there wouldn't be a phase between stress and strain, hence the phase of the angle is indicative of the viscoelasticity of a material. Materials that are highly viscoelastic have a larger tangent phase angle values while materials which are ideally elastic have a tangent phase angle value of close to zero. The elastic and shear modulus of tibia cortical bone have also been determined using DMA at a frequency of 10Hz with the results for a longitudinal specimen being 12.8GPa and 3.42GPa and for a transverse specimen 9.3GPa and 2.7GPa. The tangent phase angle was reported as a minimum value of 0.015 in the frequency range 1-100Hz. The tangent phase angle was found to increase at higher frequencies, to a maximum of approximately 0.05 at 10 kHz.

Table 2.3: summary of elastic material properties of human femoral cortical bone reported in the literature. The subscripts L, T and R refer to longitudinal, transvers and radial direction of the bone respectively (Turner *et al.*, 1999; Bayraktar *et al.*, 2004).

Author	(Reilly and Burstein 1975)	(Lappi et al. 1979)	(Ashman et al. 1984)	(katsamanis and Raftopoulos 1990)	(katsamanis and Raftopoulos 1990)	(Raftopoulos et al. 1993)	(Raftopoulos et al. 1993)	(Turner et al. 1999)	(Turner et al. 1999)	(Bayraktar et al. 2004)
Experimental method	Uniaxial tension, compression and torsion strain rate 0.02-0.05/s	Pulse propagation ultrasound	Continuous wave ultrasound	Uniaxial tension, low speed	Stress wave propagation using impact with steel ball	Uniaxial tension test strain rate 2*0-5/s	Stress wave propagation applied by dropping weights	Pulse propagation acoustic velocity	Nano-indentation	Uniaxial tension strain rate 0.2%/s
Test specimen description	Dry specimen 25mm length and 3mm diameter	Wet specimen 3.6-7.2mm length 3.6mm diameter.	Wet specimen of unknown geometry	Dry specimen 7.6*4*54mm	--	Dry specimen 7.6*2.8*56mm		Wet specimen 500μm slice	Dry specimen 10mm cube	Wet specimen 2.5*3*11mm
Elastic Modulus (GPa)	E_L: 17.6 E_T: 12.5 E_R: 12.5	E_L: 5.5 E_T: 4.9 E_R: 4.9	E_L: 20 E_T: 13.4 E_R: 12	E_L: 16.2	E_L: 19.9	E_L: 16.2	E_L: 17.9	E_L: 20.55 E_T: 14.91	E_L: 23.45 E_T: 16.58	E_L: 19.9
Shear Modulus (GPa)	G_{TL}: 3.4	G_{TL}: 2.24	G_{TL}: 6.2 G_{RL}: 5.61 G_{RT}: 4.53	--	--	--	--	--	--	--
Poisson's ratio	V_{LT}: 0.39 V_{LR}: 0.39 V_{TR}: 0.56 V_{RT}: 0.56	V_{LT}: 0.39, V_{LR}: 0.39, V_{TR}: 0.2, V_{RT}: 0.2	V_{LT}: 0.35 V_{LR}: 0.37 V_{TR}: 0.42 V_{RT}: 0.38 V_{RL}: 0.22 V_{TL}: 0.24	V_{LT}: 0.36 V_{LR}: 0.36	V_{LT}: 0.36 V_{LR}: 0.36	V_{LT}: 0.36	V_{LT}: 0.36 V_{LR}: 0.36	--	--	--
Density (Kg/m^3)	--	1870	1903	2069	--	--	--	--	--	--

2.6.4 Cancellous Bone Material Properties

Cancellous bone is an anisotropic heterogeneous material. The material properties of the cancellous bone can be obtained for individual trabecular, referred to as material properties, or for blocks of cancellous bone, referred to as structural properties due to the porous nature of cancellous bone. The same terminology applies to density measurements of cancellous bone. As with cortical bone properties, only studies using human femoral cancellous bone were considered to minimise the variability. The structural and material properties of cancellous bone are shown in Table 2.4.

The properties reported on the table were only studied along the primary axis of the specimen. The cancellous bone specimens were cut from the femur to align the long axis of the specimen with the primary orientation of the trabecular struts, the specimens were not aligned with the anatomical axes of the femur. DMA has also been used to investigate the viscoelastic properties of human tibia cancellous bone. Using compression testing to 0.4% strain, the elastic modulus at 0.4% strain, having a structural density of 342-336 kg/m^3 and a phase angle tangent of 0.3-0.31, was found to be 0.28-0.32GPa. The elastic modulus at 0.6% strain of the cancellous bone was determined to be 0.38GPa, for a second test, by employing a cyclic compression test applied at 0.2Hz to 0.6% strain.

The tangent of the phase angle was 0.22 and the structural density was 289 kg/m^3. A third study followed the same protocol using specimens that were stored using different techniques. That study found the elastic modulus at 0.4% strain to be 0.194GPa, having a structural density of 340 kg/m^3 and a phase angle tangent of 0.35 for the fresh specimen. It was also found a general increase in the elastic modulus and loss tangent when the specimens were frozen and thawed or stored in ethanol, making the results statistically insignificant (Ashman *et al.*, 1988).

Table 2.4: Structural and material properties of human femoral cancellous bone (Turner *et al.*, 1999; Bayraktar *et al.*, 2004).

Author	(Ashman and Rho 1988)	(Turner et al. 1999)	(Turner et al. 1999)	(Garner et al. 2000)	(Bayraktar et al. 2004)
Experimental method	Continuous wave ultrasound	Pulse propagation acoustic velocity	Nano-identation	Torsion strain rate 0.006/s	Uniaxial tension and compression strain rate 0.5%/s
Test specimen description	Wet specimen 15 mm lengths 5mm diameter. Orientation approximately parallel with trabecular	Wet specimen 500μm slice	Dry specimen 20mm cube	Wet specimen 35mm length 8mm diameter	Wet specimen 32mm length 8mm diameter
Structural elastic modulus (GPa)	**1.63**	-	-	-	-
Material elastic modulus (GPa)	**12.9**	**17.5**	**18.4**	-	**18**
Structural shear modulus (GPa)	-	-	-	**0.289**	-
Poisson's ratio	-	-	-	-	-
Structural density (Kg/m^3)	**334**	-	-	**560**	**620**
Material density (Kg/m^3)	-	-	-	**1950**	-

2.6.5 Effect of Soft Tissue Surrounding Bone on the Dynamic Properties

An investigation has been done (Tsuchikane *et al.,* 1995) by using vibration analysis to study the dynamic properties on the effect of the soft tissue surrounding the bone. The sensitivity of the fundamental frequency to tibia fracture was determined by the use of two fresh cadaveric legs. Both legs were placed resting on a splint support from knee to ankle and the tibias examined using a shaker fitted with an impedance head after they were removed from a full body cadaver at the mid-thigh level. The soft tissue of one leg was removed prior to testing. The results demonstrated that the presence of the soft tissue increased the fundamental frequency by 18%; yet the change in frequency as the tibia was progressively cut was the same as in the contralateral leg with intact soft tissue, also an in vivo examination in the same study found that tension in the leg muscles increased the natural frequency, indicating that a change in muscle tension between measurements could lead to inaccurate frequencies.

That examination (Tsuchikane *et al.,* 1995) was also carried out on the tibia within a fresh cadaveric leg using an impact hammer at several stages of limb dissection. The fundamental frequency of the tibia from the cadaveric leg was compared to that of previously excised fresh and dry cadaveric tibias and to an in vivo investigation impacting the tibias of 20 people. The tibia was first tested in the cadaveric leg; the leg was placed overhanging a bench simulating the seated in vivo position. The impact and accelerometer were positioned on the skin overlaying the tibia. The tibia testing was repeated with the skin of the leg removed, the calf and thigh muscles removed, the foot and ankle joint removed, the knee joint removed and finally as a freely supported fresh tibia. The study found small incremental differences in the natural frequencies of the tibia when the skin was removed and when the foot and joints were removed a maximum of 6Hz but there was a larger difference when the muscles were removed with a maximum of 47Hz (Tsuchikane *et al.*, 1995).

The in vivo investigation impacted the tibia when the participants were seated with their legs overhanging a bench. Differences in fundamental frequency were determined between the fresh cadaveric tibias and the in vivo investigation. Inferring from the results of the cadaveric leg tibia, the authors attributed the difference primarily to the added mass and damping of the muscles attached to the tibia. In addition a difference of 238Hz was found between the mean frequency of the fresh and dry excised specimens. This was attributed to the presence of bone marrow in the fresh tibias and verified by injecting a grease in to the medullary canal of a dry tibia; the natural frequency dropped by 143Hz (Tsuchikane *et al.*, 1995).

The influence of soft tissue around the tibia has been further investigated by Van der perre *et al.,* 1983, using cadaveric legs. By having the leg suspended at 90 degrees with the knee flexion over a table top and the mid-thigh clamped in a vice. Five limbs were dissected in stages and the tibia was tested using an impact hammer at each stage. The response was measured using an accelerometer and the natural frequency was determined. The tibias were tested within the leg, with the leg skin removed, the muscles removed, the foot removed, the femur removed and as a free tibia. The effect of the knee ligaments was also investigated by dissecting each ligament with various tests done at each stage. The study found that the weight of the limb was most reduced by the removal of the muscles. The natural frequency was not greatly altered by the removal of the skin but increased incrementally when the muscles and foot were removed and decreased with the removal of the femur and fibula. The damping decreased at each subsequent dissection. The results showed that the foot was found to have a greater influence on natural frequency (Van der perre *et al.*, 1983).

2.7 Age-related Bone Loss

During the growth period of the human body, bone mass increases. It starts to level off in young adults, and after the 30th birthday, it begins to decrease (Wasnich, 1997). Many factors are involved in bone loss that is age-related and caused by bone loss. For example, the tendency to fall and the risk of fracture, reflect a decrease in oestrogens (Lindsay, 1994; Schiessl *et al.*, 1998), a decrease in calcium and vitamin D (Peacock, 1998; Lau and Baylink, 1999) and also physical inactivity (Marcus, 1989; Coupland *et al.*, 1993). A major cause of bone loss in the first two decades after menopause is oestrogens deficiency (Richelson *et al.* 1984). The decrease in bone density that accompanies ageing can be also partly explained by increased parathyroid hormone secretion. This results from a deficiency of vitamin D and also a low intake of calcium (Jee, 2001).

Very similar effects on the skeleton are seen when levels of vitamin D and calcium falls. This occurs because of vitamin D, which is a major regulator for calcium homeostasis and metabolism of the skeleton. The inadequate intake of Vitamin D and calcium can be avoided with exposure to sunlight and by consuming calcium-rich foods, and with the use of dietary supplements. However, Peacock (Peacock, 1998) warns that when vitamin D is taken unnecessarily, osteoporosis may be encouraged. To maximise peak bone mass, and to reduce age-related bone loss, active lifestyle and exercise is the answer. It is needed, too, for the maintenance of muscle power, the body's ability to balance and to walk, and prevent falls. As can be seen, the recommendation is to stay active throughout life and in this way maintain bone health. (Iwamoto *et al.*, 2009) The main cause of osteoporosis is the loss of bone. The osteoporosis bone disease decreases bone mass, causes bone micro architecture to decline in bone strength. This is followed by increasing bone fragility, then to increased risks of fracture (Jee, 2001). Osteoporosis is not only a disease confined to the elderly as is popularly believed because it advances when bone desorption exceeds bone formation. Osteoporosis is bound to increase as life expectancy increases (Jee, 2001).

It can be considered a governing condition of the elderly (Rizzoli *et al.*, 2009). The statistics of people who suffer a fracture related to osteoporosis shows that from every ten women over the age of 50, approximately three of them suffering a fracture related to osteoporosis. In this age group, one in eight men is affected (Jee, 2001). The functional definition of osteoporosis relates to bone mineral density assessment or bone mineral content (BMC) assessment. A change in the way osteoporosis is defined is recommended by the World Health Organisation (WHO). It recommends the use of the BMD T-score, the standard deviation (SD) from the mean for young adult Caucasian women. Minus 2.5 on a T-score indicates osteoporosis, and between -1.0 and -2.5 refers to osteopenia or low bone mass, seen as a preliminary stage of osteoporosis. If the T-score falls below -2.5 and there has been a fracture, the condition is termed severe osteoporosis. A T-score of more than -1.0 indicates normal bone mass (WHO Study Group 1994; Kanis *et al.*, 1994).

A T-score can be better understood by stating that it compares a patient's bone mass deviation from the mean bone mass of a healthy adult. Comparing bone density to the mean for people of same age and gender uses a Z-score. However, there are doubts about the use of the Z-score to infer osteoporosis; because that means an assumption that most cases of osteoporosis do not increase with age (Kanis *et al.*, 2000). But for the diagnosis of osteoporosis in premenopausal women and in children, the use of Z-score is advisable. The WHO developed a fracture risk assessment tool known as FRAX™. Clinical risk factors alone are its basis, though BMD is also used. In FRAX™, clinical risk factors evaluated are body mass index (BMI), the history of fracture, a parental history of hip fracture, the use of oral glucocorticoids, and rheumatoid arthritis and other secondary causes of osteoporosis. The analysis is also able to predict a 10-year probability of hip fracture.

2.8 Age Dependence

After the middle years (>45 years), age-related architectural changes in human bone include first and most of all a decrease in BV/TV and Conn. D (density) for trabecular bone, a decrease in the cortical thickness (C.Th), and an increase in the porosity for cortical bones. These changes may considerably involve the mechanical performance of bone, usually leading to the reduced strength and toughness of the tissue. Perhaps the most important age-related change is the BV/TV of trabecular bone, which has been found to reduce with age in the femoral head, femoral neck, lumbar spine, distal forearm, iliac crest, and proximal tibia. Figure 2.7 shows the difference between the trabecular structures of vertebrae in two different female ages.

In the lumbar spine (another common age-related fracture site), trabecular bone volume per trabecular volume (BV/TV), trabecular number (Tb.N) and Connectivity density (Conn.D) decrease significantly with age. Age-related changes in tissue anisotropy have been demonstrated in vertebral bodies, with the thickness of the horizontal trabecular decreasing significantly with age, whereas the trabecular thickness of the vertical trabecular is age-independent. In addition, age dependent micro structural changes in the trabecular bone of the tibia metaphysic are reflected in a significant decline of BV/TV, thinning of trabecular, and a change in microstructure from plate-like to more or less rod-like.

The mean yellow (marrow) space volume, bone surface-to-volume ratio, also increases with age (Mueller *et al.*, 2009).The most significant age-related structural change in cortical bone is porosity. Increases of porosity with ageing have been observed in various anatomical locations of skeletal tissues. For instance, the cortex porosity in both the femoral neck and intertrochanteric has been shown to significantly increase with age. The porosity in femoral diaphysis increases from 4 - 6% in young adults to over 9% in the elderly. The better porosity in the elderly is due to the increasing size rather than the number of Haversian canals. Age-related increases in the porosity of cortical bone are also demonstrated at other skeletal locations, such as iliac crest and diaphysis of the humerus and tibia. In addition to porosity, 3D micro-CT images of femoral diaphysis have shown that the number of Haversian canals is nonlinearly (quadratic) correlated with age in the female population, increases up to 60 years, then starts to decrease afterwards (Cooper *et al*,. 2007).

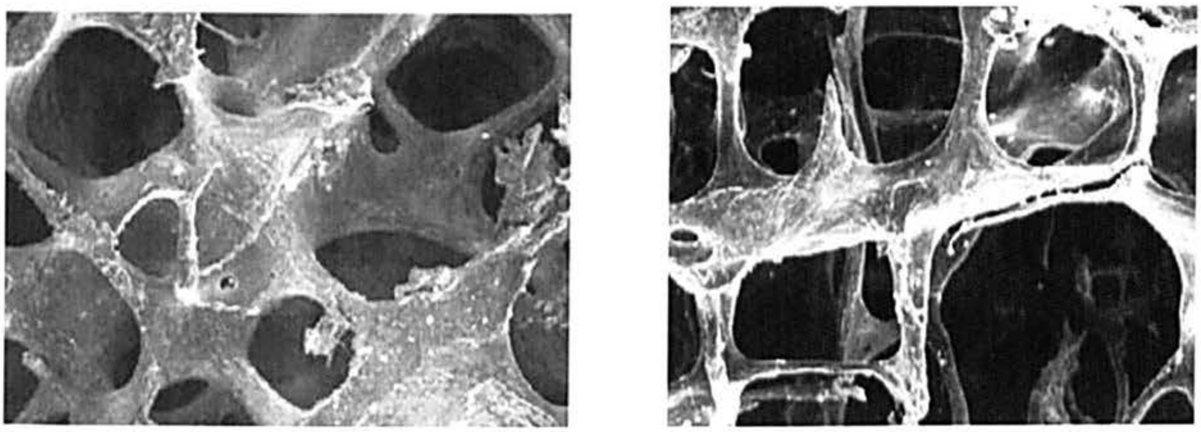

a) b)

Figure 2.7: The trabecular structure of vertebrae in a) 36 year old woman and b) in a 74 year old woman (Cowin and Raton, 2001).

2.9 Anatomical Differences

The bone structural design, mainly trabecular bone architecture, is site-dependent. Histomorphometric study has shown that the trabecular BV/TV (Bone Volume per Trabecular Volume) is much lower in the lumbar spine (8.3%) than that in the femoral neck (15.8%). In addition, 3D micro-CT investigations point out that trabecular microstructure has a similar trend in BV/TV at other sites, such as spine, femur, iliac crest, and calcaneus (Amling *et al.*, 1996). Eckstein *et al.*, 2007 compared the structural design of trabecular bone from six different anatomical sites of human bones: distal radius, femoral neck and trochanter. Figure 2.8 shows the difference between the structures of trabecular in two different parts of body.

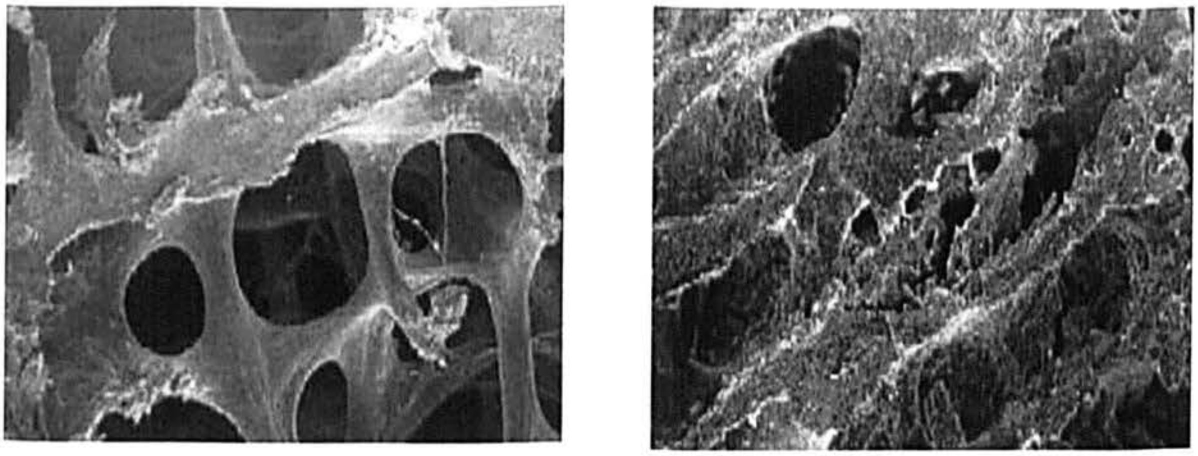

a) b)

Figure 2.8: a) and b) shows the difference between the structures of trabecular in the L1 vertebra a) and in the calcaneus b) in a 24 year old man (Cowin and Raton, 2001).

The study reported that the iliac crest displayed the most rods-like trabecular structures, whereas the femoral neck and the calcaneus displayed the most plate-like structures. In addition, the trabecular are thickest in the femoral neck (182 ± 46μm) and thinnest in the iliac crest (126 ± 19μm) (Eckstein *et al.*, 2007).

2.10 Gender Dependence

Architectural differences between men and women cause the female to be more vulnerable to osteoporosis. In the forearm radius, the trabecular compartment showed higher BV/TV (except for the mid-shaft region), Tb.N, Conn. D and lower Trabecular separation (Tb.Sp) in men in comparison with women. The cortical compartment showed higher Trabecular thickness (C.Th), tissue area, and second moment of inertia in men than in women as the Figure 2.9 shows. However, BV/TV was not gender-dependent in the forearm radius (Mueller *et al.*, 2009). At the radius and femoral neck, trabecular bone displayed a more plate-like structure, thicker trabecular, smaller separation, higher connectivity, and a higher degree of anisotropy in men than in women. At the trochanter, men displayed more plate-like structure and thicker trabecular, but there were no differences in trabecular separation or other parameters compared with the women. However, at the calcaneus, iliac crest, and second lumbar vertebra none of the bone parameters displayed significant differences between genders (Eckstein *et al.*, 2007).

Women experience more severe changes in bone with increasing age although such age-related changes are usually parallel for men and women. Men show an age-related increase in bone size (e.g., cross-sectional area of the vertebral bodies), whereas such an increase is not obvious in women. In addition, a higher tendency of disconnection of the trabecular network is present in postmenopausal women than men at a similar age. Women usually have thinner trabecular in young adulthood and may experience more micro structural damages with increasing age in comparison with men. These gender-dependent architectural changes may explain why women are more susceptible to age-related bone fractures than men (Mosekilde, 2000).

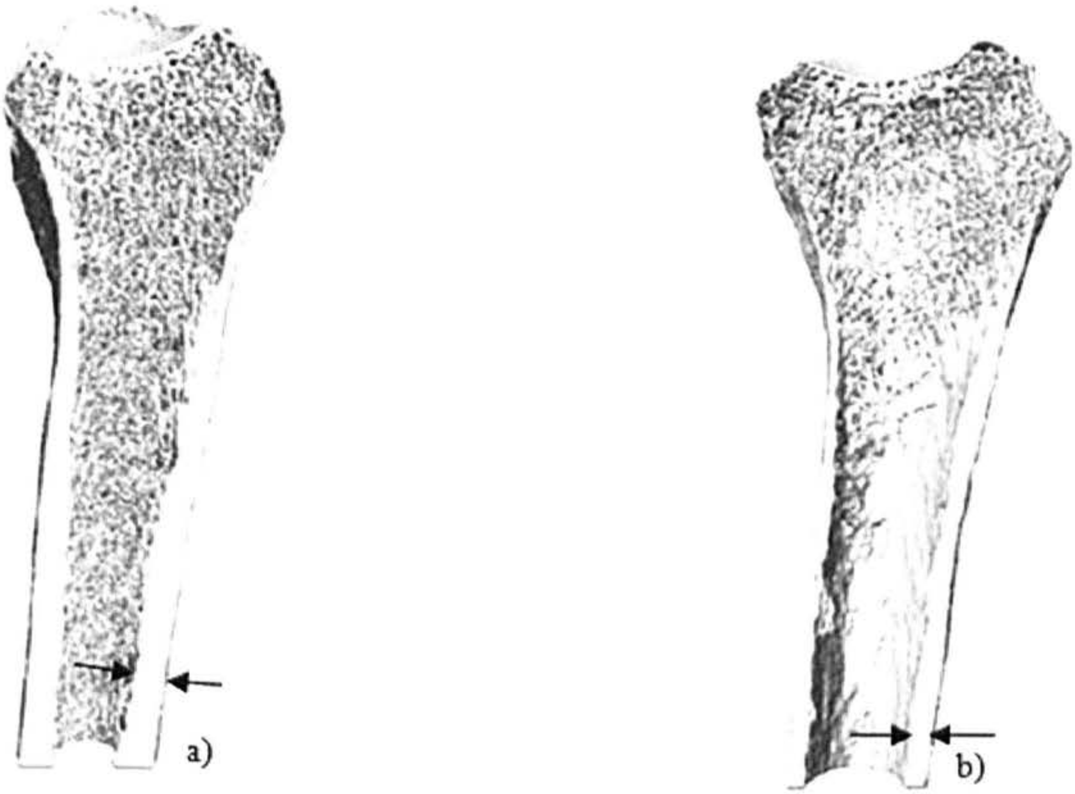

Figure 2.9: HR of a healthy and an osteoporotic human radius, a) 79-year-old man and b) a woman of the same age (Adapted from Bone, 45, Mueller *et al.*, 2009, page 882-891, with permission from Elsevier Inc).

2.11 Failures and Defects of the Skeletal System

The function of human skeletal systems involves structurally supporting the body, protecting the vital organs, and serving as a lack of minerals for balanced metabolism. Clinically, most failure sand defects of the skeletal system are induced by traumatic injuries, age-related or osteoporotic fractures, and pathological degenerations. Among the causes, age-related and osteoporotic fractures are increasingly becoming one of the major health care concerns around the world due to the increased risk of morbidity and the serious threat to the quality of life of patients. Recent studies have shown that the lifetime risk of major bone fractures is between 40-46% for Caucasian women and between 13-22% for Caucasian men at the age of 50 years (Hordon *et al.*, 2000; Kanis *et al.*, 2000; Melton 3rd, *et al.*, 1992).

Furthermore, this number is rising every year and could reach 4.5 million world-wide by 2050 (Gullberg *et al.*, 1997). A similar trend can also be found in all other ethnic groups although fragility fracture rates are different (Duan *et al.*, 2005). In many cases, surgical intervention with bone grafts and even total joint replacements are needed. Another common example of bone defects is congenital deformities, with functional and cosmetic corrections of these complications becoming a major clinical practice. The surgical procedures for such purposes primarily involve the transfer of tissues or the placement of implantable prosthesis.

2.11.1 Fracture of Bone Tissues

The main role of the musculoskeletal system is to transmit forces from one part of the body to another under controlled strain and to protect vital organs (e.g. lungs, brain). It also performs other important functions such as serving as mineral reservoir. Several skeletal tissues participate in this mechanical objective of transmission and protection: bone, cartilage, tendons, ligaments and muscles.

The mechanical properties of bone are a result of a compromise between the need for a certain stiffness (to reduce strain and achieve a more efficient kinematics), and the need for enough ductility to absorb impacts (to reduce the risk of fracture and minimize skeletal weight). Most fractures are caused when a bone suffers loads that exceed certain threshold levels (in terms of stress or damage), that may also be prolonged (creep), or repetitive (fatigue). Other fractures are caused when bone is compromised structurally as a result of disease, ageing, surgical intervention, pharmaceutical treatments, poor diet, lack of exercise, and so forth. In all cases some sense can be made by invoking either material or engineering principles to explain the effects of overload, or structure/function relationships to grapple with the effects of a materially and structurally compromised tissue (Rho *et al.*, 1998).

In general, bone is stronger in compression compared to tension, and weaker in shear. As a result, impact failure in a bone will begin on the opposite side to the impact (the tensile side) since it will reach its ultimate strength sooner than the side loaded in compression. In some cases there sultan advancing crack will reach the middle of the bone, and near compressed tissues. Due to bone's higher resistance to this type of load, it will advance in a path nearer to the bone's longitudinal direction, along the directions of maximal shear stress. This phenomenon is known as Osteoporosis. Osteoporosis is one of the most common syndromes afflicting the aging human population, and in particular post-menopausal women. It is defined as a state of increased bone fracture risk, and it is commonly linked to decreased estrogenic levels of bones in the body. In this way it will form a fracture with a so-called 'butterfly' fragment, commonly seen in practice (see Figure 2.10) (Rho *et al.*, 1998).

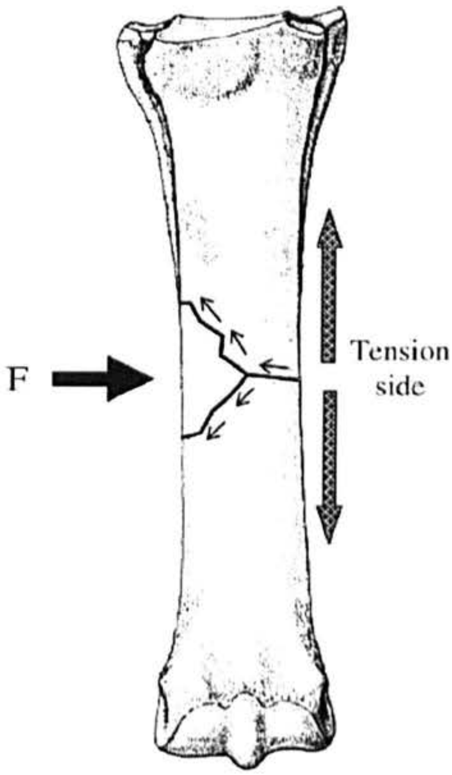

Figure 2.10: Lateral impact loading of a long bone causes bending. The fracture starts away from the site of impact and 'runs' along the direction of maximal shear, creating a butterfly fragment (Turner, 2005) and (Rho *et al.*, 1998).

2.11.2 Material Characterisation during Bone Fracture

Three stages are involved in the fracture of bone. The stress/strain curve (in tension) for bone as a material shows a (macroscopically) linear phase followed by a 'knee' region where the material yields. Then a region of strain hardening (which can be shorter or longer depending on the circumstances) follows, and then unexpected catastrophic failure, as shown in Figure 2.11. In phase I, the material deforms reversibly with little obvious remaining damage, while in phase II (the elastic-continuum damage mechanics domain) the material is still structurally integrated but absorbs energy by developing diffuse micro cracking at the expense of stiffness and remaining strength. In phase III, the fracture mechanics realm, energy is absorbed to reach the final fracture surface.

The amount of energy depends crucially on the properties of the final fracture plane and the overall number of such planes and/or fragments. The toughness of a material is defined in terms of stress or energy related requirements to run a crack through the material. Stress-based criteria, such as the stress intensity factor (Kc) postulate that fracture is initiated when the concentration of stress at the crack tip reaches a critical value. Energy-based approaches either measure the critical work to fracture of a specimen W_f, or determine critical levels of energy per unit area necessary for fracture (Zioupos, 1998).

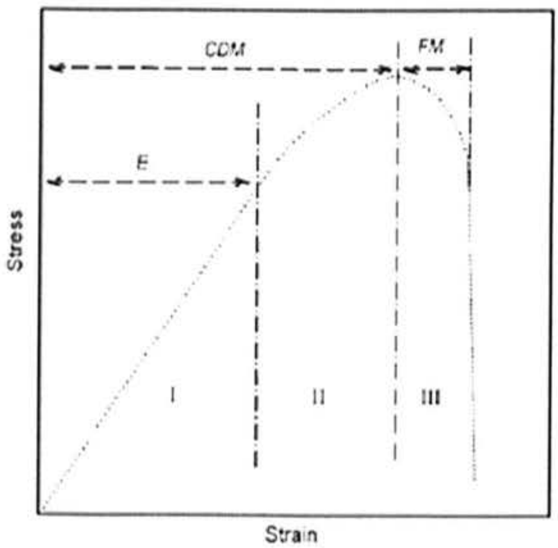

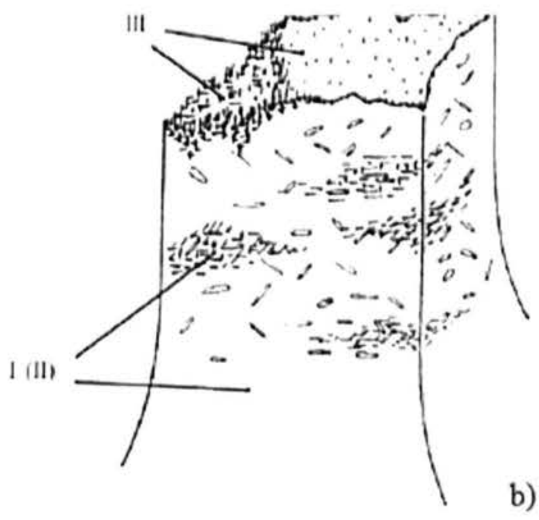

Figure 2.11: a) Consecutive stages of behaviour: E: the elastic range. CDM: the continuum damage mechanics range. FM: the fracture mechanics. b) Energy is absorbed, either elastically, or as pre -failure damage, in a slow-moving crack, or a fast-moving fracture plane (Zioupos, 1998).

Recently it has become quite clear that those modern composites (and also bone and other biological hard tissues) show weak inter-lamellar interfaces which are able to absorb energy and/or divert a crack and so deter the onset and growth of fracture (Peterlik *et al.*, 2006).

Also, it is now increasingly clear that initiation of cracks in bio mineralized (bone and other biological hard tissues) tissue is far less important than their propagation, since biological tissues utilise a number of tricks like crack diversion/deflection, fibre pull-out, crack and/or matrix bridging to increase the required amount of energy to fracture (Jackso *et al.*, 1989; Wang *et al.*, 1995). The fracture process is dependent on the direction of travel of the crack, being either brittle (in the longitudinal direction) or deflected (in the tangential direction) or toughened by micro-cracking (in the radial direction) as shown in Figure 2.12.

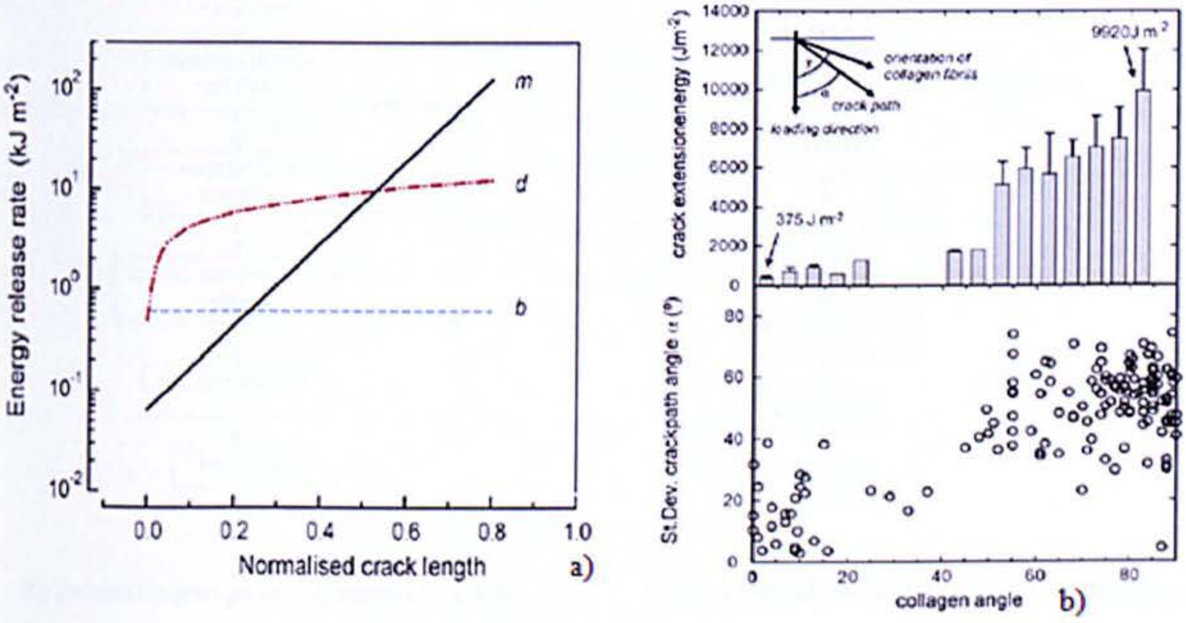

Figure 2.12: Crack propagation. a) Energy in the radial (m, micro cracking damage), tangential (d, deflected crack) and circumferential (b, brittle fracture) in bovine bone showing crack length. Bone is more resilient in micro cracking damage (m) and b) An across-the-grain crack (fibre direction) needs more power than a blow along it (Peterlik *et al.*, 2006).

2.11.3 Types of fractures

The first type of fracture is often shaped by normal loads acting on a bone that has been damaged by disease or age (Zioupos and Currey, 1998).This type of fracture is usually called pathologic. Most occur through osteoporosis in the elderly and are more frequent in women than men. Bone tumour is another important cause of pathologic fracture. It change bone mechanical properties and produces stress concentrators. Removing the tumour generally increases the risk of fracture.

In fact, a higher risk of bone fracture in the elderly is not only due to the progressive decrease of bone reliability (osteoporosis), and therefore strength, but also to extra factors such as the incapability of soft tissues to attract the energy generated in a fall and the change of the kinematic variables of the walk. Lotz and Hayes report that only a small amount of energy is necessary to break a bone (i.e. 5% of the energy available in a fall), due to the energy-absorbing action of soft tissues that are deformed in the shock or impact (Lotz, Hayes, 1990). Figure 2.13 shows a schematic sequence of stages leading to both types.

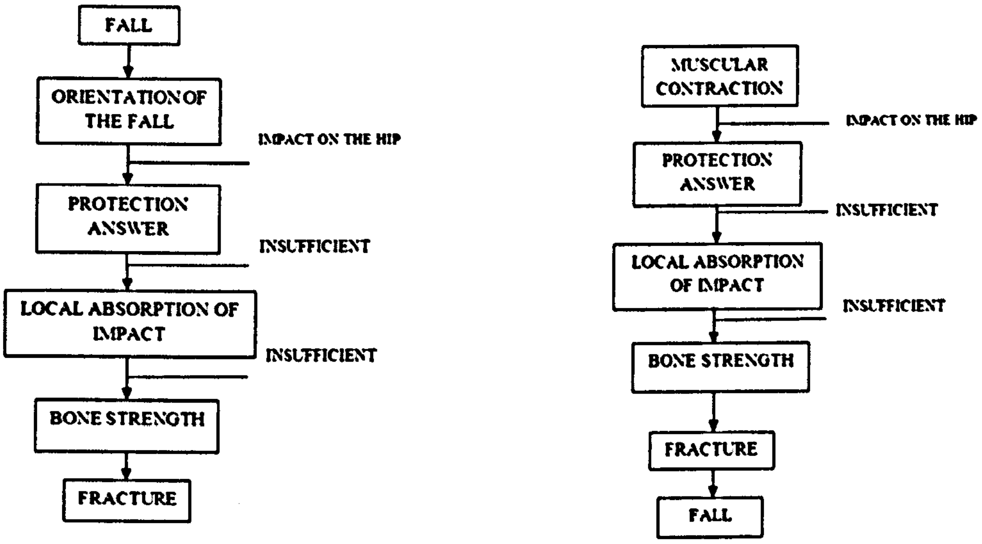

a) External impact produced fracture (first type) **b) Creep or fatigue produced fracture (second type)**

Figure 2.13: Scheme of two usual types of mechanisms of bone fracture (Sloan and Holloway, 1981).

The second type of fracture is produced by creep or fatigue. Bones often support more or less stable loads for long-lasting periods of time and cyclic loads that may produce micro damage. If the growth of micro damage is faster than repair by remodelling, micro cracks (or other kinds of micro damage) can increase and so produce macro cracks and complete fracture. Clinically, this is called a stress fracture. Fracture normally occurs in individuals who are involved in repetitive-type physical performance, such as soldiers, ballet dancers, joggers, athletes, and racehorses. It also occurs at lower activity levels in bones damaged by osteoporosis, particularly at older age when bone remodelling is almost static (Burr *et al.*, 1997).

2.11.4 Healing

Once a fracture occurs, the basic healing process is auto-activated naturally to repair the site. Healing involves the separation of several tissues (cartilage, bone, granulation, etc.), with different patterns that are directly influenced by the mechanical environment, which is in turn governed by the load applied and the constancy of the fracture site. In detail, not all fractures are totally repaired. Occasionally there are non-unions or delayed fractures depending on specific geometric, mechanical and biological factors such as ageing, poor diet and so forth, mitigating the many different kinds of fixations used to improve fracture stabilisation.

Fracture healing is a natural process that can reconstitute injured tissue and recover its original function and form. It is a very complex process that involves the coordinated participation of immigration, differentiation and proliferation of inflammatory cells, angioblasts, fibroblasts, chondroblasts and osteoblasts which synthesize and release bioactive substances of extracellular matrix components. Figure 2.14 shows the process of healing with different types of collagen and growth factors (Einhorn, 1998).

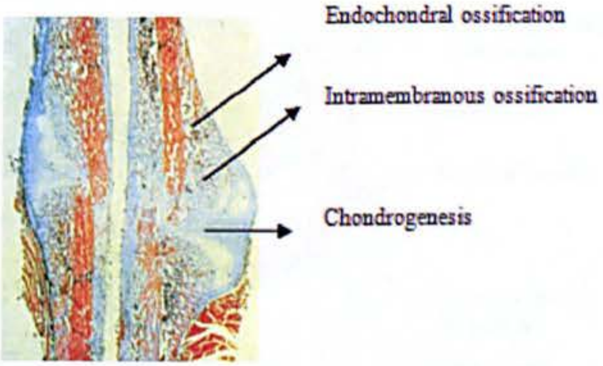

Figure 2.14: Callus at day 9 post-fracture showing more mature bone under the periosteum (intramembranous ossification) (Einhorn, 1998).

2.12 Anatomy of the Human Femur

In the human skeleton system the heaviest and longest bone is called femur which is also known as the thigh bone. It includes two sections:

I. Proximal end which articulates with the bones of the hip in forming hip joint

II. Distal end forming the knee joint which articulates with the tibia and the patella.

2.12.1 Hip Bone

Sacroiliac joint and hip joint of the bone to the proximal end of the femur and proximal portion of the posterior sacral articulating shape a bony structure at the base of the spine. This results in a connection between the trunk and lower limbs. The pubic symphysis hip bones form the pelvic girdle and pelvis forms the anterior and lateral walls. Hip bone consists of the ilium, ischium and pubis with which they meet at the acetabulum as shown below. Acetabulum bone is one of the main joint of the hip bone which locates below the spine where it joins three bones of hip and shapes as Y shape which is the concave surface of pelvis. Acetabulum forms two- fifth of the ischium and one fifth of the pubis (see Figure 2.15).

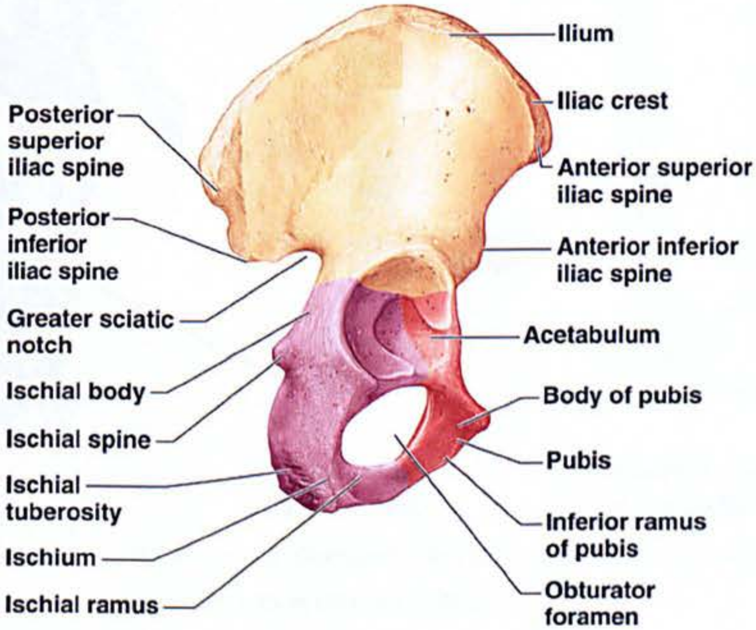

Figure 2.15: Lateral view of the hip bone showing the acetabulum formed by the ilium, ischium and the pubis. Figure based on original artwork from (Moore, 2007).

2.12.2 Femur

Femur is formed in the thigh bone which is the heaviest and the longest bone in the human body structure which is nearly one fourth to one third of the human body length. The femur is a well-built section of the insect leg which is located between the hip joint and the knee joint (see Figure 2.16 and Figure 2.17).

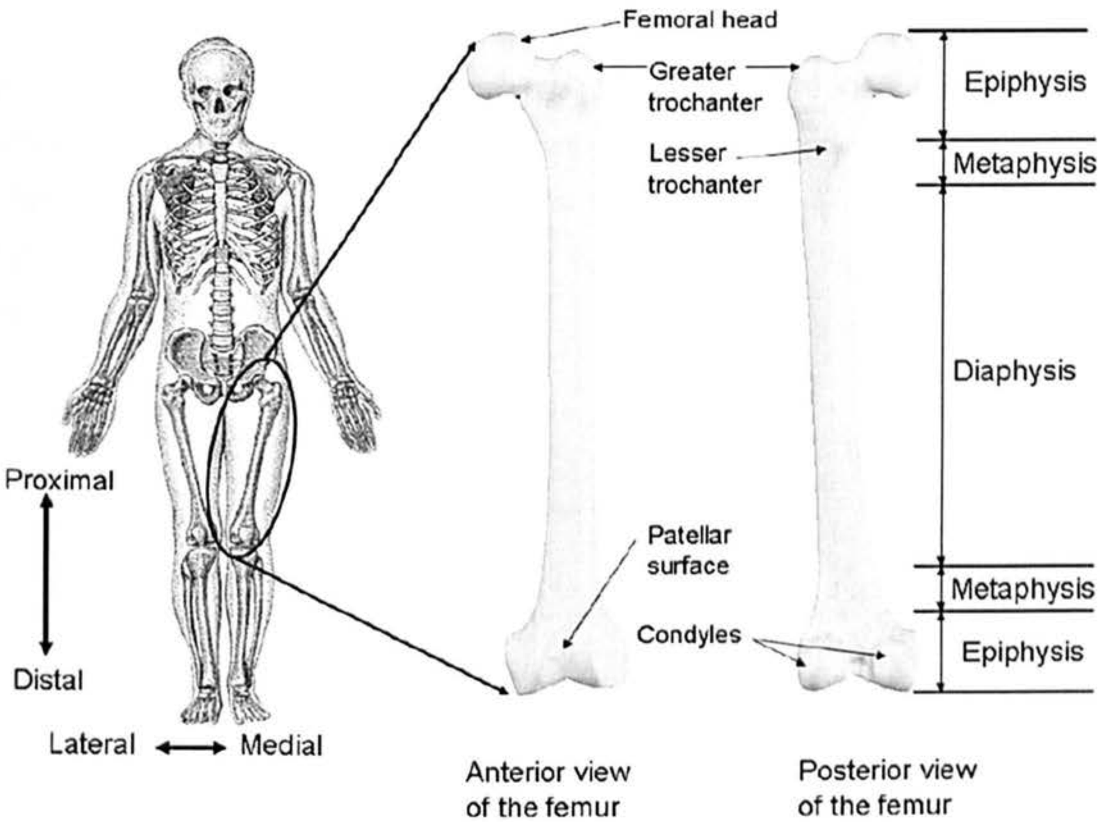

Figure 2.16: Skeletal anatomy of the femur and directional reference used to identify location of anatomical landmarks (Figure based on original artwork from (Martini, 2001).

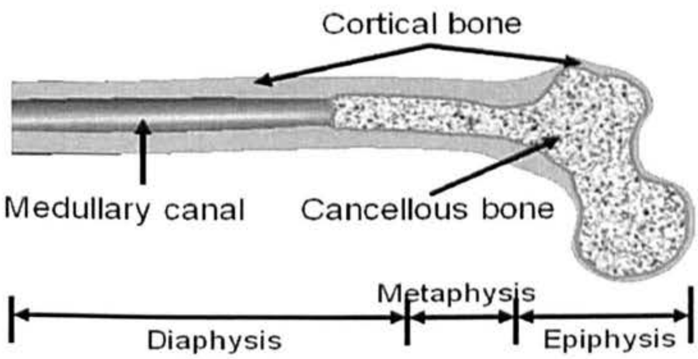

Figure 2.17: Bone tissue of the femur (Figure based on original artwork from (Martini, 2001).

2.12.3 Upper End

The Upper end of the femur consists of three main parts head, neck and greater and lesser trochanters. The femur head is a partial two thirds of a sphere that attaches to the hip joint facing upward. It is the ball rounded top part of the femur. The ligament of the head of the femur is attached to a pit known as the fovea capitis femur. The neck is connected with the head of greater trochanter region facing upward. The neck is a shaft which is 4-5 cm long and it has a narrow diameter at its middle part. At the front side of the femur bone between the neck and the trochanter region, there is a trochanteric line which runs from the greater trochanter to the lesser trochanter that projects outwards. The trochanteric line becomes less discernible towards the less trochanter. At the back of the femur bone, the intertrochanteric crest is fairly smooth and more indiscernible. Figure 2.18 shows the different parts of femur from anterior and posterior view.

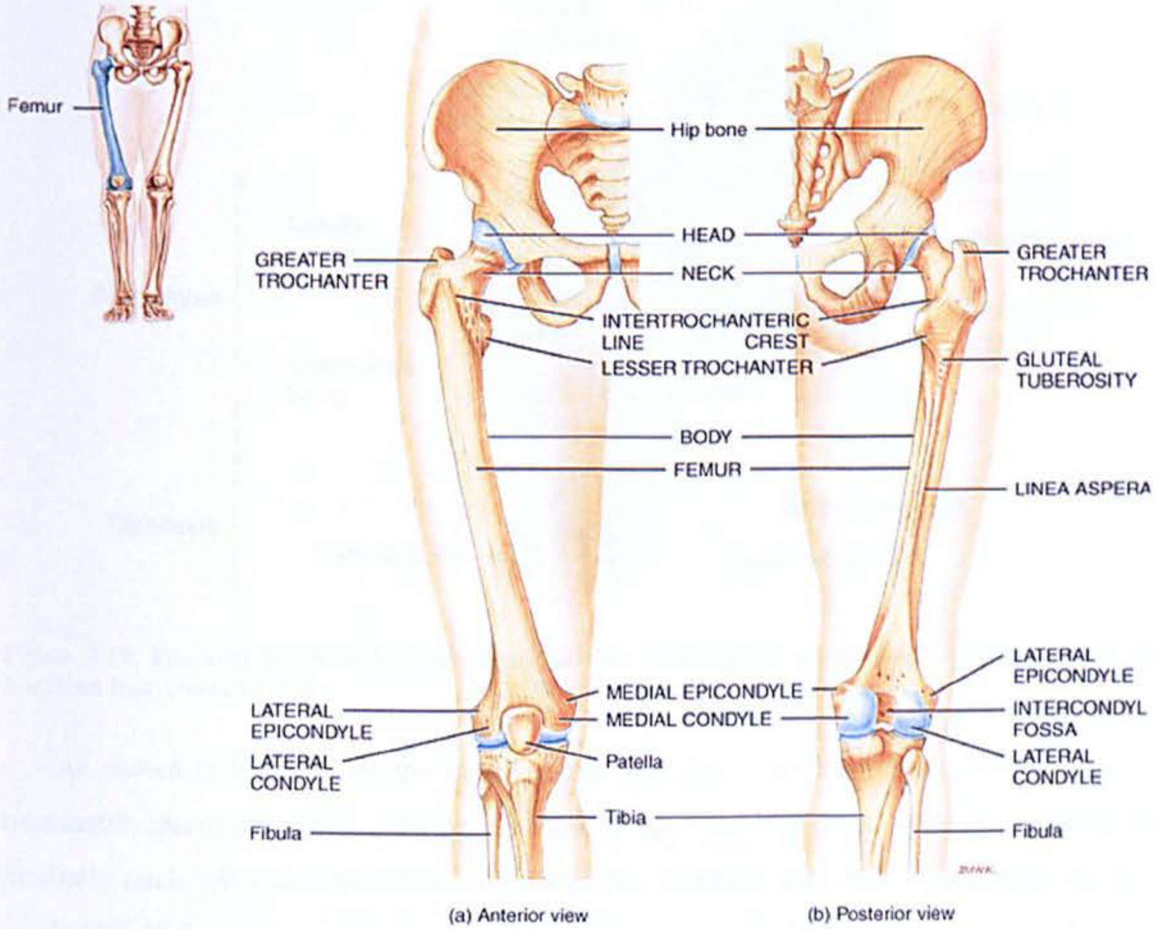

Figure 2.18: Femur (anterior and posterior view). Figure based on original artwork from (Moore, 2007).

The angle of inclination made by the neck and the linea aspera femur has a typical value of between $110^{\circ} - 145^{\circ}$, with an average angle of about 126 degrees from the longitudinal shaft axis. The angle of inclination decreases during the active growth period and it is commonly smaller in females (Manatomy, 2013). The greater trochanter is located above the junction of the shaft laterally, about 10 cm below the iliac crest where it protrudes superomedially to the junction between the neck and shaft regions. A greater reach of motion in the hip joint is possible due to the perpendicular manner in which the angle of inclination of the femur allows the axis of the neck and head to intersect with the acetabulum cup.

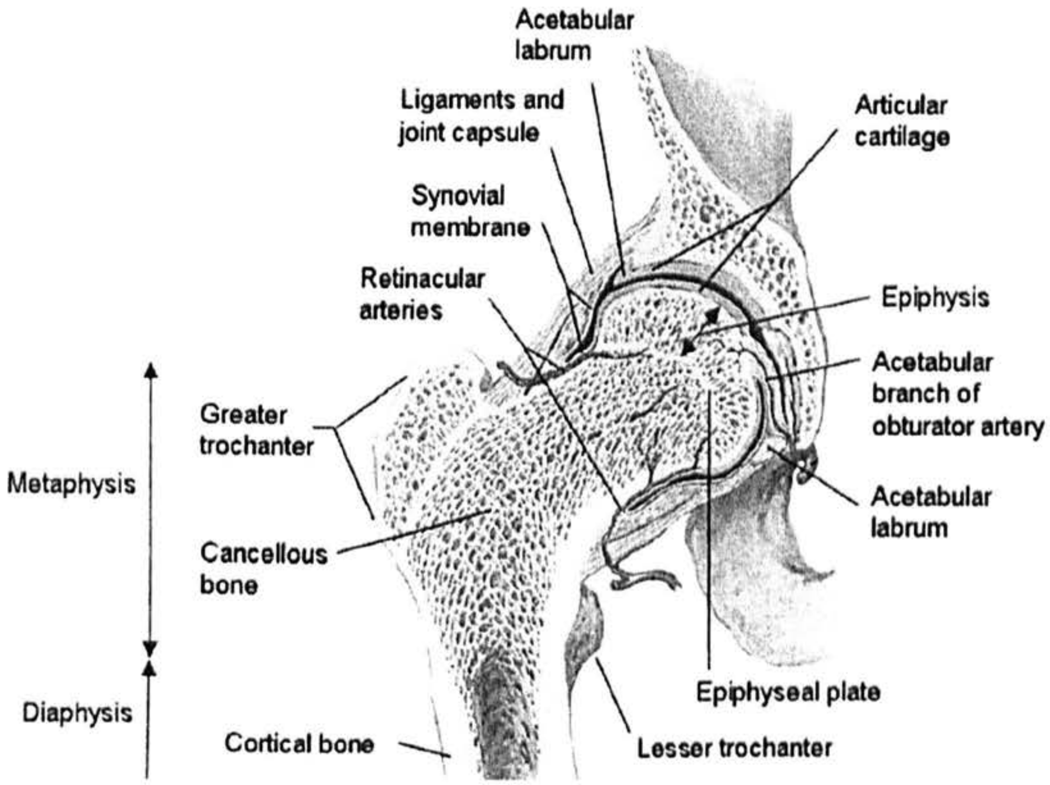

Figure 2.19: Proximal femur in a posterior-medial view showing the trochanters and femoral head region. Modified from (Netter, 2002).

As shown in Figure 2.19, the Line became less clearly near the less trochanter and lesser trochanter, intertrochanteric crest on the back of the femur becomes relatively smooth. Super medially neck joins the shaft area, and about 10 cm below the iliac crest, where the greater trochanter of the femur located at the joint of the neck and shaft. The angle of inclination as shown in Figure 2.20 and Figure 2.21 is the angle between the super medially projected neck and head axis and the shaft-axis and has a typical value of between $110^{\circ} - 140^{\circ}$, with an average of about 126˚. It is usually smaller in female and decreases during the active growth period. Angle of inclination of the long axis of the femur neck and head in a more direct manner to intersect with acetabulum cup allows for a greater range of motion in the hip joint. There is a difference between the angles of femur. The Larger angle is called anteverted and the smaller angle is called retroverted. This could be noted by external and internal rotation of the femur, causing out-toeing and in-toeing (pigeon toe) respectively (Norkin, 1992).

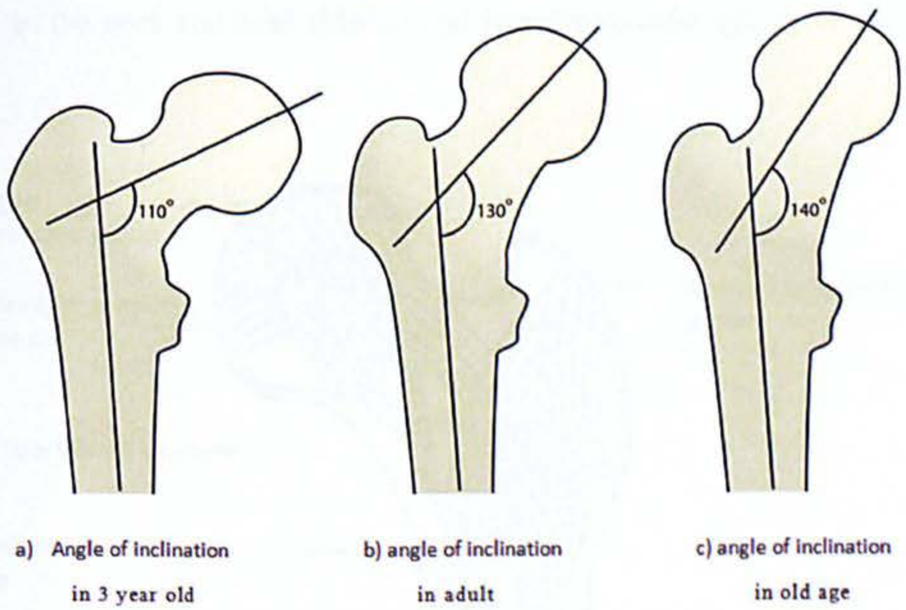

Figure 2.20: Angle of inclination (Anterior view) is defined as the angle span between the femoral axis and the neck axis, and decrease over active growth period. Figure based on original artwork from (Moore, 2007).

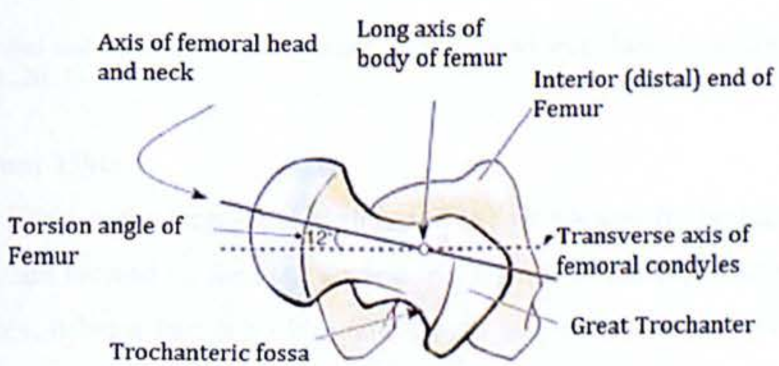

Figure 2.21: The torsion angle is often defined as the angle spanned by the femoral neck axis and the distal condylar axis. Figure based on original artwork from (Moore, 2007).

2.12.4 Bone Structure Femur

Bone structure femur is categorised by its almost spherical head, slightly flattened neck and also two trochanters with their communicating intertrochanteric ridge. Frontal section of the uppermost third of the femur shows the powerful cortex and fragile medulla of the shaft (see Figure 2.22). Above the lesser trochanter this arrangement is reversed, and a thin cortical shell clothes the dense arrangement of cancellous bone which forms the internal weight-bearing system in the neck and head (Medial and lateral trabecular system of the femoral neck, 2011).

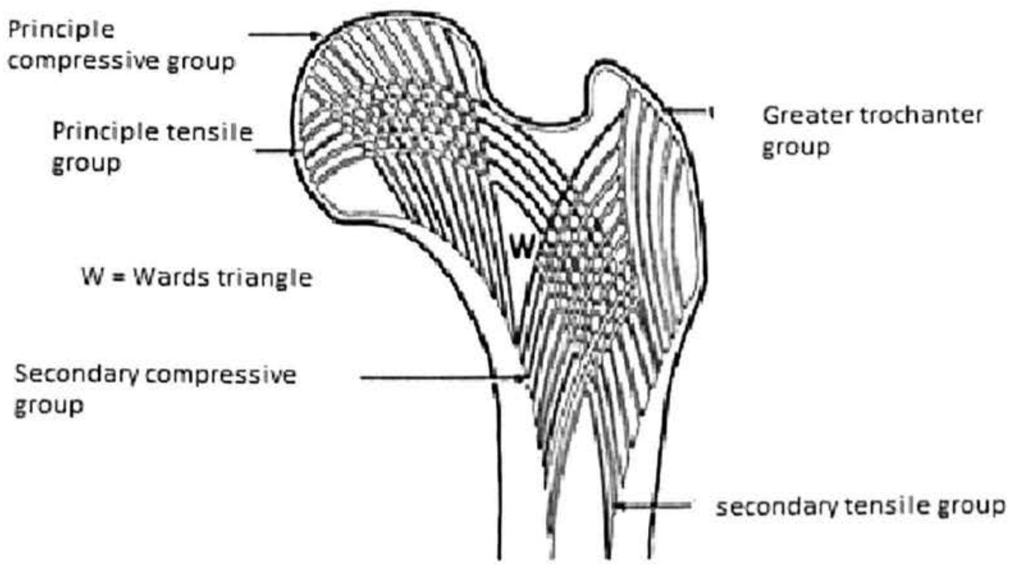

Figure 2.22: Medial and lateral trabecular systems of the femoral neck (Medial and lateral trabecular system of the femoral neck, 2011).

2.12.5 Proximal Tibia

Proximal Tibia is the larger and stronger of the two bones in the leg, it's also known as the shin bone and located on the anterior and medial side of the leg. It connects the knee with the ankle bones. It has a length roughly one-fourth to one-fifth of the body length. The body weight is transmitted from the femur to the ankle and foot by this. The tibia has an upper and lower end, divided by a shaft, with the upper end rotated more medially than the lower in superior axial view. The upper end of the tibia is curved backwards and it is bigger than the lower end. The upper surface comprises of the medial and lateral condyles, a large ovoid and smooth surface that articulates with the femoral condyles (See Figure 2.23).

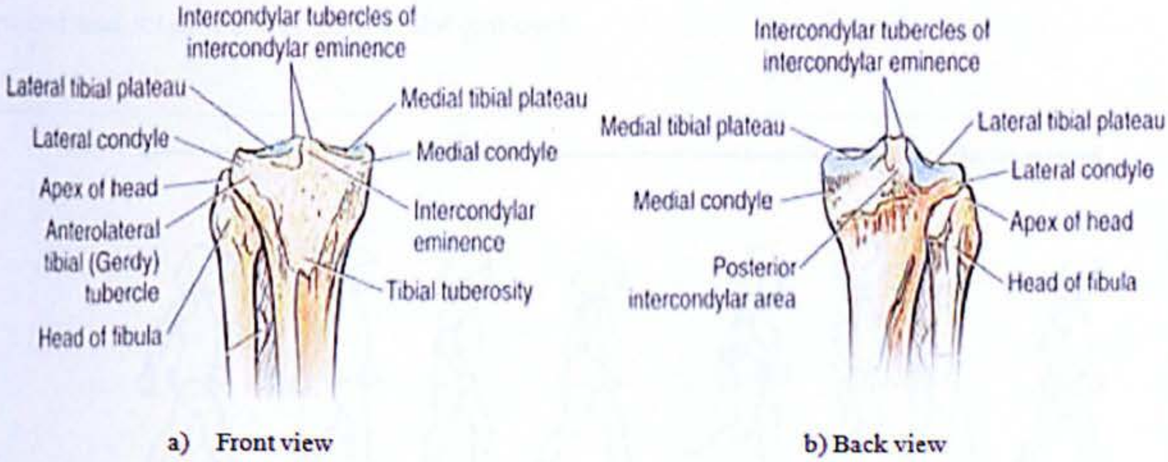

Figure 2.23: Proximal tibia. Figure based on original artwork from (Moore, 2007).

2.12.6 Sexual Dimorphism in the Femur

Sexual Dimorphism in the Femur is a phenotypic differences between male and females of the same species. Sexual dimorphism in humans has been a subject of much controversy, especially when extended beyond physical differences to mental ability and psychological gender. According to Wescott (2005), females show more platymeria than males because of the wider pelvic breadth. The female constriction differs from males because of a bigger pelvic width in the ability to bear children, this wider distance of females would result in greater Medio lateral bending of the sub trochanteric region, and it can cause greater platymeria. Within-group variation in the proximal femur, expressed as sexual dimorphism, may also reduce the validity the proximal femur shape has in predicting ancestry. Hence, the differences of sex may reduce the validity in assessing heritage (Wescott, 2005).

2.12.7 Femoral Loading during Gait

Human Gait Cycle is explained as the type of locomotion carried out by limbs. Human gait is essential to complete day to day physical tasks such as walking, jumping and running. Depending on the type of gait, the limbs experience different mechanisms including overall velocity, force, kinetic energy, and potential energy. Walking, the simplest form of activity is produced by repeating the gait cycles. According to the gait cycle developed by Perry, gait cycle can be divided into two phases as Figure 2.24 shows, the stance phase and the swing phase (University of Vienna, 2006). Swing phase is when the limb is not in contact with the ground and it takes about 38% of the gait cycle.

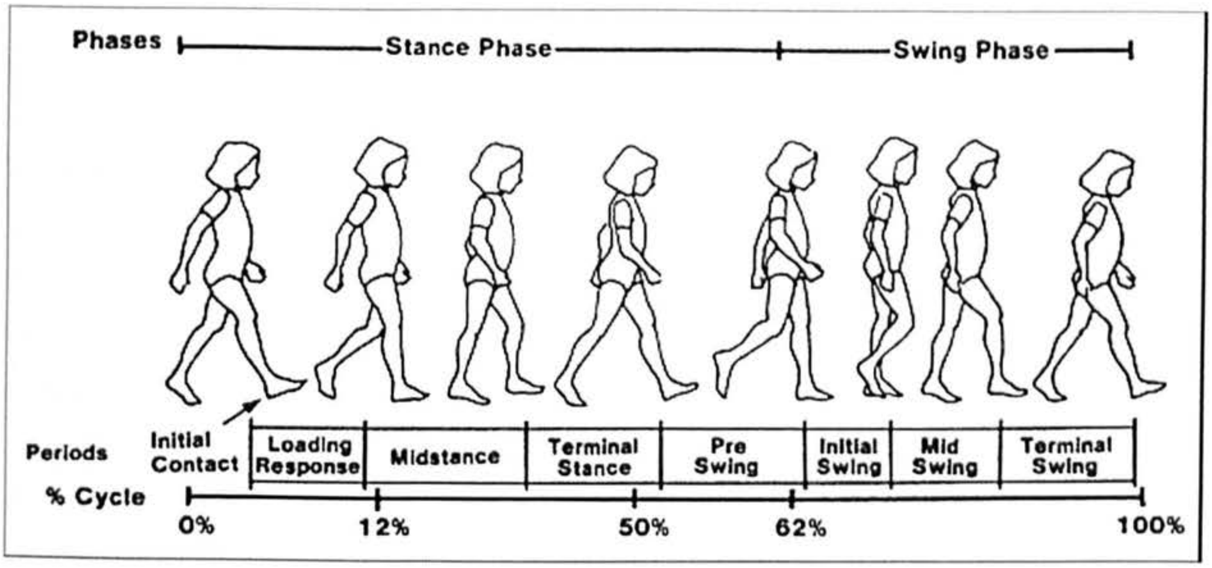

Figure 2.24: Phases of gait cycle for walking (University of Vienna, 2006).

Stance phase is divided into four stages the loading response (see Figure 2.24 and Figure 2.25), mid-stance, terminal stance and pre-swing. To understand the purpose, the various stages of the human gate will be described assuming that the subject stepped forward with their right foot as shown in Figure 2.24. In this case, the loading response starts as the right heel contacts the ground. When the rest of the right foot approaches full contact with the ground and achieves a flat position, the left foot stands on its toes. The loading response stage ends once the toes of the left foot leaves the ground. During the loading response stage, the body experiences double limb stance (Nordin, 2001).

The mid-stance represents the first half of a single support. It begins when the foot leaves the ground and continuous as the body weight travels along the length of the foot until it is aligned over the forefoot with the toes of the left foot leaving the ground and ends when the centre of gravity is shifted directly over the right (standing) foot. The terminal stance follows the mid-stance and ends when the left foot touches the ground. Over 90% of the mid-stance and terminal stance is carried by a single limb stance (University of Vienna, 2006; Human gait cycle, 2011). The pre-swing is the terminal double limb support period and occupies the last present of stance phase; it follows the mid-stance and is the last stage in the stance phase. The pre-swing begins when the left foot makes its initial contact with the ground. It ends when the right toes leave the ground. The pre-swing stage is performed with a double limb stance.

The swing phase is divided into 3 stages (see Figure 2.25): the initial swing, mid-swing and terminal swing. The initial swing begins when the right toes leave the ground and ends when the right knee reaches its maximum flexion of approximately 60°. The mid-swing begins from the moment of maximum knee flexion and ends when the tibia is perpendicular to the ground. Lastly, the terminal swing follows the mid-swing and ends when the right foot contacts the ground. The single limb stances during the stance phase are carried out by the initially responding leg, which is the right leg in the example above. During the swing phase the weight is then transferred to the contra lateral leg, or the left leg in the above example (Human gait cycle, 2011).

Gait Cycle	Stance phase 0-60%	Loading response 0-10%	Initial contact to contralateral toe-off
		Midstance	Contralateral toe-off to when the body CG is directly above the reference foot; weight loading begins
		Terminal stance	CG directly above the reference foot to contralateral initial contact; weight loading ends and heel of the reference foot leaves ground at ~35%
		Preswing 50-60%	Contralateral initial contact to toe-off
	Swing phase 60-100%	Initial swing	Toe-off to maximum knee flexion
		Midswing	From maximum knee flexion to when the tibia is perpendicular to the ground
		Terminal swing	Tibia perpendicular to the ground until initial contact; knee reaches maximum extension just before initial contact

Figure 2.25: Sequence of the typical gait cycle (Typical motion ranges of hip, 2011).

2.12.8 Motion of the Hip

The hip joint motion during gait is tri-axial: flexion-extension occurs about a mediolateral axis in the sagittal plane; adduction-abduction occurs about an anteroposterior axis in the frontal (coronal) plane; and internal-external rotation occurs about a longitudinal axis in the transverse plane as shown in Figure 2.26. However, as people age, the range of motion becomes limited. Murray in his study observed older men had shorter strides and a decreased range of hip flexion and extension. Johnson and Schmidt studied the range of motion during common daily activities and concluded that at least 120° hip flexion and at least 20° of abduction and external rotation were required to do routine activities without any hindrance (Typical motion ranges of hip, 2011).

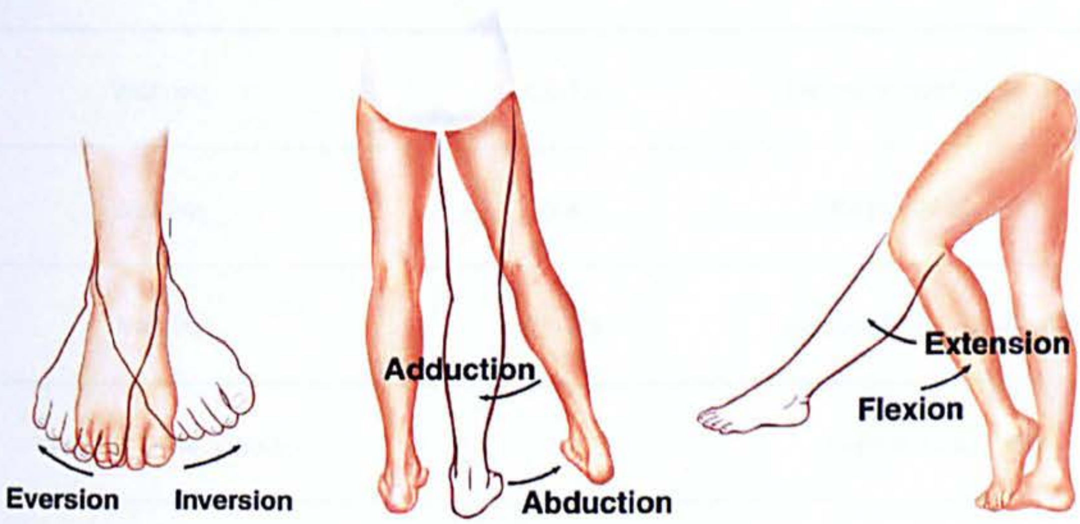

Figure 2.26: Typical motion ranges of the hip joint (Typical motion ranges of hip, 2011).

2.12.9 Range of Forces on Hip Joints during Routine Activities

Studies have shown that substantial forces act on joints during routine activities. Table 2.5 show range of typical peak forces on the hip during routine activities. The peak resultant forces for patients with prosthesis during gait ranged from 1.8 to 4.36 times the body.

Table 2.5: Typical peak forces on the hip joint due to routine activities (BW = body weight).

RANGE OF TYPICAL REPORTED PEAK JOINT FORCES FOR SELECTED STUDIES		
ACTIVITY	**REPORTED PEAK FORCE (BW)**	**REFERENCE**
Walking Ascending Stairs Descending Stairs	2.7-4.3 3.4-5.5 3.9-5.1	Bergmann et al., 1993, 1995
Walking	1.8-3.3	Rydell, 1966
Walking	4.9-7.0	Paul, 1967
Walking	4.5-7.5	Crowninshield et al., 1978
Walking	5.0-8.0	Rohrle et al., 1978
Walking	2.2-2.8	van den Bogert et al., 1999
Walking Slow Speed	2.7	English et al., 1979
Walking Normal to Fast Speeds Stair Climbing	2.7-3.6 2.6	Kotzar et al., 1991
Walking Slow Speed (Crutches) Ascending Stairs	2.6 2.6	Davy et al, 1988

2.13 Introduction to Fracture Mechanics

Broken bones, cracked engine blocks, broken pottery utensils, or damaged aircraft components; the problem of fractures has dogged society ever since humans began making things. Although there has never been a more technological age than now, there has not been any diminishing of the total numbers of fractures, and variations of the fracture. This study concentrates on just one, however, but a particularly troublesome fracture for many people who are at risk the longer they live.

A reason why the problem of fractures might well be worse today is because more can go wrong in our complex tech society. It has been found that most structural failures occur through the fracture. In that case, fracture failure is known as one of the main failure modes which are caused by:

I. Fault of negligence at the stage of design, construction, or in its operation.

II. The application of a new design or material that reacts unexpectedly and undesirably.

Human error is seen as the cause of the first type of failure and includes the possibilities of ignorance or wilful misconduct. It might happen through poor workmanship, or through the use of inappropriate or substandard materials. A likely cause can follow when there have been errors in stress analysis, where the correct technology is available but was not applied. The second cause is when new designs, are employed before they have been tested rigorously. Fracture mechanics, broadly speaking, is the area of solid mechanics that deals with the mechanical behaviour of products that do fracture.

The expert in the field is C. E. Inglis, who in 1913 published the results of stress analysis for an elliptical hole in an infinite linear elastic plate loaded at its outer boundaries. By making the minor axis very much less than the major, a crack like discontinuity was modelled (see Figure 2.27).

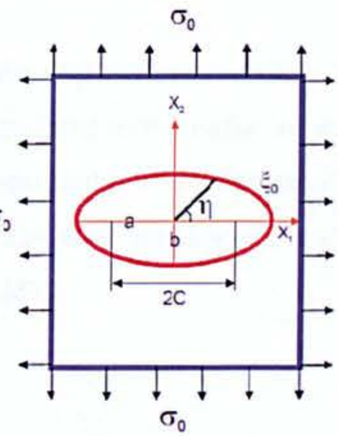

Figure 2.27: Through-thickness crack in an infinite plate loaded in biaxial tension (Mirzaei, 2011).

The complete solution of the above problem can be found in the Elasticity textbooks. Extremism of the stresses can be shown as follow:

$$(\sigma_\eta)^{max}_{\eta=0,\pi} = 2\sigma_0 \frac{a}{b} \tag{2-1}$$

$$(\sigma_\eta)^{min}_{\eta=\frac{\pi}{2},\frac{3\pi}{2}} = 2\sigma_0 \frac{a}{b} \tag{2-2}$$

The above equations show that as b→0 (the ellipse becomes a crack) a stress singularity develops at the crack tip. The effects of scratches and flaws on aircraft engine components were investigated by A. A. Griffith, who transformed the Inglis analysis by calculating the effect of the crack on the strain energy stored in an infinite cracked plate. This energy, which is a finite quantity, should be taken as a measure of the tendency of the crack to propagate, Griffith reported. He tested cracked glass spheres and his results revealed that the simple elastic analysis could be used to describe the propagation of different sized cracks at different stress levels.

After the Second World War, a fracture mechanics research group at the Naval Research Laboratory in the US, led by G.R. Irwin, who was considered to be the pioneer of modern fracture mechanics, analysed the findings of Inglis, Griffith, and others. Irwin discovered that the instruments needed to analyse fractures were readily available. His first major contribution was to extend the Griffith approach to metals by including energy dissipated by local plastic flow.

He developed the energy release rate concept in 1956. This was closely related to the Griffith theory though in a form considered more useful for solving engineering problems. He used an approach developed by Westergard to show that the stresses and displacements near a crack tip could be described by a parameter, later known as the stress intensity factor, related to energy release rate (see Figure 2.28).

$$G = -\frac{d\Pi}{dA} \geq R \tag{2-3}$$

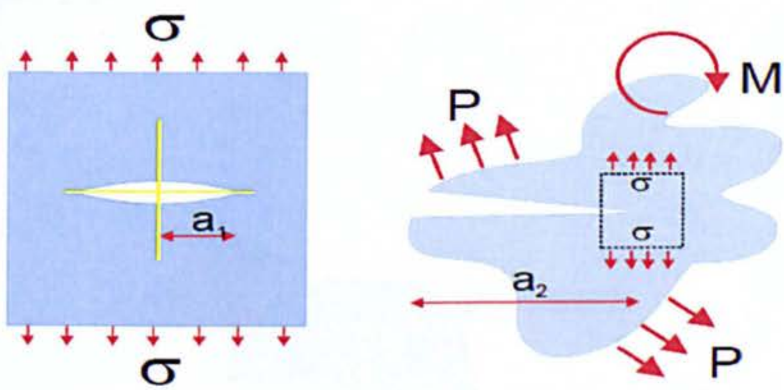

Figure 2.28: Elliptical hole in a flat plate (Mirzaei, 2011).

$$\begin{bmatrix} \sigma_x \\ \sigma_y \\ \tau_{x.y} \end{bmatrix} = \mathrm{K_c} \frac{\cos\frac{\theta}{2}}{\sqrt{2\pi r}} \begin{bmatrix} 1 & -\sin\frac{\theta}{2} & \sin 3\frac{\theta}{2} \\ 1 & +\sin\frac{\theta}{2} & \sin 3\frac{\theta}{2} \\ & \sin\frac{\theta}{2} & \cos 3\frac{\theta}{2} \end{bmatrix} + \text{negligible higher order terms; } \mathrm{K_0} = \sigma\sqrt{\pi a} \tag{2-4}$$

In practice, all this work was largely ignored by engineers as it seemed too mathematical and it was only in the 1970's that fracture mechanics came to be accepted as a useful and even essential tool.

2.14 Elasto-Plastic Fracture Mechanics

In the regime where the global stress-strain response of the body is linear and elastic (LEFM), the elastic energy release rate, G, and the stress intensity factor K can be used for characterizing cracks in structures. In the elastic-plastic region (EPFM) also called yielding fracture mechanics (YFM), the fracture characterizing parameters are the J-integral and the crack-tip-opening displacement, CTOD. The J contour integral is extensively used in fracture mechanics, as both the energy and the stress based criteria, for determining the onset of crack growth. The original form of the J-Integral for a line contour surrounding the crack tip can be written as (see Figure. 2.29):

$$J = \int_{\Gamma} \left(w dy - T_i \frac{\partial u_i}{\partial x} \right) ds \tag{2-5}$$

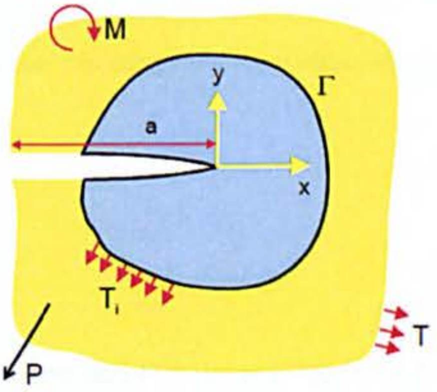

Figure 2.29: In cases where fracture is accompanied by substantial plastic deformation, an alternative description of the crack tip state has been established, designated the "crack-tip-opening displacement (CTOD) approach". This idea is based on the experimental finding that cracks tend to open up under load, as shown below in the magnified view. The basis of the CTOD approach is that forward propagation of the crack, as shown in the right figure, should only occur when the CTOD reaches a specific value which is characteristic of the material (Mirzaei, 2011).

2.15 Linear Elastic Fracture Mechanics (LEFM)

Fracture is the separation of a component into, at least, two parts. This separation can also occur locally due to formation and growth of cracks. Let us investigate the force required for such a separation in a very basic way. A material fractures when sufficient stress and work are applied on the atomic level to break the bonds that hold atoms together.

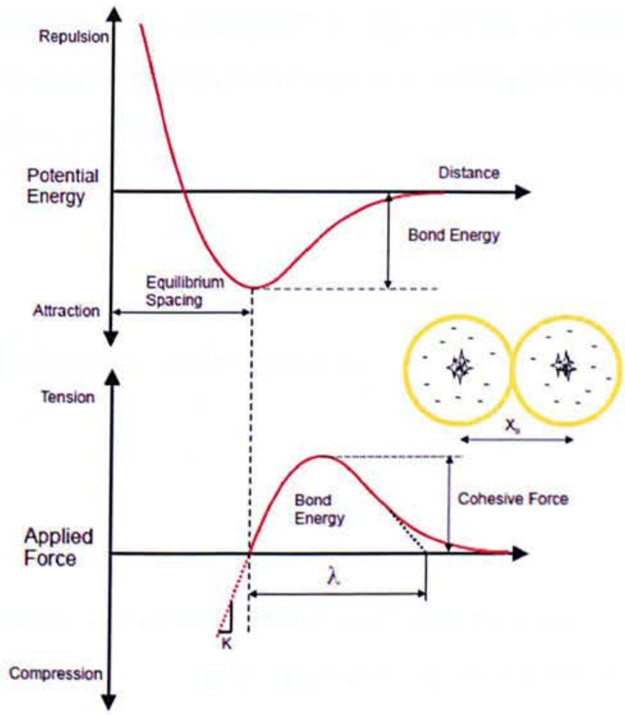

Figure 2.30: A schematic plot of the potential energy and force versus separation distance between atoms (Mirzaei, 2011).

The bond energy is given by:

$$E_b = \int_{x_0}^{\infty} P dx \tag{2-6}$$

Where x_0 is the equilibrium spacing and P is the applied force (see Figure 2.30). A reasonable estimate of the cohesive strength at the atomic level can be obtained by idealizing the inter-atomic force-displacement relationship as one half the period of a sine wave, so we may write:

$$P = P_c \sin\left(\frac{\pi x}{\lambda}\right) \tag{2-7}$$

where λ is defined in Figure 2.30. For small displacements, we may consider further simplification by assuming:

$$K = \frac{P_c \pi}{\lambda} \tag{2-8}$$

If both sides of this equation are multiplied by the number of bonds per unit area and the equilibrium spacing x_0 (gauge length), then k can be converted to Young's modulus E and P to the cohesive stress σ_c gives:

$$\sigma_c = \frac{E\lambda}{\pi x_0} \tag{2-9}$$

Assuming $\lambda \approx x_0$, Equation (2-5) can be written as:

$$\sigma_c \approx \frac{E}{\pi} \tag{2-10}$$

The reason behind the above huge discrepancy is the existence of numerous defects in ordinary materials. These defects can be quite diverse by nature. Starting from the atomic scale, they may include point defects (for example vacancies: atoms missing), line defects, extra atomic planes (dislocations). On the microstructural level we may consider defects due to grain boundaries, porosity, etc. Some of these defects may also evolve during the processes of deformation and fracture. For instance, plastic deformation involves various movements of dislocations which may interact and eventually result in local damages. Plastic deformation may also lead to the formation of microvoids which may coalesce and evolve to microcracks.

On the other hand, the term fracture mechanics has a special meaning: description of fractures which occur by propagation of an existing sharp crack. Hence, the assumption of a pre existing crack is essential in fracture mechanics. It is evident that numerous microscopic defects and/or microcracks naturally exist in ordinary materials. However, the scope of Engineering Fracture Mechanics is almost entirely concerned with macrocracks which are either present in the components (as a result of manufacturing processes like welding) or develop during the service by various failure mechanisms such as fatigue or creep. The crack propagation can occur in many ways. For instance we may have fast-unstable and slow-stable crack growth under monotonic loading, or a cycle by cycle growth under alternating loads. In general, the resistance to crack growth can be defined by a special term called the toughness of the material.

2.16 Ductile Versus Brittle

By definition, ductile fracture is always accompanied by a significant amount of plastic deformation, while brittle fracture is characterized by very little plastic deformation. Both types of fracture have distinctive features on macro and micro levels (see Figure 2.31).

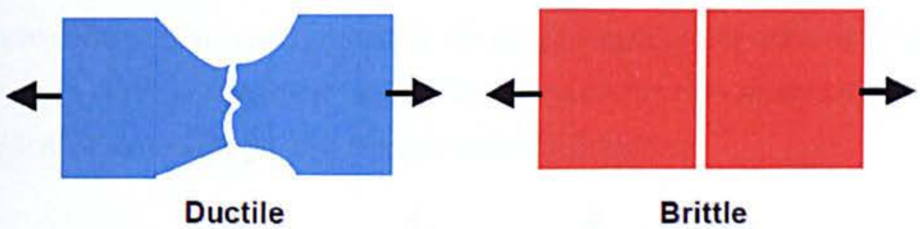

Figure 2.31: The Ductile and Brittle fracture (Mirzaei, 2011).

To a large extent, ductility and brittleness depend on the intrinsic characteristics ofb materials such as chemical composition and microstructure. Nevertheless, extrinsic parameters like temperature, state of stress, and loading rate may also have substantial influences on the fracture properties of materials. In general, materials show brittleness at low temperatures, high strain rates, and triaxial state of tensile stress. Let us consider the deformation and fracture mechanisms of a ductile material subject to a simple tension test during which several strength levels can be defined. As Figure 2.32 shows, the first level is the proportional limit, below which there is a linear relationship between the stress and strain (point A).

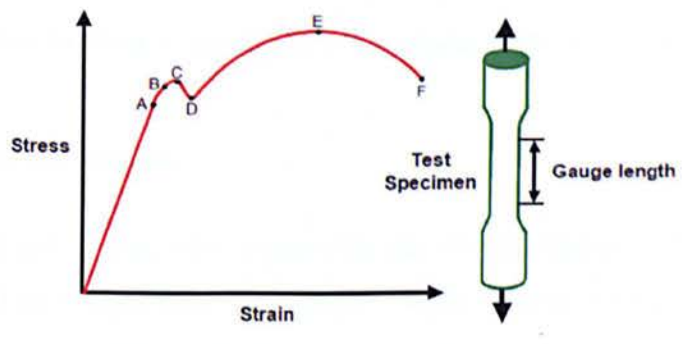

Figure 2.32: Fracture mechanisms of a ductile material subject to a simple tension test (Mirzaei, 2011).

The second one is the elastic limit which defines the stress level below which the deformation is totally reversible (point B). The third level is the yield strength which marks the beginning of irreversible plastic deformation (point C). Some materials show a clear yield point and also a lower yield point like point D. For others the yield strength is a point that is difficult to define and, in practice, it is defined as the intersection of the σ-ε curve and a line parallel to the elastic portion of the curve but offset from the origin by 0.2% strain.

Beyond this point and up to the next level, which is the ultimate tensile strength (point E), the plastic deformation is uniform along the gauge length of the specimen. The inflection point in the σ - ε curve is due to the onset of localized plastic flow or necking as depicted in the Fig. 2.33(A). Finally, the point F represents the final fracture.

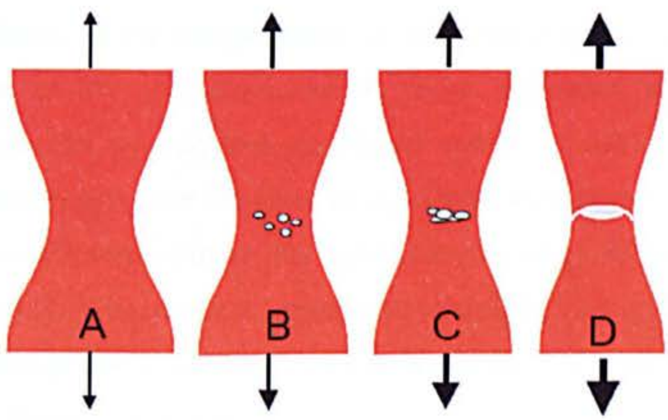

Figure 2.33: Steps of fracture in ductile material (Mirzaei, 2011).

The occurrence of necking results in a tri-axial state of stress. Accordingly the plastic deformation becomes more difficult and small particles within the microstructure start to fracture or separate from the matrix causing micro voids, as depicted in Figure 2.33 (B).

2.17 Fixed Displacement Condition

In continuation of our discussions concerning the energy approach, we will investigate the behaviour of cracked components under two distinct loading conditions. First, suppose that we have stretched a cracked component by the amount Δ and have constrained it as depicted in Figure 2.34.

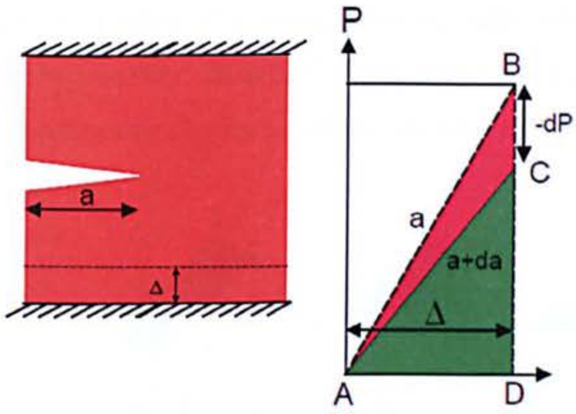

Figure 2.34: The cracked component in the Fixed Displacement Condition (Mirzaei, 2011).

The amount of elastic strain energy stored in the component is equal to the triangle ABD, and the slope of the load-displacement curve represents the stiffness of the component. Let us initially assume that the stored energy is sufficient to maintain an incremental crack growth (da) under the fixed displacement condition. Since the component with a longer crack has a lower stiffness, the stored elastic energy decreases to a new level equal to the triangle ACD. Since there is no externally applied load in the system, the total potential energy is equal to the strain energy (the only source to provide the required energy for the crack growth). Hence, we may write:

$$(V = 0), (\prod = U), U = \int_0^{\Delta} P d\Delta = \frac{P\Delta}{2} \tag{2-11}$$

$$G = -\frac{1}{B}\left(\frac{dU}{da}\right)_{\Delta} = -\frac{\Delta}{2B}\left(\frac{dP}{da}\right)_{\Delta} \tag{2-12}$$

In practice, however, crack growth may occur in very complicated stress fields. In general, we consider three basic modes for crack growth, although mixed-mode growth is also possible (see Figure 2.35). Mode I is the opening or tensile mode where the crack faces separate symmetrically with respect to the x_1-x_2 and x_1-x_3 planes. In Mode II, the sliding or in plane shearing mode, the crack faces slide relative to each other symmetrically about the x_1-x_2 plane but anti-symmetrically with respect to the x_1-x_3 plane. In the tearing or anti plane mode, Mode III, the crack faces also slide relative to each other but ant symmetrically with respect to the x_1-x_2 and x_1-x_3 planes. The energy release rates related to these modes are termed GI, GII, and GIII respectively. In mixed mode problems we simply add the energy release rates of different contributing modes to obtain the total energy release rate.

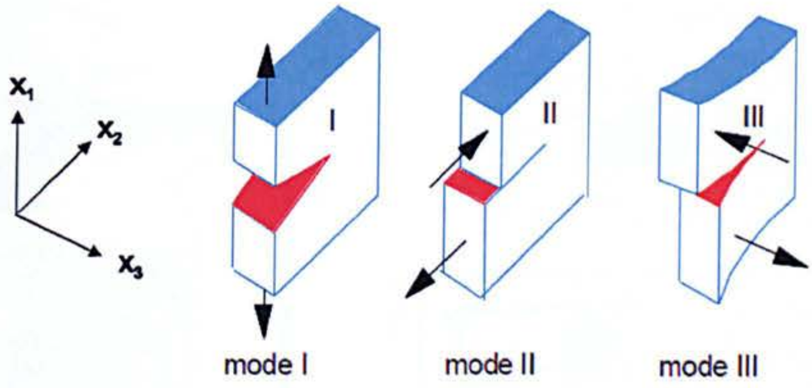

Figure 2.35: Three basic loading modes for a cracked body: Mode I, opening mode; Mode II, sliding mode and Mode III, tearing mode (Mirzaei, 2011).

2.18 Fracture Mechanics in Bone

Bones establish the skeleton of the body and enable the body to function, shift and operate as well as supporting the body against the gravity. Moreover, some body parts are shielded by bones and the production centre for blood products is known to be bone marrow. The reservoir of calcium in body is bone and upon the influence of hormones the calcium reservoir is always undergoing change, therefore, results in bone not to be a stagnant organ. The level of blood calcium is increased by parathyroid hormone through leeching calcium from bone, whereas the opposite effect is seen by calcitonin hormone which causes bone to accept calcium from the blood.

Bone fracture is a complex phenomenon that may be understood from the perspective of the multi-dimensional hierarchical nature of the bone-matrix structure. Resistance to such bone fracture, which is characterized macroscopically by such parameters as the work-of-fracture and the fracture toughness, evolves from a suite of physical structure-related mechanisms that act at multiple length-scales ranging from nano- to near macro-scale dimensions (shown in Figure 2.36). These mechanisms can be classified as "plasticity" mechanisms, that operate principally at sub-micrometer dimensions to promote intrinsic toughness (i.e., molecular uncoiling of collagen molecules, fibrillar sliding of both mineralized collagen fibrils and individual collagen fibers, and microcracking), and crack-tip shielding mechanisms, that operate at length-scales of w1e100 mm to promote extrinsic crack-growth toughness (i.e., crack deflection/twist and crack bridging).

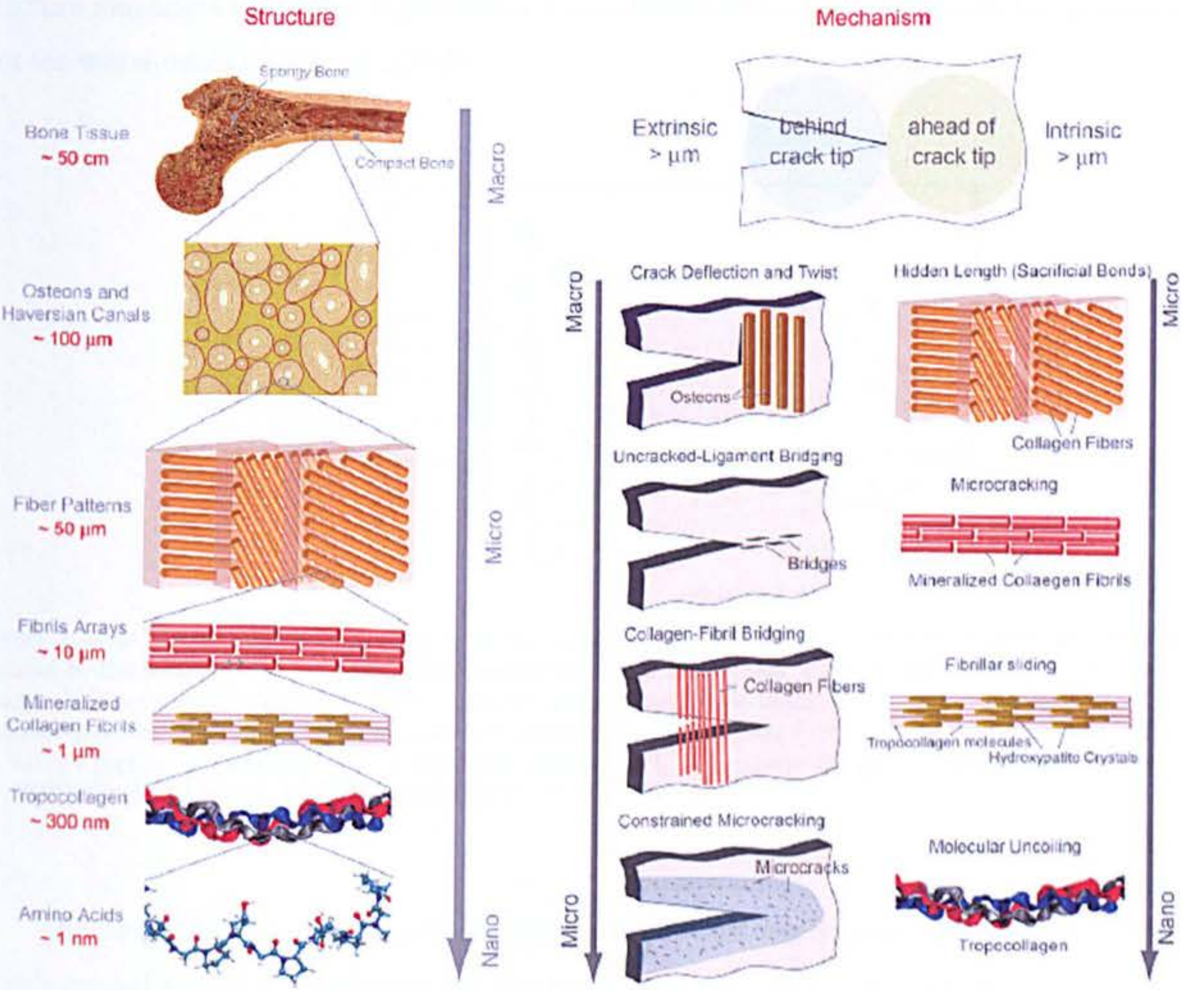

Figure 2.36: The structure of bone showing the seven levels of hierarchy with the prevailing toughening mechanisms (Launey *et al.*, 2010; Ritchie *et al.*, 2009).

A central factor of the latter toughening mechanisms is the specific nature of the crack path which is controlled by the applied forces and the nature of the bone-matrix microstructure, in particular the hyper-mineralized interfaces of the osteons (cement lines) (see Figuer 2.37 a), which provide microstructurally "weak", and hence preferred, paths for cracking. As the osteons are aligned nominally along the long axis of the bone, this is the basis of the marked anisotropy in the fracture properties of bone, in that bone is easier to split than to break (Nalla *et al.*, 2003; Yeni and Fyhrie, 2003) and that the transverse toughness is lower in shear than in tension (Nalla *et al.*, 2005; Zimmermann *et al.*, 2009). Fracture mechanics measurements afford the most appropriate methodology to characterize the toughness of bone by providing a quantitative measure of its fracture resistance. Recent studies have shown that for human cortical bone in the transverse (breaking) orientation, the fracture toughness in shear is significantly lower than in tension, i.e., the mode I toughness is not the worst-case (see Figuer 2.37 b).

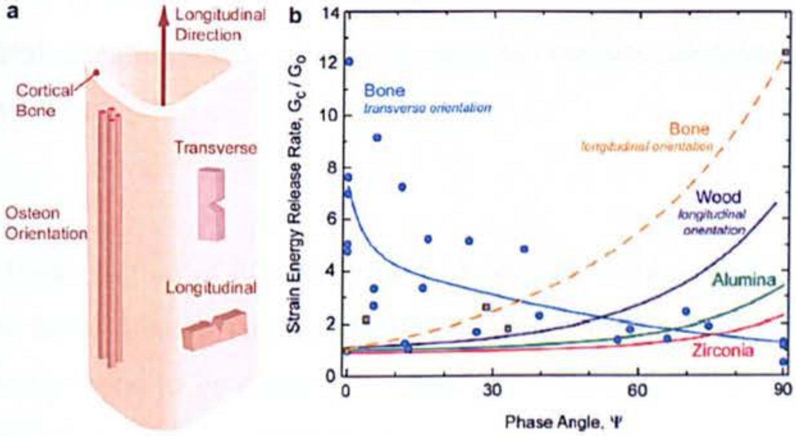

Figure 2.37: a) A schematic of the cortical bone in a human femur. The secondary osteons are generally oriented parallel to the long axis of the bone, while the cement lines are located at the boundaries of the secondary osteons b) The critical strain-energy release rate, i.e., toughness, of bone under mixed-mode conditions, is highly dependent on the orientation. In the transverse orientation (L-R), bone has a higher toughness in tension (mode I), while a preliminary analysis of the longitudinal orientation (C-L) suggests an opposite trend (Zimmermann *et al.*, 2009; Singh and Shetty, 1989 and Norman *et al.*, 1996).

Since fractures are unpleasant debilitating events, the mechanical performance of bone play a crucial role in the quality of life that we experience. Some types of fractures are quite clearly caused by the fact that bone is exposed to loads that surmount certain threshold levels (with regard to stress or damage), which can also be protracted (creep), or persistent (fatigue). Other types of fractures are due to structural compromise of the bone such as disease, surgical intervention, poor diet, ageing, lack of exercise, pharmaceutical treatments, and etc. In all conditions it can be postulated that by implementing either material/engineering principles to demonstrate the influences of overload, or structure/function correlations to encounter with the consequences of a materially and structurally compromised tissue (Rho *et al.*, 1998).

2.19 Femur Fracture: The Clinical Aspects

The longest and strongest bone in the human body which is able to bear an enormous magnitude of compressive load before fracture is the femur. The downside of a material property such as that is that, potentially life threatening injuries could occur in the case of a traumatic event (American Academy of Orthopaedic Surgeons, 2013). Also an injured femur can cause a disruption to the blood flow to the thigh muscle (quadriceps, hamstrings) and also will result in excessive bruising and blood loss (American Academy of Orthopaedic Surgeons, 2013). It is essential that patients who suffer from femur fracture are required immediate medical attention. Bone disease or physical impacts are usually the cause for femur fractures to occur.

2.19.1 Bone Disease

The risk of bone fracture of bone fracture is drastically increased by Osteoporosis and occurs when the bone mineral density (BMD) decreases to the level which causes the microstructure of the bone to be disrupted. (American Academy of Orthopaedic Surgeons, 2013) There are 6 major causes to osteoporosis:

1. Aging - All men and women have some risk of developing osteoporosis as they become older, particularly over the age of 60. Women who have had their menopause before the age of 45 are likely to also suffer from osteoporosis (Patient, 2013).

2. Heredity - Have a strong family history of osteoporosis (that is, a mother, father, sister or brother affected) (Patient, 2013).

3. Nutrition/lifestyle – lack of calcium and or vitamin D due to poor diet and exercise. Having an alcohol intake of more than four units per day and smoking (Patient, 2013).

4. Medical conditions. An overactive thyroid, coeliac disease, Cushing's syndrome, Crohn's disease, chronic kidney failure, rheumatoid arthritis, chronic liver disease, type 1 diabetes or any condition that causes poor mobility (Patient, 2013).

5. Physical impact – this could be from a quick fall or heavy impact during sports activities. Both healthy adults and children can suffer from this.

6. Motor vehicle accident – these accidents have a high source of traumatic energy when they occur which can cause serious injuries to the bone. There are specific fracture patterns which are related to a specific type of vehicle impact; the most common fracture is to the femoral head (Sanders, 2008).

2.19.2 Symptoms

Symptoms can include severe pain, inability to move the leg, deformity and swelling. A fractured femur will result in the thigh to become shorter than a healthy one due to the thigh muscles forcing the broken edges of the femur out of alignment (American Academy of Orthopaedic Surgeons, 2013).

A simple fall to the ground which has a small amount of force can cause the femur bone to fracture (Patient, 2013). This is classed as a symptom of osteoporosis because a simple fall will not harm or affect a person who doesn't have osteoporosis in the hip.

2.19.3 Biomechanical Aspects of Femur Fractures

The study of hip fracture requires an understanding of biomechanics of hip fracture, including the mechanism of fracture, the characteristics of falls, load distributions in the femur, the contribution of cortical and trabecular bone to the strength of the femoral neck, fracture initiation and previous biomechanical research. Figure 2.38, shows the loading on the femur during gait is much different than that seen in fall. The diagram is a simplification of the stress in the femoral neck as it only shows the force applied to the femur from pelvis.

These fractures usually occur due to high or low impact in patients who suffer from osteoporosis. Osteoporosis patients who already have orthopaedic implants such as hip joints are highly likely to fracture their femur compared to the average person (Lochmüller *et al.*, 2002, Turner & Burr 2001). There are three categories of femur fractures which are proximal femur fractures, femoral shaft fractures and distal femur fractures.

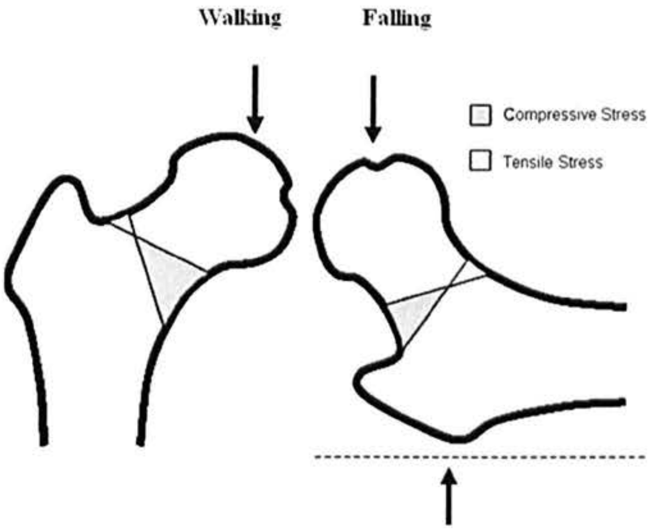

Figure 2.38: The direction of load applied to proximal femur from acetabulum and general stress distribution through the cross section of neck (Turner, 2005).

2.19.3.1 Proximal Femur Fracture

Hip fractures (proximal femoral fractures) commonly occur from a fall or from a direct blow to the side of the hip. Hip fractures are more common in older people, often in 80-year-olds, and happen four times more often to women. The UK treats about 75,000 hip fractures annually and the numbers are increasing. The Proximal femur fracture occurs closest to the upper portion of the femur which is closest to the hip. This fracture usually comes with a hip fracture or a hip joint failure which is common in elderly patients who suffer from osteoporosis (Sanders, 2008). There are three main types of proximal femur fractures:

1- Femoral neck fracture
2- Intertrochanteric femur fracture
3- Subchanteric femur fracture

The femoral neck fracture occurs when the ball of the hip joint (femoral head) is fractured off the femur.

1- Subcapital neck fracture – below the head of the neck region is where this type of neck fracture usually occurs. This is generally caused by a sharp reduction in cross – cross sectional area which acts as a stress rise in the bone (see Figure 2.39a) (Sanders, 2008).

2- Transcervical neck fracture – this stress usually occurs in the middle of the neck of the femur bone. This is where the cross sectional area is at its lowest however results in high mechanical stresses (see Figure 2.39b) (Sanders, 2008).

3- Basicervical neck fracture – this neck fracture usually happens at the base of the neck of the bone, the hair line crack runs along a line joining the top of the greater trochanter to the top of the lesser trochanter (see Figure 2.39c) (Sanders, 2008).

The intertrochanteric fracture occurs where the fracture line runs the greater and lesser trochanter. The subtrochanteric fracture extends below the femoral shaft, sometimes it can also occur below the lesser trochanter (see Figure 2.39d) (Sanders, 2008).

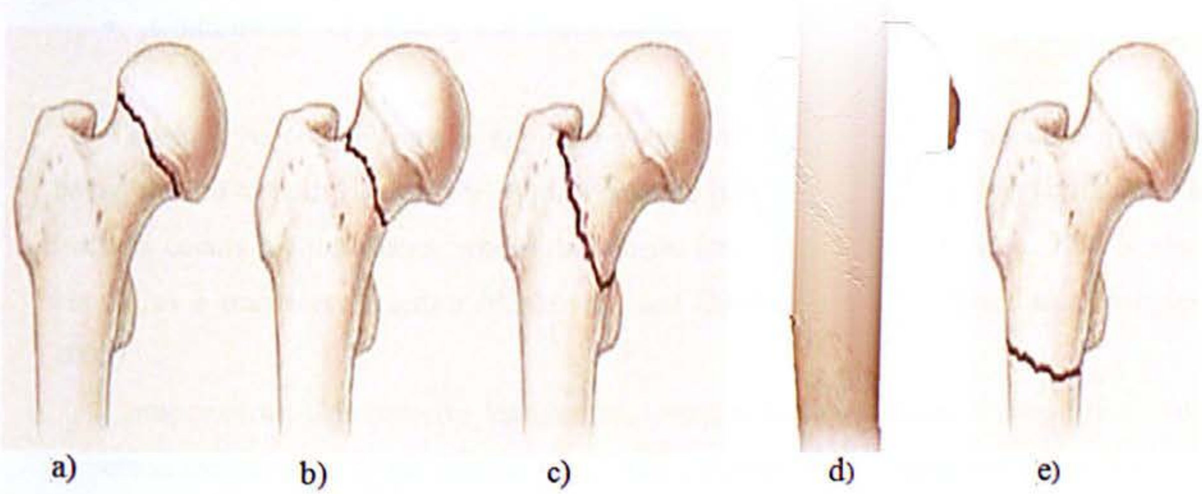

Figure 2.39: Four types of proximal femur fractures: a) subcapital neck fracture, b) transcervical neck fracture, c) basicervical neck fracture, d) intertrochanteric fracture, e) subtrochanteric fracture (Georgetown University Medical Center, 2011).

2.19.3.2 Femoral Shaft Fracture

Femoral fractures occur due to high energy impact or incorrectly fitted orthopaedic implants which increase the stress carried by the femur (Sanders, 2008). If the femur bone is considered just as a cylindrical shaft (a bone structure on its own) loading fracture can be analysed. There are five types of loading modes that cause fracture on the shaft of the bone (Cullinance and Einhorn, 2002):

- Tension
- Compression
- Torsion
- Bending
- Combination of bending and compression

Tension: As tensile force is applied on the shaft, assuming equal amount of forces being applied to both sides of the shaft, a fracture pattern can be seen in the middle. The fracture occurs on the planes where the tensile stresses are at their peak. This is also known as a transverse fracture (Pankovich and Davenport, 2006; Carter and Spengler 2002).

Compression: Compressive loading can result in a slope/slanting fracture line with respect to the direction of the applied load. Along planes of high shear stress is where the compressive force can produce a fracture (Pankovich and Davenport, 2006; Carter and Spengler 2002).

Torsional: Torsional forces usually result in a continuous spiral like fracture across the shaft of the bone. This type of fracture is also known as an oblique spiral fracture (Pankovich and Davenport, 2006; Carter and Spengler 2002).

Bending: The bending forces are where half of the femur bone goes into tension and the other half goes into compression. As seen is Figure 2.40, the fracture pattern appears to be that of tensile and compression forces (Pankovich and Davenport, 2006; Carter and Spengler 2002).

Combination of bending and compression: As illustrated in Figure 2.40 the pattern has two oblique fractures at the end along with a fracture in the middle of the bone. This type of fracture is also known the butterfly fracture. As the compressive force increases, the butterfly fragment will consist of more than just one piece (Pankovich and Davenport, 2006; Carter and Spengler 2002).

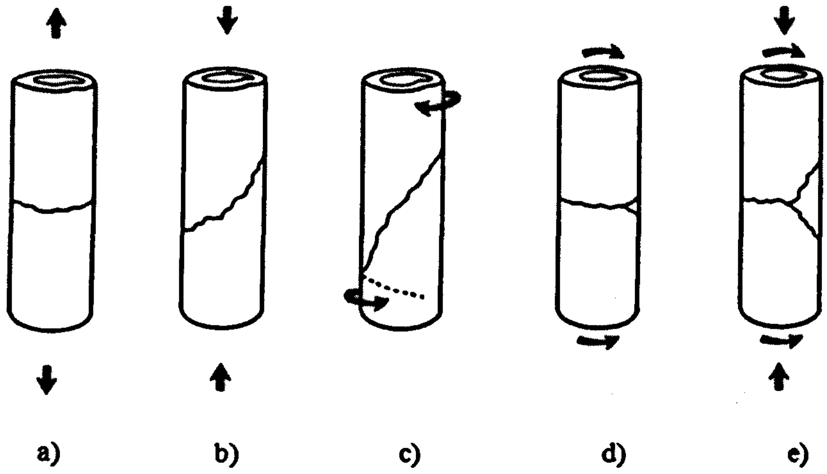

Figure 2.40: Five modes of force that fracture femoral shaft: a) tensile force, b) compressive force, c) torsional force, d) bending force and e) combination of bending and compressive forces (Thakur, 2007).

2.19.3.3 Distal Femur Fracture

Distal femur fractures occur within the distal (bottom) 15cm of the femur. Distal fractures are generally caused by either high-energy trauma or low-energy injuries for patients with osteoporosis. These types of fractures most commonly occur in patients with ill-fitting total knee prostheses (see Figure 2.41). On the other hand, high-energy trauma can be transmitted to the flexed knee and will create fractures at the distal femur. The distal femur fractures are mainly divided into four categories: Supracondylar fracture, inter condylar fracture, condylar fracture and distal femoral epiphyseal fracture (Sanders, 2008).

- **Supracondylar fracture:** The fracture breaks off the distal femur from the rest of the femur in a transverse direction. Supracondylar fractures occur on the plane normal to the axis of the femur around the edges of the epiphysis where the stresses are concentrated due to the change in cross-sectional area.
- **Inter condylar fracture:** The inter condylar fracture runs between the lateral condyle and the medial condyle. This fracture segments the femur into at least three parts if not more depending on the severity of the event of injury.

- **Condylar fracture:** The condylar fracture produces an oblique fracture pattern across the epiphysis. This results in a femur with one of the condyles intact and an oblique fracture of the other condyle. The distal femoral epiphyseal fracture occurs across the epiphysis.

- **Distal femoral:** The distal femoral epiphyseal fracture occurs across the epiphysis. In other words, parts of epiphysis are intact with the femoral shaft while the rest of the epiphysis is fractured in a transverse direction with respect to the axis of the femur.

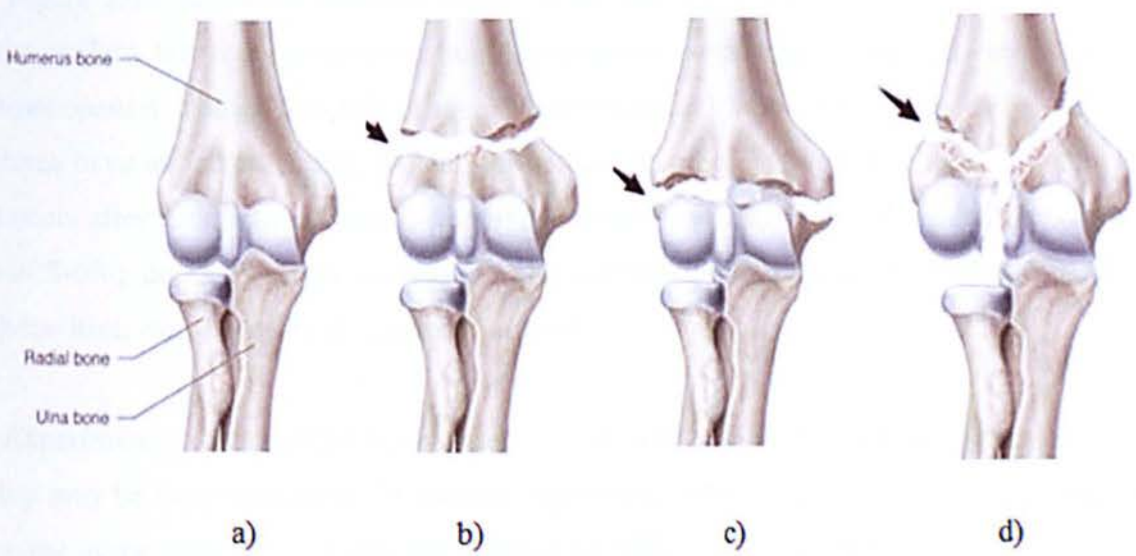

Figure 2.41: Four types of distal femur fractures: a) supracondylar fracture, b) inter condylar fracture, c) condylar fracture and d) distal femoral epiphyseal fracture (Sanders, 2008).

2.19.4 What Causes a Hip Fracture and How Diagnosis the Hip Fracture?

Osteoporosis, cancer, or stress injuries can weaken the bone and make the hip more susceptible to breaking. In severe cases, the hip can fracture simply through the act of standing and making a slight twist. The pain associated with the injury will be concentrated in the outer upper thigh or groin. The diagnosis of a hip fracture is generally made by X-ray. However, in some instances an incomplete fracture may not be seen on a regular X-ray.

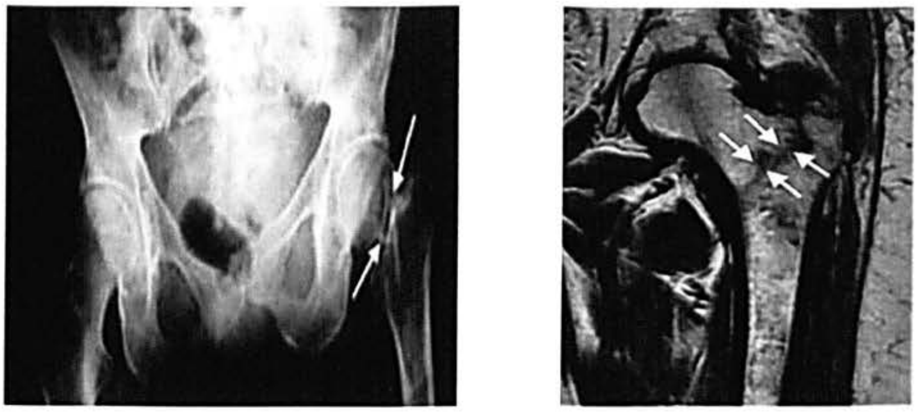

a) b)

Figure 2.42: Shows a) the X-ray image of the hip and femur and b) the MRI scan of the hip and femur (David *et al.*, 2012).

Figure 2.42 shows the different image of the hip and femur in X –ray and MRI scan. Statistics show that it is age-specific, but the population percentage is not high - about 14% in postmenopausal women and 6% in men. Postmenopausal women suffering earlier non-hip fractures have an increased risk of later hip fracture and the relative risk is highest within the first years after the fracture. Patients in nursing homes have a high risk of hip fracture (annual rate of 5-6%), and they might suffer one and a half falls per person per year. The strength of the bone itself may not offer the greatest protection.

Experiments which carried out by Melton et al, 1992, show that the soft tissue covering the hip may be more protective. In another experiment, external hip protectors were tested in a nursing home study and the rate was reduced by 50%. The review found that the essentials in the development of hip fracture are, risk of fall, type of fall, type of impact, energy absorption, and bone strength. Risk estimation and prevention of hip fracture may prove realistic when these issues are taken into consideration. An estimate of the total hip fractures globally twenty years ago was 1.7 million. The world's ageing population is likely to take this total to 6.3 million by 2050 (Cooper *et al.*, 1992).

The resources needed for patients with hip fracture equal about 17% of hospital orthopaedic surgery beds. Every fifth patient will be referred to a nursing home (Jensen *et al.*, 1980). As Figure 2.43 shows age has a most significant part in the injury. About 80% of hip fractures occur in the women older than 70 years old while in men 50%. Melton et al, 1992 estimate the lifetime risk for people of 50 to be 17.5% for women and 6% for men. A 60-year-oldwoman with a life expectancy of 81 years has an estimated lifetime risk of hip fracture of 14%. A man of 60 with a life expectancy of 77 years has an estimated risk of hip fracture of 6% (Melton *et al.*, 1992).

The fatty covering of the hip that offers significant protection against hip fracture was found by Lauritzenet et al, 1993 (see Figure 2.43). Women who experienced hip fracture had an average 22 mm of subcutaneous tissue compared with 32 mm in healthy women who had not suffered hip fractures. The investigation found that the thickness of the soft tissue was related to body weight (BW) and BMI, but no relation was found to height and age, except for women with hip fracture, among whom age and soft tissue thickness correlated negatively (Lauritzen *et al.*, 1993).

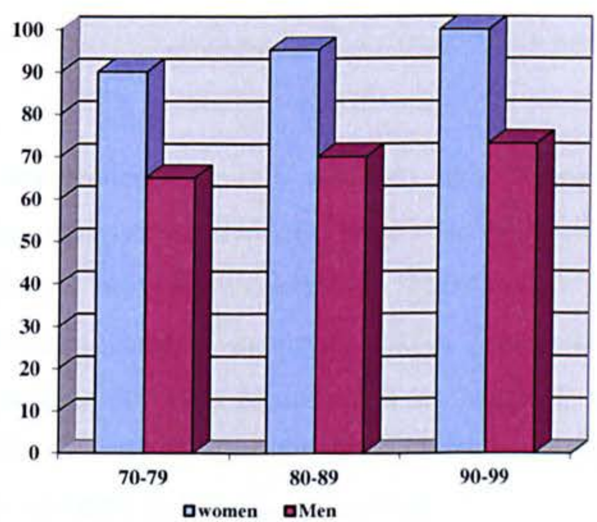

Figure 2.43: The annual age-specific rate of fallers in women and men in nursing homes (Lauritzen *et al.*, 1993).

Those having pattern-falls tend to have more functional disability, to have increased impairment of mobility, to use more aids to mobility, to be older, and to have poorer vision and lower systolic blood pressure. Three fourths of femoral neck fractures occur in the "home" and approximately two-thirds of these are due to a fall precipitated by an environmental hazard. The causes of falls among patients with hip fracture are either tripped or lost balance (57%), spontaneous (23%), or lost consciousness (20%).

Risk factors for hip fracture have been narrowed by investigating teams to one or more of these factors (Campbell *et al.*, 1981) (see Figure 2.44):

I. The faller must be orientated to impact near the hip

II. Protective responses must fail and local soft tissues must absorb less energy than necessary for prevention of fracture.

III. The residual energy of the fall applied to the proximal femur must exceed its strength.

Fall → Protective responses → Energy absorption → Bone strength → Hip fracture

Figure 2.44: The cascade of events leading to hip fracture (Cummings and Nevitt, 1989; Lauritzen *et al.*, 1993).

Other risk factors are tendency to fall, disability and immobilisation, low physical activity, use of psychotropic/anxiolytic/hypnotic drugs, use of corticosteroids, low calcium intake in the elderly, osteomalacia, thyreotoxicosis, cigarette smoking, chronic alcoholism, diabetes mellitus, insufficient sunlight exposure, and a protective effect from thiazide diuretics. Evidence is lacking for risk factors such as heredity, nutrition, and medical conditions. No information is available on the combined effects of the different risk factors. This relationship is rather complex and poorly understood.

The risk of fracture is especially increased in persons who walk with sticks or help from another person or have experienced a recent fall (Boyce and Vessey, 1988; Copper *et al.*, 1988; Grisso *et al.*, 1991) and (Stott and Gray, 1980). Many patients with a hip fracture have suffered an earlier fracture and in nursing homes many residents will share several of the aforementioned characteristics. Nutritional factors may be important, although difficult to assessable. In elderly women, it has been shown that nutritional status correlates closely with both food intake and disability. This may also explain why being overweight protects against hip fracture (Lanritzen and Lund, 1993; Morgan *et al.*, 1986). Other explanations are that a protective effect may be related to oestrone production from and the androstenedione level in fat cells in postmenopausal women or overweight status induces greater stress on the skeleton, which stimulates bone strength.

Chapter 3 - 3D Proximal Femur Model Generated from CT scan Data

3.1 Introduction Imaging Technology

Techniques that can acquire detailed anatomical information in the field of medical imaging from bone fractures are Computed Tomography (CT) and Magnetic Resonance Imaging (MRI). Hip fractures are known as common injury and it can lead to permanent disability, pneumonia, pulmonary embolism, and death.

However, the specialist who wants to use the techniques to treat fractures needs training and experience to reach the correct diagnosis. The technical problem for the doctor is that the images achieved from the techniques are not platform-independent. The images can only be accessed at the platform with the scanner attached. Specialists expect that 3D models will come from slices taken from the CT scan, once it has been analysed by a method known as Finite Element. Methods it will show the responses to be expected at various loading conditions. This will help the specialists to advise patients on important precautions to prevent possible further damage.

Integrating these important medical supporting technologies such as medical imaging, computer-aided modelling, rapid prototyping (RP) and computer aided engineering (CAE) will reduce risks, help with the cost, and be invaluable for decisions by specialists. However, CT scanning, or MRI, which shows the specialist the precise cause and region of the affected part, is stored in DICOM form. The images can be visualised for easy decoding when the proper hardware is employed. This is associated with the scanner and this puts the cost beyond many GP practice finances. Another problem that comes from such a sophisticated technology is the difficulty of not only explaining to patients exactly what the scans reveal, but for the doctor to interpret the information fully.

3.2 Imaging Technology

Various modalities which are commonly in use in medical imaging are computed tomography (CT) and magnetic resonance imaging (MRI). These methods are used to create a digital geometry. Computer processing is used to generate a three-dimensional image of the human body from a large series of two-dimensional images.

CT imaging is ideal to use for scanning when the objects have different density, depending on an absorption coefficient. However, CT imaging is not efficient at distinguishing between different soft tissues which causes poor image quality. The MRI allows excellent soft-tissue contrast, so CT and MRI are sensitive to different tissue properties. The appearance of images obtained with these two techniques differs markedly.

3.2.1 Computed Tomography

The CT software processes a large volume of data to create two-dimensional cross-sectional images of the body. Pixels in an image obtained by CT scanning are displayed in terms of relative radio density, as shown in Figure 3.1. At each sampling point within the volume, each type of scanner will measure a value relating the density of the material at that point and converting it into a pixel greyscale value. The measurement relates to the amount of X-rays absorbed by the object. Organs with different density will get different pixel values. In this way, the different organs, tissues or volumes can be defined (Forman *et al.*, 2009).

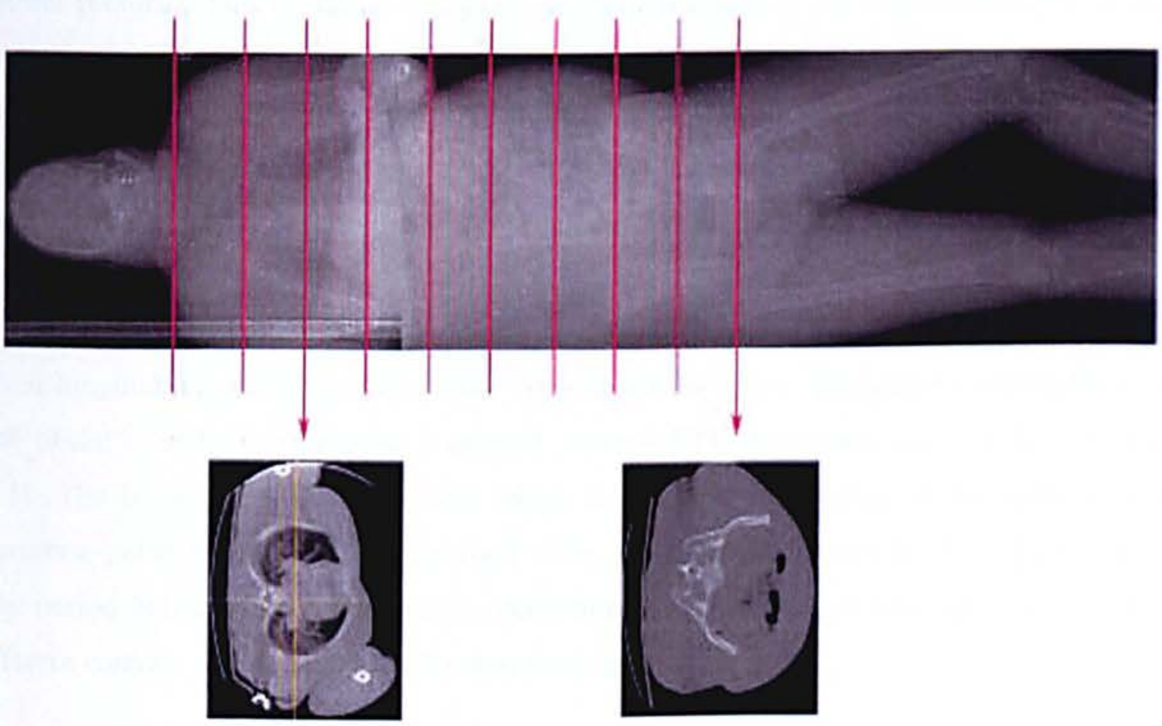

Figure 3.1: Image of CT (Forman *et al.*, 2009).

3.3 Magnetic Resonance Imaging

Magnetic resonance imaging (MRI) is known as nuclear magnetic resonance imaging, it's a test that uses magnetic field and pulses of radio wave energy to visualize internal structures of the body in details. MRI has a higher contrast on soft tissue comparing to CT and thus a very suitable candidate for distinguishing pathologic tissue, and imaging in the cardiovascular and oncological disciplines. The explanation of physics involved in MRI is beyond the matter of discussion here, however MRI makes use of the nuclear resonance of an elementary subatomic particle with an odd atomic number, such as 1H, 31P or 13C, which acts like magnetic dipoles. Under strong magnetic field, usually generated by an electromagnet in an MRI machine, the atoms start to align with the axis of the external magnetic field with a resonance frequency known as the Larmor frequency, named after a French physicist.

The Larmor equation is $\omega_0 = g \times B_0$;where ω_0 is the Larmor frequency, B_0 is the magnetic field and g is the constant gyromagnetic ratio, specific to each type of atomic nucleus mentioned above. However, only a slight majority of atoms are aligned (parallel protons) in the direction of the magnetic field and the remaining is aligned in an opposite fashion (anti-parallel protons). This creates a slight net magnetic moment in the tissues under the strong magnetic field. When a radio wave pulse exactly the same as the Larmor frequency is applied, some of the already aligned protons will be pushed out of their alignment under the original magnetic field. A receiver coil can detect a tiny but detectable change in the magnetic field when the protons relax back to their original states (Forman *et al.,* 2009).

The realignment of the nuclei relaxation after short pulse in the Larmor frequency is called longitudinal relaxation. The time required for the tissue magnetism to reach back to 63% of the value before the pulse is applied, is termed T1. A common value of T1 is 500ms to 1s. The transverse relaxation time, which is the local de-phasing of the spins after a transverse pulse, is named T2. A common value of T2 is 50ms to 100ms. By using different time period between the radios pulses, echo time and other parameters, images with very different contrast can be achieved (Forman *et al.,* 2009).

3.3.1 CT Scan vs MRI

An x-ray of the hip will be explained here to understand the difference between CT imaging and other techniques. The bone structures of the hip can be viewed using basic x-ray techniques. With magnetic resonance imaging (MRI), blood vessels and soft tissue can be viewed, but clear, complete images of bony structures cannot be obtained. On the other hand, x-ray angiography can show the blood vessels of the hip and not soft tissue. CT imaging of the hip can provide clear images not only soft tissue, but also bones and blood vessels. Figure 3.2 and 3.3 shows the different CT scan and MRI from the proximal femur fracture. CAD data implants can be imported and positioned into the image data and then Simpleware software automatically allows the multipart models to be converted into high quality meshes.

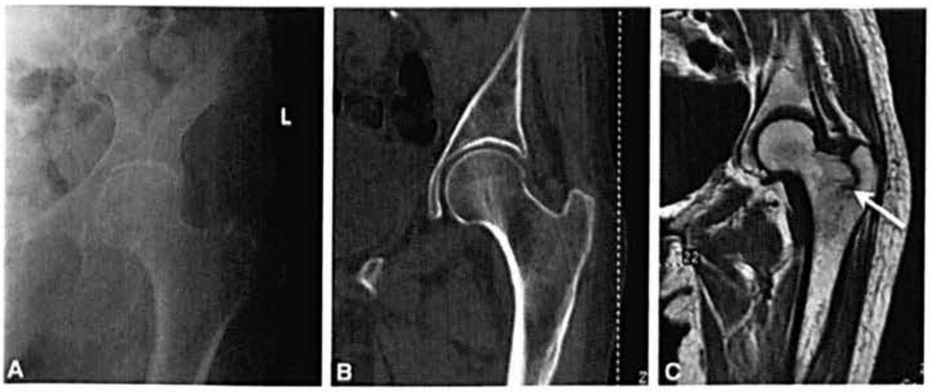

Figure 3.2: Plain films (A) and 64-slice CT scan (B) did not demonstrate the intertrochanteric fracture that was apparent on magnetic resonance imaging scan (C) of this 82-year-old woman (David *et al.*, 2012).

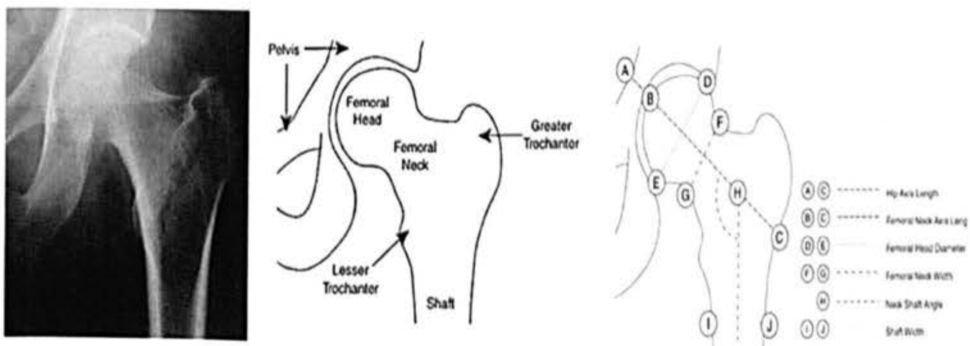

a) b) c)

Figure 3.3: a) The proximal femur taken from a digitised pelvic radiograph b) The key anatomical features of the proximal femur c) some common geometrical measurements of the proximal femur (David *et al.*, 2012).

3.4 Simpleware Software

Computed tomography (CT) imaging is also referred to as a computed axial tomography (CAT) scan. Rotating x-ray equipment is combined with a digital computer to obtain images of parts of the body. Images of cross-sections of a body's organs and tissue are produced with CT imaging. There are other imaging techniques, but CT imaging's advantage has the unique ability to produce clear images of different types of tissue. It offers views of soft tissue, bone, muscle, and blood vessels, yet without sacrificing clarity. Other imaging techniques are available which are less demanding on the practitioner's knowledge, but the image types produced are limited. Software that transfers CT or MRI images in a scan is a radiology technique that uses a combination of magnetism, radio waves, and a computer capable of producing images of body structures.

The MRI scanner is a tube surrounded by a giant circular magnet in which a moveable bed is inserted. The magnet generates a strong magnetic field that aligns the protons of hydrogen atoms which are exposed to a beam of radio waves. Various protons of the body are acted upon. A faint signal is produced which is detected by a receiver in the MRI scanner. The computer processes this information, and produces an image. Simpleware offers three important functions: It lets the operator see and analyse anatomical structures, and allows the operator to design required solutions as dynamic and static systems are portrayed accurately.

3.5 Simpleware Software Overview

Simpleware, the software solution for converting 3D images into computer-aided design tools (CAD), rapid prototype (RP), and finite element (FE) models, has three options for processing and meshing 3D image data as Figure 3.4 shows. The ScanIP component is the core image processing platform, and the +FE module integrates mesh generation, while the +CAD module caters for CAD integration. To enlarge on the capabilities, the ScanIP program offers a wide range of image visualising and processing with segmenting capabilities, which are sufficiently intuitive to suit the casual user as well as the experienced. For CAD analysis, segmented images are exportable as STL or IGES files or RP manufacturing. Importing directly into commercial finite element (FE) packages is enabled with the +FE module. An extensive selection of image processing tools comes with ScanIP which assists in visualising and segmenting regions of interest from 3D data, such as MRI, CT, micro CT, and microscopy.

The +FE module can convert 3D image data into multi-part volumetric models. It was formerly known as +ScanFE and it can provide unique meshing capabilities that allow the creation of extraordinarily accurate 3D image-based models. ScanIP's capabilities have been extended considerably, and it can produce volume and surface meshes, and with grey level data automatically assign the material properties. The analysis-ready meshes are importable by many commercial FE and CFD packages. The +CAD Module offers an uncomplicated importing of interactive positioning and integration of CAD models. The +CAD module was called +ScanCAD and it is now a bolt-on component for ScanIP to integrate CAD objects into 3D imaging. This means that these combined models are exportable as multi-part CAD models. When they are used with the +FE module, they can be converted into multi-part volumes.

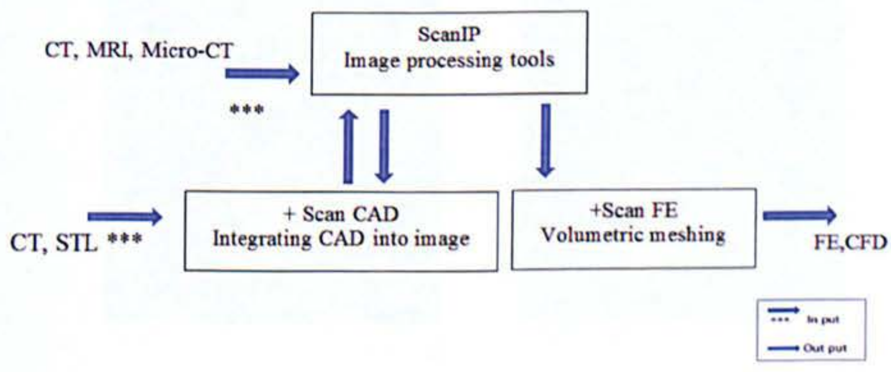

Figure 3.4: Simpleware Software products.

3.6 Image Reconstruction

The signal arrives at the computer in analogue format and an analogue to digital converter turns it into a binary file. The digital signal is stored and the image is reconstructed. Each of the pictures is now termed a pixel and is displayed on a matrix. This is assigned a number, called a Hounsfield unit, based on the amount of energy recorded by the detector. The anatomy of an object, made up of a large number of tiny elongated blocks, is reconstructed and then represents a volume of tissue called voxel, which stands for 'volume of pixel'.

3.6.1 Importing Data

In this study the geometry of the pelvic–femur complex has been selected from a male of 60 years. His stature and weight are 183 cm and 77.4 kg respectively. This subject has the characteristic mass and stature close to the average adult male. The data was collected by the Department of Radiology, Millad Hospital, Tehran, Iran. Material properties included cancellous bone. Its thickness and the thickness of cortical bone were based on in-situ CT scan data [Siemens, 110 KVp, 105m, 5mm thick slices at 2.5mm interval, 255 numbers of slices, acquisition matrix and in-plane resolution 0.7mm×0.7mm (pixel size)]. Depending on the pixel spacing and slice thickness, the image quality will vary. If the image quality is higher, the picture has more detail. Figure 3.5 shows two pictures with different dimensions of the pixel.

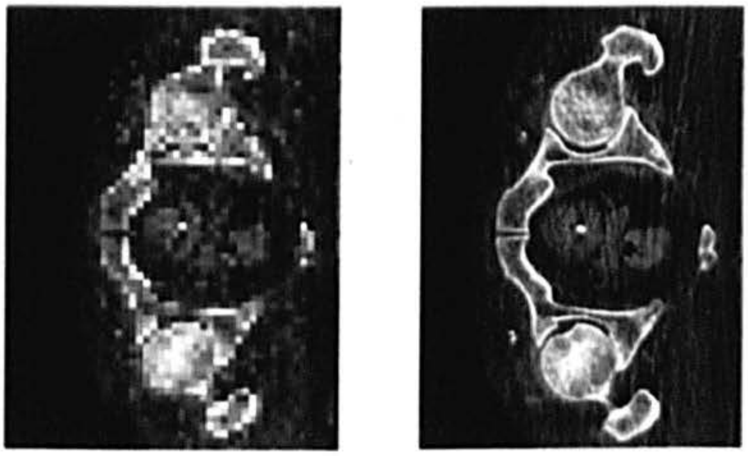

a) b)

Figure 3.5: Two images with different pixel size. In (a), the pixel size is 0.5x0.5 (mm). In image (b) the pixel size is 0.97x0.97 (mm^2) (Forman *et al.*, 2009).

The 255 CT-Scan in DICOM (Digital Imaging and Communications in Medicine) format, after proper thresholding and segmentation of the bone, was loaded in the trial version 3.1, SIMPLEWARE Software, UK, to produce the solid model. The output was converted in the DXF format and transferred to the IGS format by using mechanical software, ANSYS. The IGS data produces the three dimensional (3D) FE model of human pelvis femur soft tissue in ANSYS.

The CT scans of proximal femur, stored in DICOM forms, were imported by the ScanIP equipment and decoded as Computer-Aided Design (CAD). This 3D modelling is the prerequisite for analysis by finite element modelling (FEM). The (DICOM) standard was created by the National Electrical Manufacturers Association (NEMA) for distributing and viewing medical images, such as CT scans, MRIs, and Ultrasound. DICOM is now a comprehensive set of standards for the handling, storing, printing and the transmission of medical imaging information.

DICOM includes a file format definition, as well as a network communication protocol. The header consists of a 128-bytes file preamble, followed by a 4-byte DICOM prefix. Down sampling data to a resolution where features remain identifiable and reducing the size of an image itself is often recommended. Lower memory requirements usually make the segmentation step easier and consequently number of elements in FE mesh is also reduced. The voxel size (spacing in mm) decides the size of the base element in the mesh and thus influences the density of the generated mesh. Small base elements mean higher density in the system. Figure 3.6 shows the import of DICOM file (slice 0) in Simpleware.

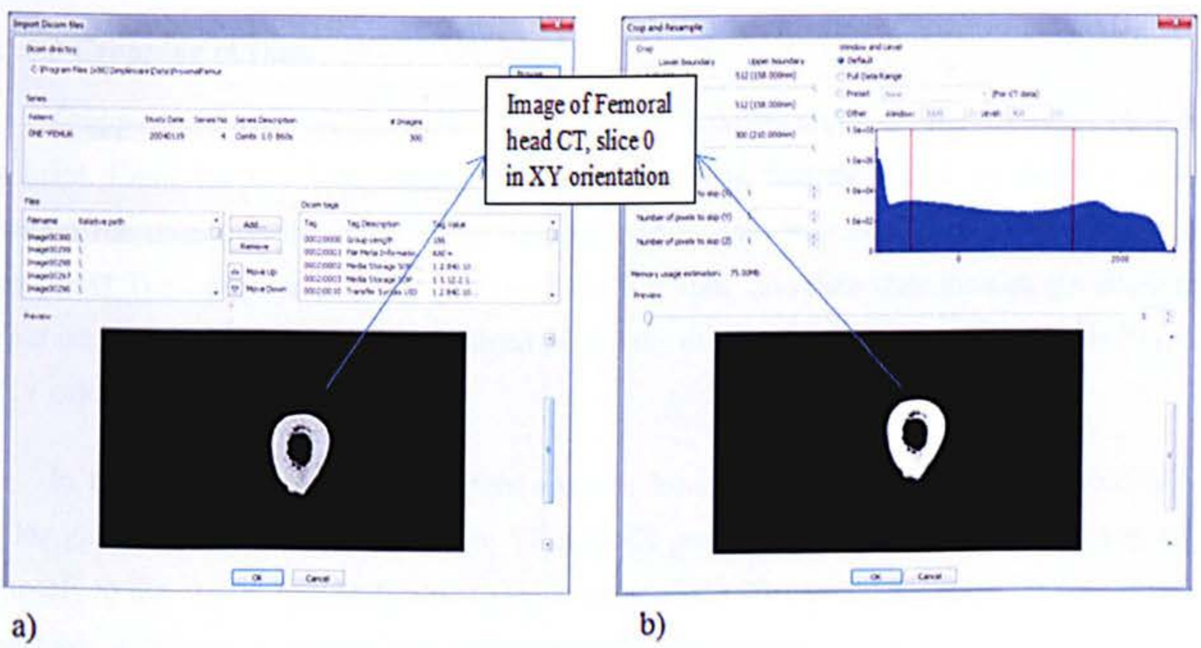

Figure 3.6: a) Import of DICOM files dialog box and, b) Transformation dialog box.

3.6.2 Resampling of Data

Assuming a mesh with minimum element size of 0.7mm, the highest mesh density is likely to be generated. In this case, elements are resampled down to a voxel size of, say, $0.7 \times 0.7 \times 0.7$ (see Figure 3.7).

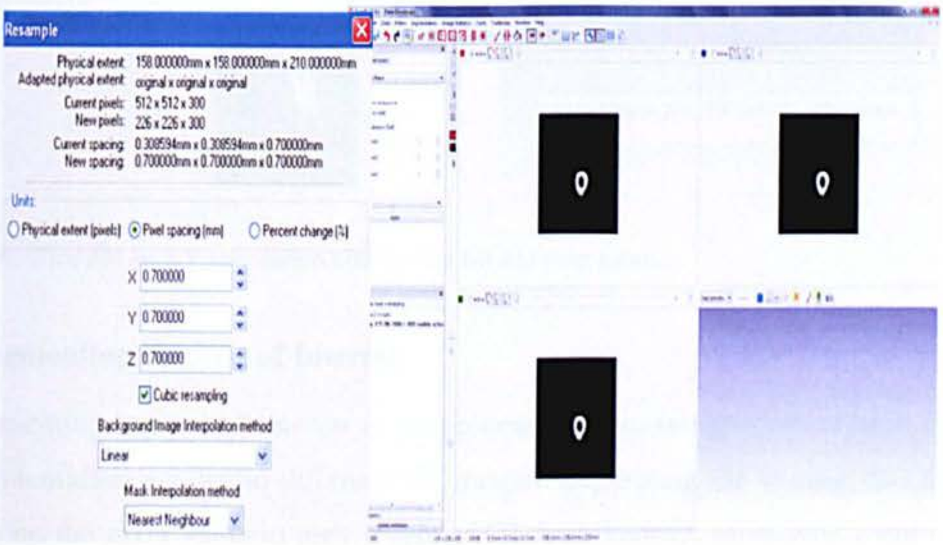

Figure 3.7: Resampling slices in Simpleware.

3.6.3 Cropping of Data

Cropping is highly recommended for reducing the image until only the necessary objects remain. Using an XY view, sliding through the slices to find the actual number contained within the object, is the most appropriate method to crop the data. How much should be cropped? The easiest answer is to start with the XY view, and then slide through the slices to find out how many are actually contained within the object. Figure 3.8 shows the slice 231 in XY orientation after cavity fill.

In this particular example, the bone extends from slice 1 to, approximately, slice 287. This guides the ideal cropping for the YZ and ZX positions. It is important not to crop too closely to the object. It is preferable to leave some space. The mesh generator cannot smooth surfaces at the volume border, and consequentially would leave them flat.

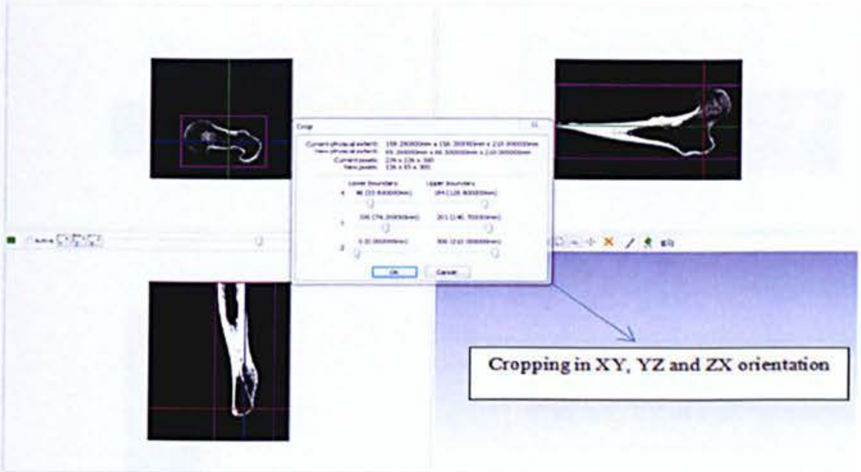

Figure 3.8: Slice 231 in XY orientation after cavity fill and crop panel.

3.6.4 Segmenting Regions of Interest

Segmenting regions of interest is the process of identifying to where each pixel belongs. The segmentation applies to different CT images. Separating the images into different parts depends on the pixel value in grey levels of CT scan images. Most time spent on the model generation process goes to segmentation process. Each organ has a different density, so the organ or soft tissue is defined depending on pixel values (see Figure 3.9). Each pixel creates a voxel, and the volume images can be considered as three-dimensional tables containing intensity values for particular positions in space. We can use semi-automatic methods to determine the structure manually, when the contrast between different parts is not clear, manual methods. Figure 3.10 shows slides in XY, YZ and ZX orientation after morphological close.

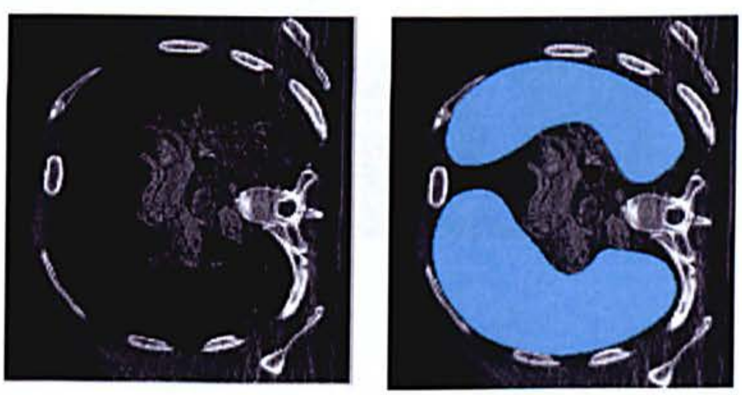

Figure 3.9: Example of segmentation of the lungs from PMHS M457(Forman et al., 2009).

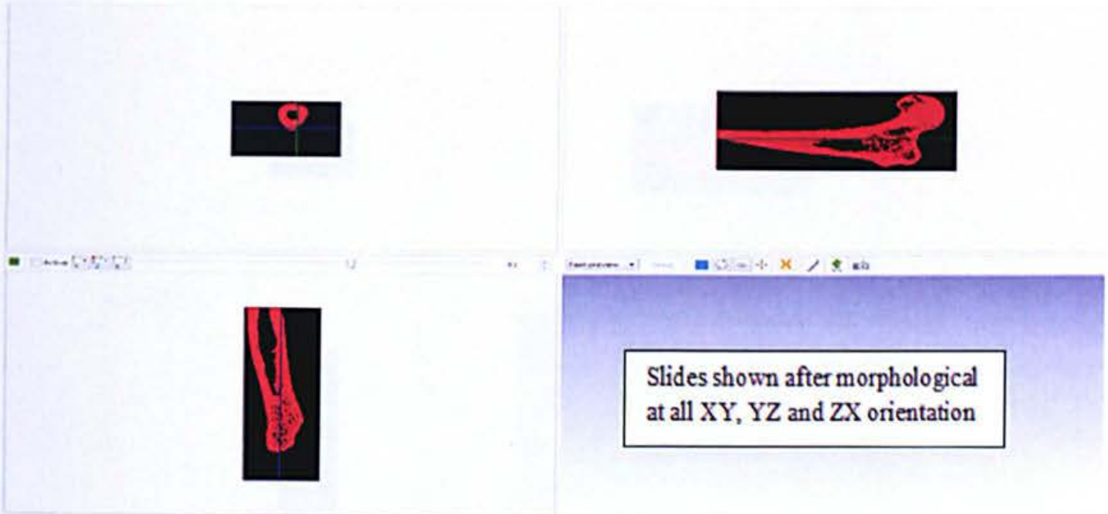

Figure 3.10: Slides after morphological close.

It should be noted how the inside of the bone features fine structures/trabecular (e g slice 0 in XY). In many cases, a merging of slices will simplify the surface. Trabecular region bones are of a low density and this can be shown by using material properties in the signal strength. A Morphological close, which effectively simplifies the shape of the object, leads to a simpler mesh. Internal holes of the structure which show at this stage can be solved with the Cavity Fill function of the Floodfill tool. The main aim is to eradicate small holes yet preserve the marrow as a cavity within the femur. The FloodFill algorithm is the answer, used by left-clicking on a pixel belonging to the femur, not the air as shown in Figure 3.11 and Figure 3.12. This will create a new mask (Mask 1).

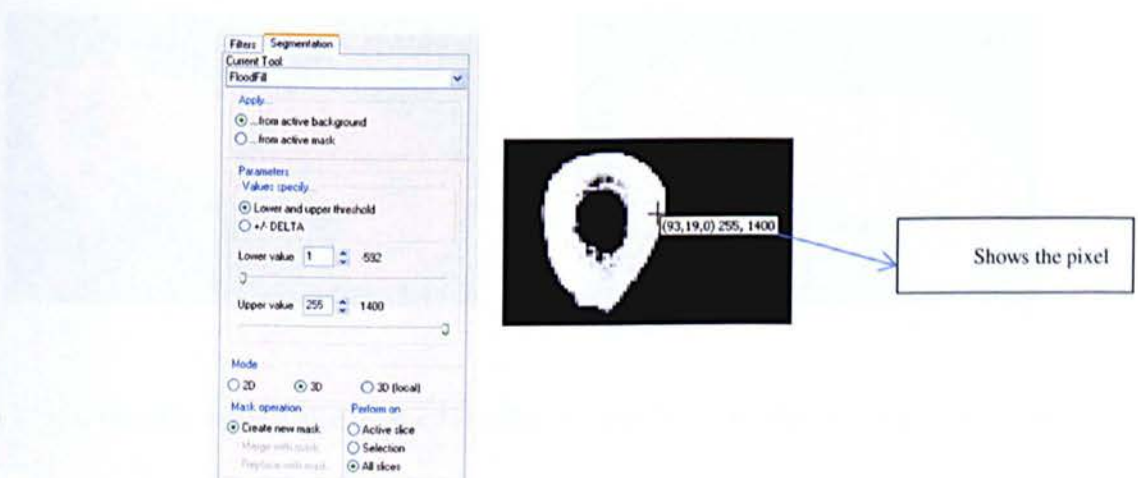

Figure 3.11: Floodfill tool panel and slice 0 in XY orientation.

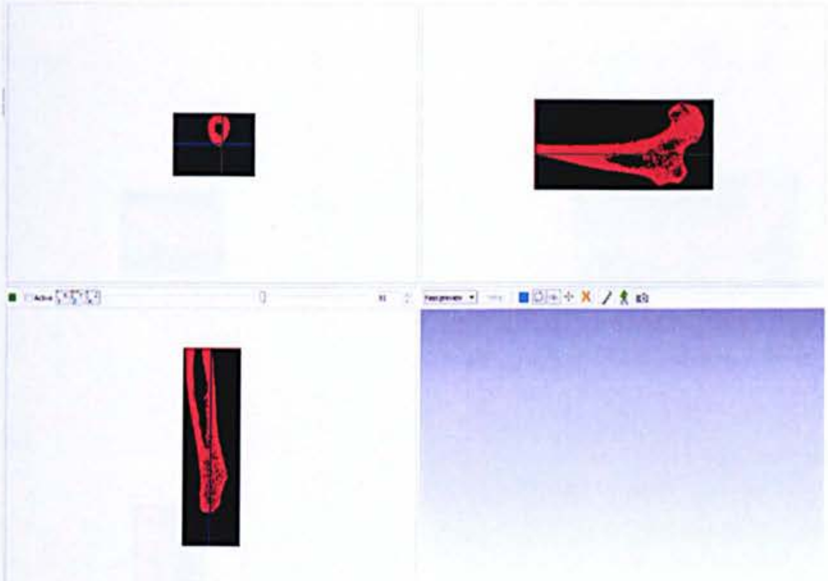

Figure 3.12: Floodfill on slice 0 in XY, slice 44 in XZ and slice 81 in YZ orientation.

All holes that should not show should be filled. It is necessary to ensure that the marrow is not seen by the software as a hole. This is achieved by padding it in the Z direction by connecting it with the outside of the bone (see Figure 3.13 and Figure 3.14).

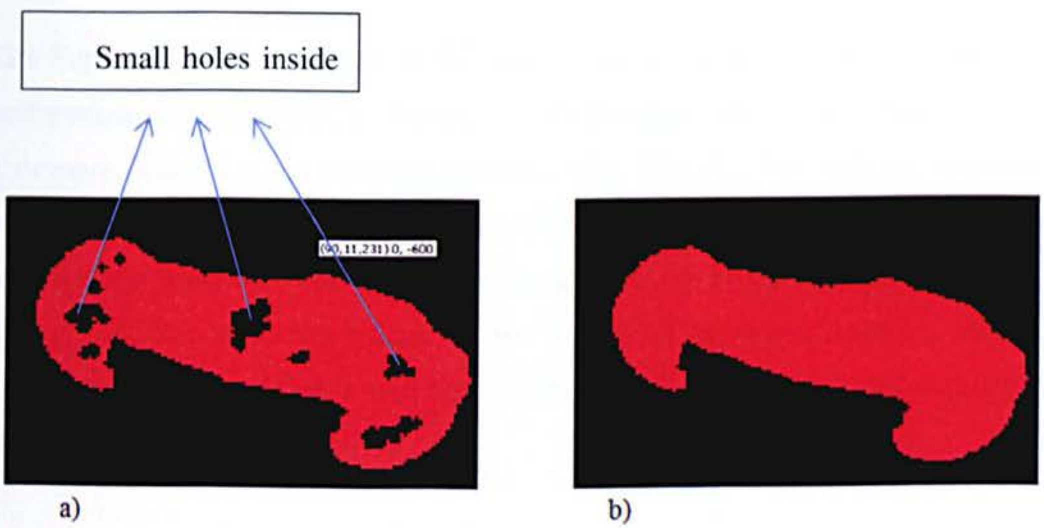

Figure 3.13: a) Floodfill segmentation in slice 231 in XY, b) Slice 231 in XY orientation after cavity fill.

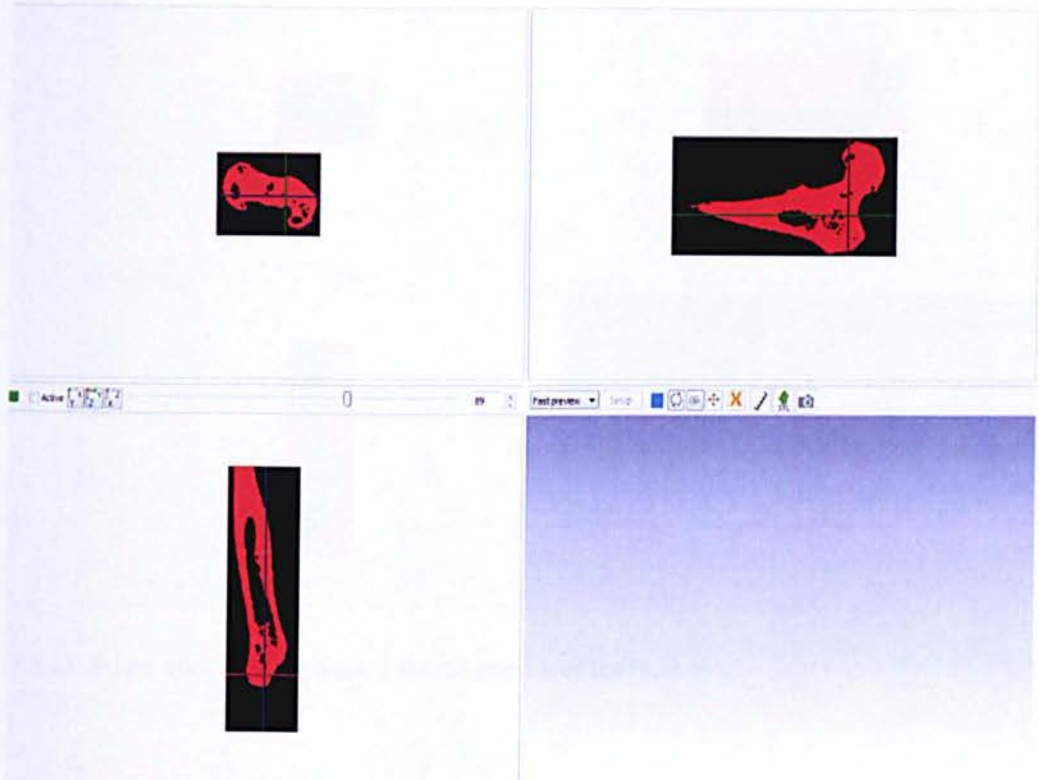

Figure 3.14: Slice 234 in XY, slice 49 in XZ and slice 89 in YZ orientation after cavity fill.

The Figure 3.15 indicates that all the holes are gone. However, the XY view shows that and some remaining holes remain. These actually belong to the marrow, currently connected to the exterior because of the padding operation. Slice 214 in XY orientation shows that close to the head of the femur some fine structures still exist. They could be eliminated by applying a morphological open but that would also create holes in the surface of the bone in places where it is very thin. Creating a mask for the interior of the bone (marrow), closing it, and then subtracting it from Mask 1 will have a similar effect to Mask 1, but without affecting the bone's outer surface.

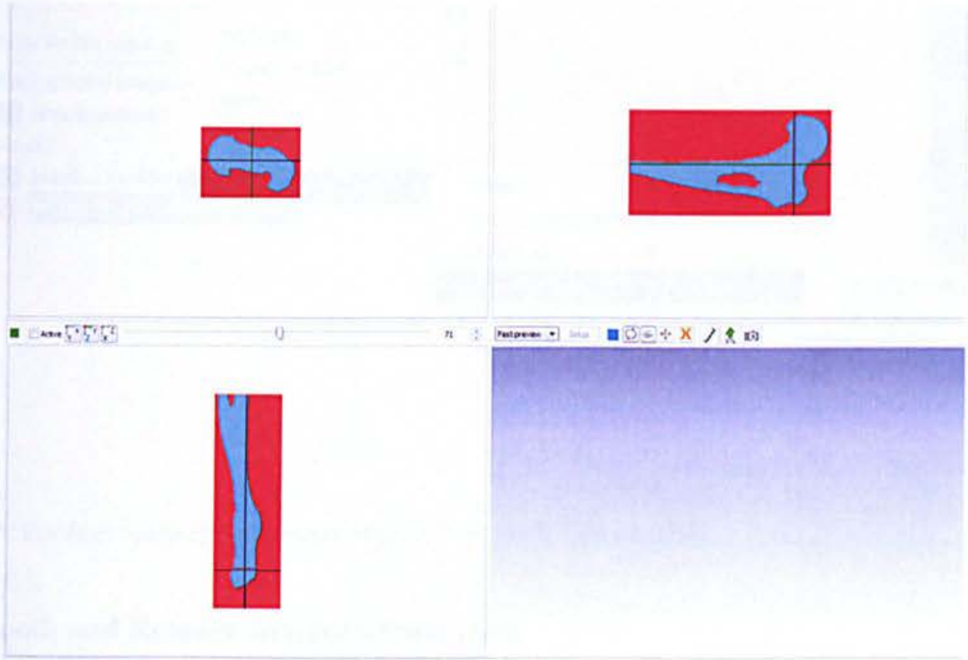

Figure 3.15: Slides after creating mask 2 for the interior of the bone.

The software offers a wide range of filters for different applications such as smoothing and noise reduction. Smoothing reduces noise but also attenuates contours. The noise reduction filters preserve features, as much as is possible. Boolean operations are applied for intersections or unions, and for inverting or subtracting between masks.

The incorrect use of filters causes loss of characteristics of shape and size of the organs, or parts that have been modelled. The filter and number of iterations depends on each form and the dimensions of the organ or bone. In order to remove any overlap between Masks 1 and 2, a subtract-boolean operation can be applied. Figure 3.16 shows the Boolean operation to subtract Mask 2 from Mask 1 on all slices.

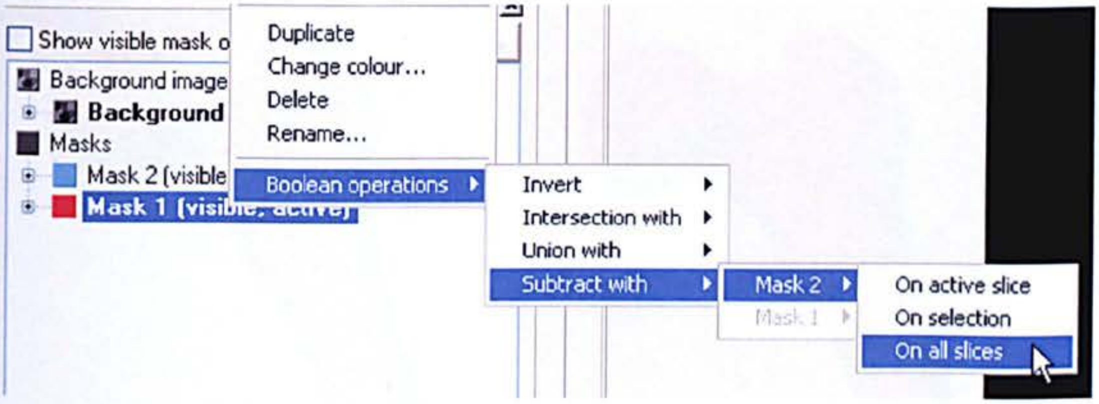

Figure 3.16: Boolean operation to subtract Mask 2 from Mask 1 on all slices.

3.6.5 Smooth and Remove Artefacts from Data

It is desirable to keep the grayscale information of the background because this will allow more accurate and faithful surfaces to be shown. This is achieved by smoothing algorithms in ScanIP. A powerful way to smooth the data is to use the recursive Gaussian smoothing. Figure 3.17 presents a screenshot before and after applying this smoothing. Usually a value of 1 to 3 times the spacing - in the given direction - gives an initial good smoothing.

The threshold values used for the masks in the exercise are 1-255. The value is set at this level due to the window and level settings. The values are really too close to the boundary 0-255. This makes the greyscale values less useful. Topology and volume preserving of the pre-smoothing algorithm involves too many constraints. An appropriate smoothing would be achieved with the mask binaries.

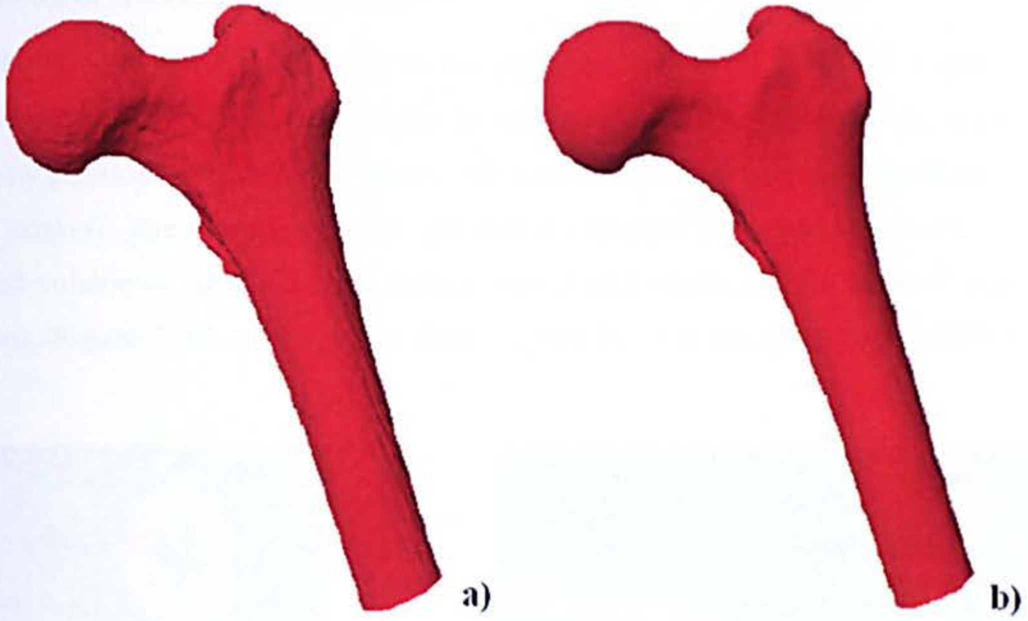

Figure 3.17: Difference before (a) and (b) after applying the recursive guassian filter.

3.6.6 Generating a FE Preview

First make sure mask 2 is invisible by right clicking on it in the Mask browser then selecting Toggle and after that in the 3D view, select FE in the 3D preview type. The FE preview should look similar to the one shown in Figure 3.18.

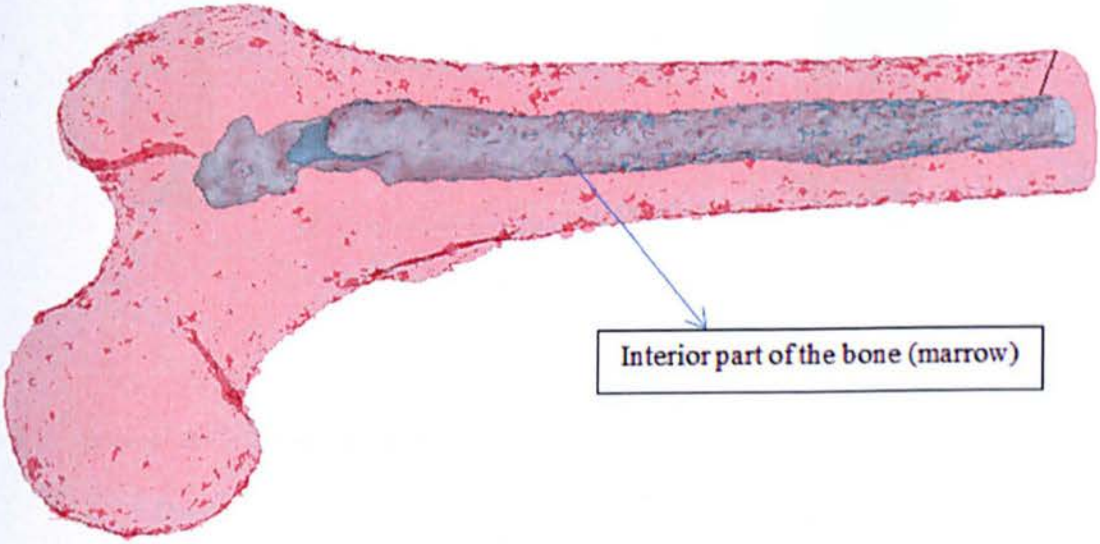

Figure 3.18: FE preview in the 3D.

3.6.7 Planes of Geometry in a 3D Model

In the 3D view, it would be easily to visualise the planes of the 2D views. This is a useful tool to locate areas of interest more easily. In order to use the slice slider, the slices are moved to the new position of the 2D view planes. 3D view will provide useful information about the visible mask(s). The information also includes the number of polygons of each mask, the estimated volume of each mask, the surface area of each mask, and the number of points of each mask. Figures 3.19, 3.20 and 3.21 show the viewing of active slices in 2D and 3D.

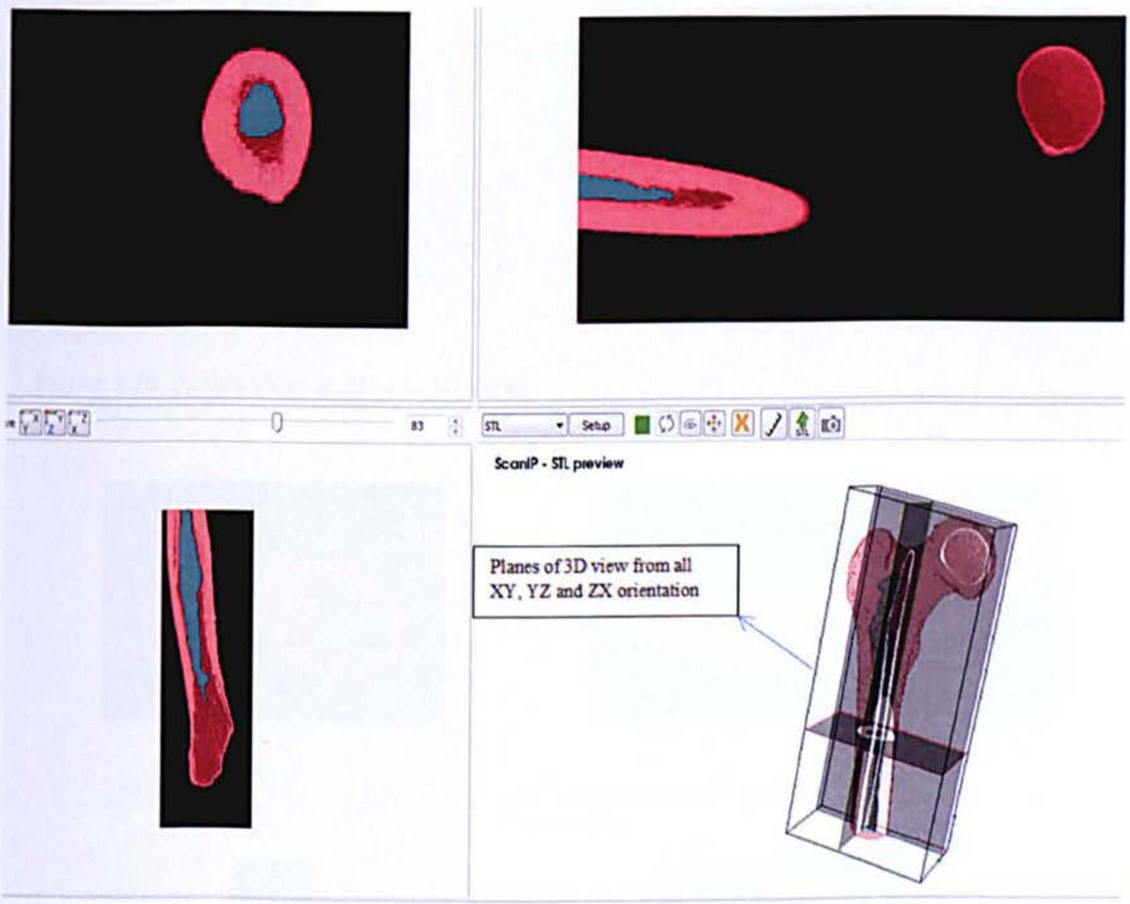

Figure 3.19: Active slices in 2D and 3D views.

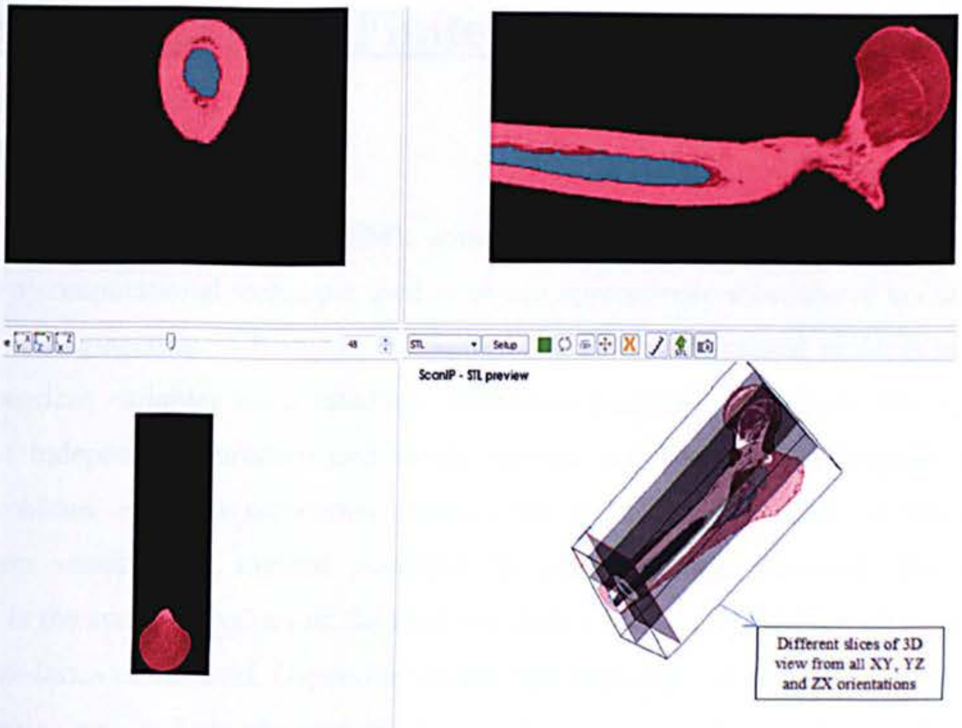

Figure 3.20: Active slices in 2D and 3D views

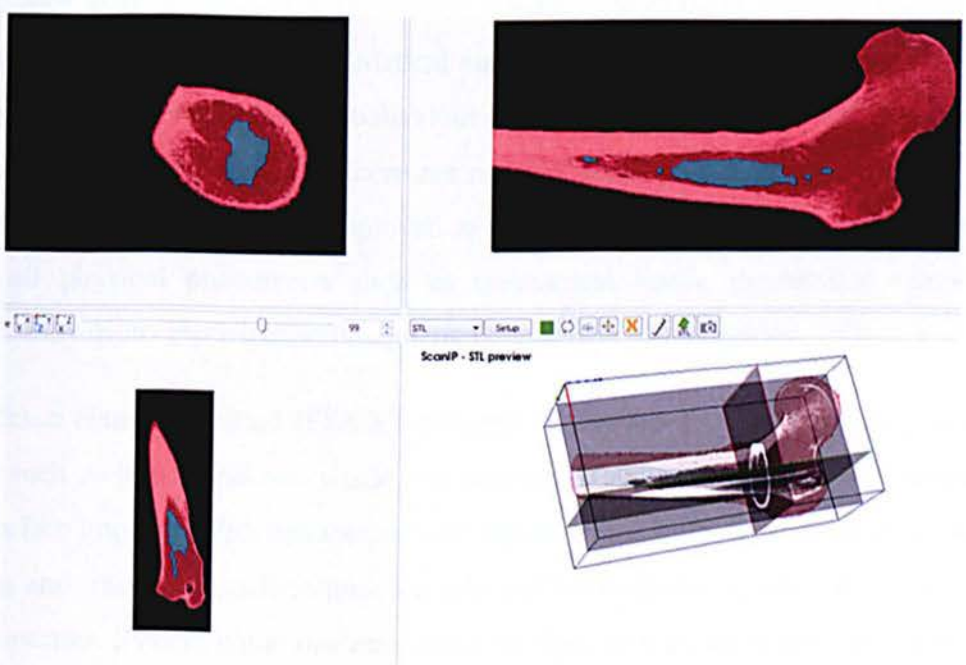

Figure 3.21: Active slices in 2D and 3D views.

Chapter 4 - Explicit Finite Element Analysis

4.1 Introduction to FEA

The finite element method (FEM), sometimes referred to as finite element analysis (FEA), is a computational technique used to obtain approximate solutions of boundary value problems in engineering. A boundary value problem is a mathematical problem in which or more dependent variables must satisfy a differential equation everywhere within a known domain of independent variables and satisfy specific conditions on the domain. Boundary values problems are also sometimes called field problems. The field variables are the independent variables of interest governed by the differential equation. The boundary condition is the specified values of the field variables or related variables such as derivatives on the boundaries of the field. Depending on the type of physical problem being analyzed, the field variables may include physical displacement, temperature, heat flux, and fluid velocity to name only few (Hallquist, 2003).

The finite element method works by breaking a real object down into a large number of elements, such as little cubes. The behaviour of each little element, which is regular in shape, is readily predicted by set of mathematical equations. The computer then adds up all of the individual behaviours to predict the behaviour of the actual object. The finite in finite element analysis comes from the idea that there are a finite number of elements in a finite element model. Finite element method is employed to predict the behaviour of things with respect to virtually all physical phenomena such as mechanical stress, mechanical vibration, heat transfer fluid, various electrical and magnetic phenomena and acoustics.

The finite element method (FEM) represents an optimal tool for modelling complicated materials such as bones and soft tissue and understanding their response to unusual loading conditions like impacts. With this method, the continuum is discretised in elements with finite dimension and interpolation functions are selected for assembling element properties to get global properties. System equations are solved for obtaining nodal unknowns and then, using the nodal values, additional calculations are made to obtain other results such as stresses, strains, moments, etc.

4.2 LS-DYNA

The explicit LS-DYNA FE-analysis software was used to carry out the simulations in the present study. LS-DYNA is a highly advanced general purpose nonlinear finite element program that is capable of simulating complex real world problems. The distributed and shared memory solver provides very short turnaround times on desktop computers and clusters operated using Linux, Windows, and UNIX. LS-DYNA is suitable to investigate phenomena involving large deformations, sophisticated material models and complex contact conditions for structural dynamics problems. It allows switching between explicit and different implicit time stepping schemes. Disparate disciplines, such as Coupled Thermal analyses, Computational Fluid Dynamics (CFD), Fluid-Structure Interaction, Smooth Particle Hydrodynamics (SPH), Element Free Galerkin (EFG), Corpuscular Method (CPM), and the Boundary Element Method (BEM) can be combined with structural dynamics (Livermore Software Technology Corp, 2012).

By determining product characteristics before a prototype is built, for many products LS-DYNA is the key to reducing time to market. Carrying out investigations with the aid of LS-DYNA supports the design of robust products with superior performance. For pre- and post-processing, LS-DYNA comes with the LS-PrePost tool. LS-PrePost can be utilized to generate inputs and visualize numerical results. The software package LS-OPT for optimization and robust design is also supplied with LS-DYNA. With the option of multidisciplinary simulations, LS-DYNA significantly increases potentials for developing innovative products. These advantages contribute towards reducing development costs. All above-mentioned features and software packages are supplied as a single unit. LS-DYNA is not split for special applications, and the licensing scheme enables the different disciplines to be combined without limitations (Livermore Software Technology Corp, 2012).

In the initial section of this chapter, elementary concept about mechanical dynamics, shell elements, time integration and overall adaptive procedures will be conferred.

4.3 Basic Structural Dynamics

LS-DYNA is a FEM-program principally for examining enormous distortion dynamic response of structures. How dynamic difficulties are referred to mathematically and which approaches that are applied to solve the governing equations will be preserved in the subsequent sections.

4.3.1 Governing Equations

Taking into account a statically evaluated structure, the equations of equilibrium for a linear problem necessitates this:

$$f_{int} = f_{ext} \Leftrightarrow ku = f \quad (4.1)$$

It means, internal forces are equivalent to external forces. k represents the linear stiffness of the structure and u is the displacement. In a static non-linear analysis the internal force fluctuates as a nonlinear function of displacements consistent with:

$$f_{\text{int}}(\mathrm{u}) = f_{\text{ext}} \quad (4.2)$$

Now, consider the damped dynamic single degree of freedom, SDOF, system in Figure 4.1.

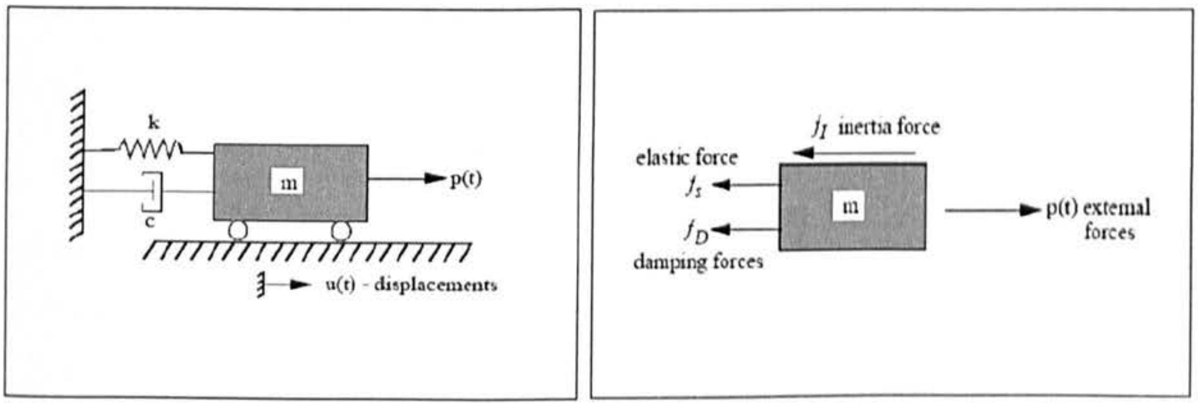

Figure 4.1: Single degree of freedom system (Heath, 2002).

Dynamic equilibrium requires that (d'Alembert's principle):

$$f_I + f_D + f_{int} = p\,(t) \quad (4.3)$$

Where:

$f_I = m\ddot{u}\,; \quad \ddot{u} = \frac{d^2 u}{dt^2}\,; \qquad \ddot{u}$ = acceleration (4.4)

$f_D = c\dot{u}\,; \quad \dot{u} = \frac{du}{dt}\,; \qquad \dot{u}$ = velocity (4.5)

$f_{int} = ku; \quad u;$ u = displacement (4.6)

K is, as in static analysis, the linear stiffness, c is the damping coefficient and m is the mass of the body. Introducing equations 4.4 - 4.6 in 4.1 indicates the equation of motion. In the linear case the equation of motion performs as a linear ordinary differential equation as;

$$m\ddot{u} + c\dot{u} + ku = p(t) \tag{4.7}$$

In the nonlinear example, the internal force differs in the same mode as in the static nonlinear case. Hence, the equation of motion acts as a non-linear (Heath, 2002);

$$m\ddot{u} + c\dot{u} + f_{int}(u) = p(t) \tag{4.8}$$

4.3.2 Structural Damping

In structural dynamic analyses the functional force is a utility of time. If a typical load curve is applied as in Figure 4.2 the respond for a certain node in an undamped structure, -

c = 0, will act as presented in Figure 4.3.

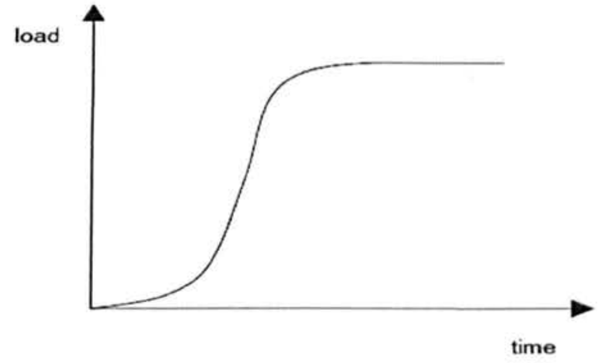

Figure 4.2: Typical load curve (Heath, 2002).

That is, the structure will initiate to vibrate with a specific frequency, the natural angular frequency, ω_n. To achieve the static solution to the problem, structural damping has to be considered. Some concepts about structural damping and how the damping can be used in a dynamic structure follows. Study the equation of motion, Equation 4.7, for an SDOF system. Then, the change that the vibration is supposed to be free needs to be taken into account. That is, the structure has been exposed to a displacement, u (0), and subsequently been unconfined. There is no excitation force acting on the structure.

$$m\ddot{u} + c\dot{u} + ku = 0 \tag{4.9}$$

C as described, earlier the damping coefficient. It describes the energy loss in a cycle of free vibration. The natural frequency is also calculated as:

$$\omega_n = \sqrt{\frac{k}{m}} \tag{4.10}$$

A new term called the damping ratio, ζ, is introduced. The relation between c and ζ is as follows:

$$\zeta = \frac{c}{2m\omega_n} \tag{4.11}$$

Dividing Equation 4.12 by m gives:

$$\ddot{u} + 2\zeta\omega_n\dot{u} + \omega_n^2 u = 0 \tag{4.12}$$

The solution to this differential equation has the form:

$$U = e^{st} \rightarrow (s^2 + 2\zeta\omega_n s + \omega_n^2)e^{st} = 0 \tag{4.13}$$

This equation is satisfied for all t if:

$$s^2 + 2\zeta\omega_n s + \omega_n^2 = 0 \tag{4.14}$$

Equation 4.15, known as the characteristic equation, has two roots:

$$s_{1,2} = \omega_n \left(-\zeta \pm i\sqrt{1-\zeta^2}\right) \tag{4.15}$$

In the case when $\zeta = \pm 1$, the imaginary part will be zero. The solution to $S_{1,2}$ is exactly the undamped natural angular frequency. This case is called the critical damping of a system and c_{cr} is called the critical damping coefficient and can be expressed as:

$$c_{cr} = 2m\omega_n = 2\sqrt{km} = \frac{2k}{\omega_n} \tag{4.16}$$

Other types of damping that can occur in a dynamic system are underdamped and over damped. The differences between undamped, underdamped and critical damping are shown in Figure 4.3.

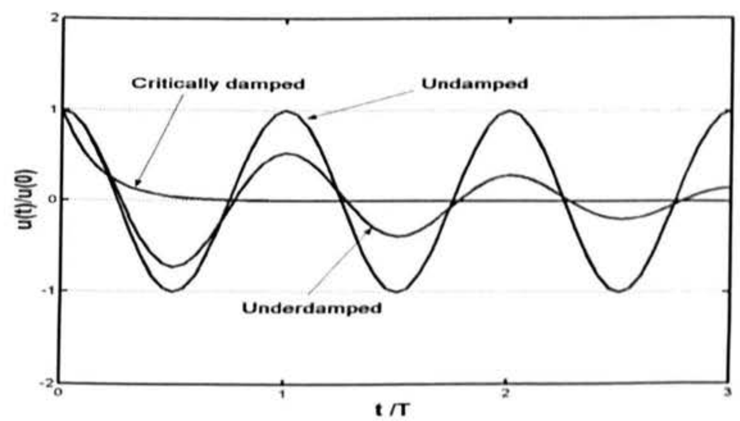

Figure 4.3: Dynamic response for different types of damping (adopted from (Chopra, 2001)).

On the y-axis, one has the ratio between the response at time t, u (t), and the initial displacement, u (0), and on the x-axis the ratio between the time t and the natural period time of the system, T_n, which is defined as:

$$T_n = \frac{2\pi}{\omega_n} \tag{4.17}$$

The above theory is described for one-dimensional single degree of freedom problems, scalar problems. In multi degree of freedom, MDOF, the same theory applies, with parameters described as matrices and vectors. The MDOF-system has a set of different natural angular frequencies. Every frequency is said to describe a mode that is a special vibration part of the structure. For every mode there is a corresponding c_{cr} and therefore a corresponding response. There are different methods of applying damping to a structure. Unlike the elastic modulus of a material, the properties of damping are not that well established.

In classical damping theory there are different ways to express the damping coefficient c. One usually utilizes two main techniques, either mass-proportional damping or stiffness-proportional damping. Mix of these two makes the so called Rayleigh damping. Since the damping coefficient, as described earlier, varies in different modes it is a complex procedure to express the damping for a structure. Normally in structural dynamics, only the lowest modes (frequencies) are of interest for the response (Chopra, 2001).

4.3.3 Damping in LS-DYNA

LS-DYNA includes both Rayleigh and mass-proportional damping. For lower frequencies the mass-proportional damping is more efficient and therefore used. The damping is applied on the nodes of the deformable structure. The best damping is usually based on the critical damping of the lowest mode of interest. The damping affects both translations and rotations of the structure. The damping force is calculated as:

$$F^n_{damp} = D_s \mathrm{M}\dot{u} \tag{4.18}$$

where D_s is a function of the lowest frequency of interest:

$$D_s = 2\omega_{min} \tag{4.19}$$

4.4 Shell Elements

Shell elements can be regarded as plate bending elements combined with plane membrane elements. A shell element carries load both in the plane, membrane forces, and perpendicular to the surface. Shells can also have a curved surface, though, only flat linear elements are considered in this work. The definition of a thin shell is that its thickness t is small compared to the overall dimensions. The thickness can be constant or vary within an element. Consider the quadrilateral shell element in Figure 4.4a. The four corner nodes have 5 degrees of freedom each, 3 translations and 2 rotations (Cook *et al.*, 2002).

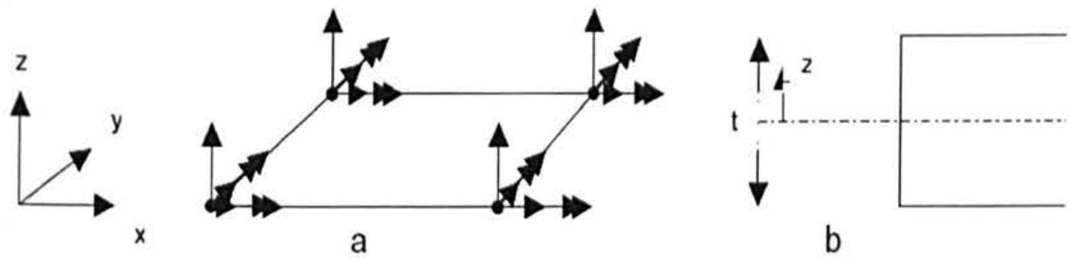

Figure 4.4: a) Quadrilateral shell element with DOF, and b) Definition of mid plane (Cook *et al.*, 2002).

The stresses in a shell generate membrane forces N, measured in force per unit length.

$$N_x = \int_{-t/2}^{t/2} \sigma_x dz; \tag{4.20}$$

$$N_y = \int_{-t/2}^{t/2} \sigma_y dz; \tag{4.21}$$

$$N_{xy} = \int_{-t/2}^{t/2} \sigma_{xy} dz; \tag{4.22}$$

The stresses are calculated as a superposition of membrane and bending stresses. For a linear elastic thin shell the normal forces are independent of z and the bending stress varies linearly with z.

$$\sigma_x = \frac{N_x}{t} + \frac{12M_x Z}{t^3}; \tag{4.23}$$

$$\sigma_y = \frac{N_y}{t} + \frac{12M_y Z}{t^3}; \tag{4.24}$$

$$\sigma_{xy} = \frac{N_{yx}}{t} + \frac{12M_{xy}Z}{t^3}; \tag{4.25}$$

Stresses are evaluated at so called integration points within the element. An element needs 4 integration points to be stable, fully integrated. Elements with less integration points are called under-integrated. At every integration point a number of integration points through the thickness can be used to describe the stress variation.

4.4.1 Belytschko-Lin-Tsay Shell

The most frequently used shell element is the so called Belytschko-Lin-Tsay element. It was first implemented in LS-DYNA as a computationally more efficient element than its precursor. It is considerably more efficient than the other types of shells and this advantage depends on several mathematical simplifications. However, because of these simplifications, it has some disadvantages. It loses stiffness considerably when it is warped and it is therefore not appropriate for analysing warped structures. Since only one integration point in the plane is used, zero energy modes may occur. The difference between an under integrated and a fully integrated element is shown in Figure 4.5a. Zero energy modes are also known as "hourglass" modes because of their shape. Two typical hourglass modes are shown in Figure 4.5b.

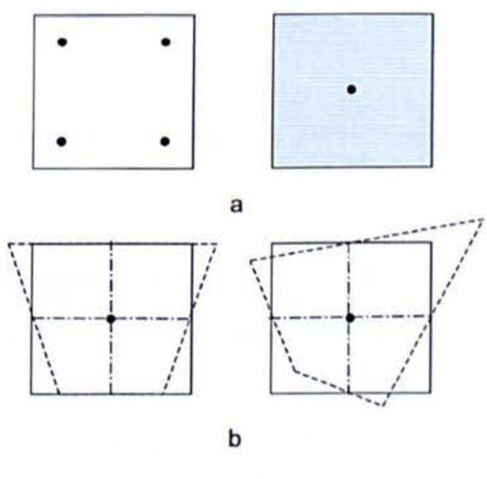

Figure 4.5: a) A fully integrated element to the left and a under integrated element to the right b) Two hourglass modes for the under integrated element (Engineering Research AB, 2005; Hallquist, 2003).

Since the strain is only evaluated in one point it is possible that no strains occur in that point. Therefore, the strain energy of the element is zero even though the element is considerably deformed. For a fully integrated element, the hourglass effect will not have an influence on the solution. As discussed earlier, an hourglass force is added to the equation of motion in LS-DYNA. The aim with this force is to control the formation of these modes. After the analysis, it is essential to control that the hourglass energy is small compared to the total energy otherwise, the solution will be inaccurate. Displacements are only evaluated at the element nodes. The element is linear and therefore no bending deformation of the element is obtained within the element. An element formulation of higher degree would affect the critical time step considerably and is therefore rarely used in an explicit FEM-solver (Engineering Research AB, 2005; Hallquist, 2003).

4.4.2 Explicit Time Integration

LS-DYNA uses the central difference method to solve the equation of motion. In matrix form, the equation of motion appears as:

$$M\ddot{u} + C\dot{u} + f^{int}(u) = f^{ext}(t) \tag{4.26}$$

M and C have the dimensions (*dof* × *dof*), f and u have the dimensions (*1*× *dof*). However, the formulation in LS-DYNA differs from the original equation. Because of the reduced integration that discussed in above, an "hourglass" force is added. There might also be contact between different parts involved. Therefore a second force is added to the equation. Thus, the formulation in LS-DYNA appears as:

$$M\ddot{u} + C\dot{u} + f^{int}(u) = f^{ext}(t) + f^{hour}(u,\dot{u}) + f^{cont}(u,\dot{u}) \tag{4.27}$$

If we from now on disregard from "hourglass" and contact forces and return to the equation for an SDOF system, the following expression appears:

$$\left(M + \tfrac{1}{2}\,2\Delta t c\right) u_{n+1} = \left((\Delta t)^2\, p_n \;-\; ((\Delta t)^2)k - 2m)u_n \;-\; \left(m - \tfrac{\Delta t}{2} c\right) u_{n-1} \right) \tag{4.28}$$

When M is a matrix and therefore an inversion is necessary. In a system with a large number of DOFs this will be computationally expensive to do in every single time step. Therefore, LS-DYNA uses a lumped mass matrix which has only non-zero values in the diagonal. Also the damping matrix is diagonal. The inversion of a diagonal matrix is trivial. A lumped mass matrix can be seen as every node obtaining a contribution which is proportional to the area of influence of the node as shown in Figure 4.6 (Hallquist, 2003).

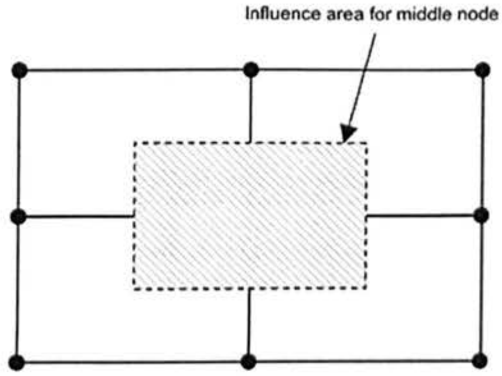

Figure 4.6: Influence area when calculating lumped masses (Hallquist, 2003).

For the MDOF system the solution to u_{n+1} appears as:

$$u_{n+1} = (M + \frac{1}{2}\, 2\Delta t C)^{-1}\ \left((\Delta t)^2\, P_n - ((\Delta t)^2\, \mathrm{K} - 2\mathrm{M}) u_n - (\mathrm{M} - \frac{\Delta t}{2}\mathrm{C})\, u_{n-1} \right) \tag{4.29}$$

The explicit time integration has many merits, it is memory efficient since no major matrix inverse operations need to be performed. It also makes it possible to describe a complex problem with a relative simple algorithm. However, it is as earlier described only conditionally stable which means that the time step may not exceed a critical value. This makes the explicit solver, as mentioned, appropriate for short time loading situations. If a slow process needs to be described, the computational effort will be too high. For example, the actual time to perform a metal forming may perhaps be 10 seconds but the simulations made in LS-DYNA are only performed during 50ms. The critical time step, Δt_{cr}, depends on the size of the elements in the model. Small elements require a small time step to make the central difference method stable. This critical time step is based on wave propagation. Basically it says that a wave cannot pass an entire element in one time step. This leads to:

$$\Delta t_{cr} = \frac{L_{min}}{c} \tag{4.30}$$

where L_{min} the shortest element side in the model and c is wave propagation velocity which is calculated as:

$$c \approx \sqrt{\frac{E}{\rho}} \tag{4.31}$$

However, different methods can be used to increase the time step and also an implicit solver is included in LS-DYNA for slower processes.

4.4.3 Contacts Modelling

The contact option in LS-DYNA treats interaction between different parts in a model. When different parts are interacting, forces appear in the contact interface. There are numbers of different contact options in LS-DYNA and the majority of them are based on the penalty method that will be treated later. The contact used in this thesis is mainly a surface to surface contact, that is, one surface is impacting another surface. Node to surface and node to node contacts are other types of contact that work in a similar way. The surface to surface contact computationally is more expensive than the other two but more stable and accurate when a coarse mesh is used. The contacts are usually defined by a master and a slave side. Generally the part with highest mesh density is used as a master side.

Although, in the surface to surface contact the choice of master and slave side is arbitrary. The penalty method consists of placing springs between all penetrating parts and the contact surface. The function of the penalty method for a node to surface contact is illustrated in Figure 4.7.

The contact force is calculated as:

$$F = \delta k \tag{4.32}$$

where k is the spring stiffness.

The surface to surface contact is treated symmetrically. In that case, both master and slave nodes are checked against penetration. If the contact pressures become large, it is possible that unacceptable penetration occur. The method checks for initial penetration, that is, if a node already has penetrated a surface before the analysis starts. It is also possible to add friction and damping in the contact interface (Engineering Research AB, 2005).

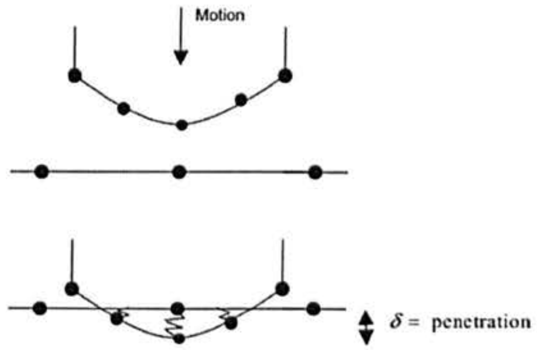

Figure 4.7: Penalty method (adopted from (Engineering Research AB, 2005).

4.5 Generating CAD/FEM Preview

The Simpleware software (v3.1) was used to produce the solid model with the 255 CT-Scan in DICOM (Digital Imaging and Communications in Medicine) format, after uploading of the proper thresholding and segmentation of the bone. The output was initially in the DXF format and then it was converted to the IGS format with mechanical software. The IGS data produced 3D dimensional FE models of human pelvis femur in LSDYNA®.

A file format definition and a network communication protocol were included in DICOM. The header consists of a 128-bytes file preamble, followed by a 4-byte DICOM prefix. It is worth mentioning that the size of the base element in the mesh is decided by the voxel size (the spacing in mm) which influences the density of the generated mesh. If a mesh with a minimum element size of 0.7mm is assumed, the highest mesh density is expected to come from the data. Elements were resampled down to a voxel size of $0.7 \times 0.7 \times 0.7$ mm^3. Finally, the IGS data of CT images was translated to generate a 3D- FE model of the human pelvis–femur complex (see Figure 4.8).

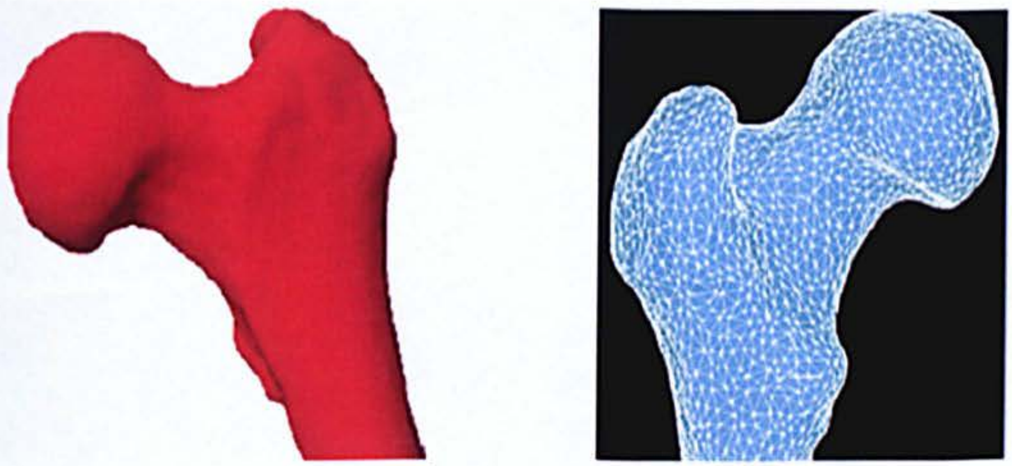

a) b)

Figure 4.8: The 3D model of proximal femur a) CAD model and b) FEM.

The FE modelling was carried by using finite element software LS-DYNA. The LS PREPOST 3.1 was used to analyse the results and also to create the models in the pre/post-processor. The finite element analysis or method is a numerical approach when similar solutions of partial differential equations exist in sub-regions, or elements. Using certain relations between the solutions of all elements gives a complete approximate solution for the entire region.

4.6 Build a Proximal Femur Model

LS DYNA has a vast selection of possible choices for the material model but before building a model, it must decide which element types and material models will best represent the physical system. The following section provides the background information needed to make these decisions.

First, the model to represent the physical system for explicit dynamic analysis has to be created. For this exercise, the proximal femur model built from CT images will transfer from Simpleware to ANSYS software (see Figure 4.9). To perform the analysis with the ANSYS graphical user interface (GUI), the Preferences options must first be set (Main Menu> Preferences) to "LS-DYNA Explicit". This will cause menus to be filtering properly to show explicit dynamics input options. (It is important to note that setting the preference to LS-DYNA Explicit it does not activate an LS-DYNA solution).

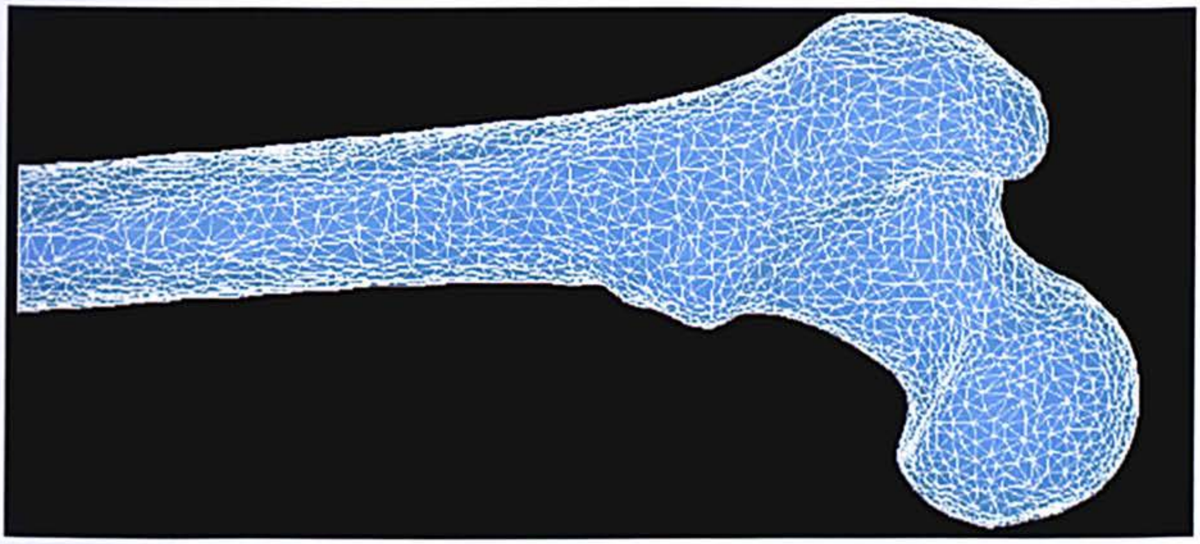

Figure 4.9: 3D model of proximal femur built from CT images in Simpleware transfer to ANSYS software.

4.7 Material properties of Cortical bone

The classical bilinear isotropic hardening model requires an elastic and plastic slope to represent the stress-strain behaviour of a cortical bone material (see Table 4.1), (Majumder *et al.,* 2008). The cortical bone specimen was simulated with Piecewise linear plasticity material. With Piecewise linear plasticity material it can be defined an elasto-plastic material with an arbitrary stress versus strain curve and arbitrary strain rate dependency. The stress strain behaviour may be treated by a bilinear stress strain curve by defining the tangent modulus. This material includes two attributes: Strain-rate effects and failure criteria.

In LS-DYNA the cortical bone was modelled by type 24 which is defined as MATERIAL_PIECEWISE_LINEAR_PLASTICITY, pertaining to von misses yield condition with isotropic strain hardening, and strain rate-dependent dynamic yield stress based on Cowper and Symonds model. The progression of stress beyond yield (according to scaling algorithm) for this model is:

$$\sigma_y\left(\varepsilon_{eff}^P, \dot{\varepsilon}_{eff}^P\right) = \sigma_y\left(\varepsilon_{eff}^P\right)\left[1 + \left(\frac{\dot{\varepsilon}_{eff}^P}{q}\right)^{1/p}\right] \tag{4.41}$$

where $\varepsilon_{eff}^P, \dot{\varepsilon}_{eff}^P$ are the effective plastic strain and strain rate, p and q are strain rate parameters.

4.8 Material Properties of Cancellous Bone

Cancellous bone is known as a composite material with a complex hierarchical structure. At macroscopic continuum level, bone exhibits orthotropic behaviour with inhomogeneous material properties. It has been also observed that the tensile strength of bone is smaller than its compressive strength suggesting that it exhibits a quasi-brittle material behaviour (see Table 4.1), (Hambli *et al.*, 2012).

Table 4.1: Details of material properties for the 3D FE model of the pelvis-femur complex (Hambli *et al.*, 2012).

Modelling entities	Density (gm/cm³)	Young's modulus (MPa)	Yield stress (MPa)	Post yield tangent modulus (MPa)	Poisson's ratio
Cancellous bone	0.042-0.541[a]	32-3340[a]	0.354-40[a]	0.032-3.34[a]	0.2[b]
Cortical bone	1.8[c]	22,700[c]	158[c]	1135[b]	0.3[a]

Determining the elastic constants of cancellous bone by conventional mechanical test procedures is very difficult due to the small size of specimens of human cancellous bone. The data analysis methods (Hambli *et al.*, 2012; Van Rietbergen *et al.*, 1996; Kabel *et al.*, 1999) permit the identification of the elastic constants of trabecular bone in function of volume fraction (BV/TV). The final results are the solid volume fraction dependent orthotropic Hooke's law for cancellous bone with correlation coefficient of 0.934 as follow:

$$E_1 = 1240E_t\left(\frac{BV}{TV}\right)^{1.8} \tag{4.42}$$

$$E_2 = 885E_t\left(\frac{BV}{TV}\right)^{1.89} \tag{4.43}$$

$$G_{12} = 486.3E_t\left(\frac{BV}{TV}\right)^{1.98} \tag{4.44}$$

$$\upsilon_{12} = \upsilon_{21} = \frac{1}{2}\left(0.176\left(\frac{BV}{TV}\right)^{-0.25} + 0.125\left(\frac{BV}{TV}\right)^{-0.16}\right) \tag{4.45}$$

The anisotropic properties of cancellous bone are presented in Table 4.1. Material model 54 of LS-DYNA was selected to model the damage of cancellous bone. The Chang-Chang failure criterion which is the modification of the Hashin's failure criterion was chosen for assessing the failure.

4.9 Mesh Sensitivity Analysis

The cortical bone has been simulated like a shell. And it has been simulated using different mesh sizes to choose the most appropriate element size. The two parameters used to choose the element size were convergence and simulation time. The simulation has been done in Ls-Dyna with Piecewise linear plasticity material type and under integrated shell elements (integration with four point).

4.10 Contact Constraint

Contacts between separately meshed objects have to be set as a substitution for boundary conditions. As gaps initially exist between the boundaries of side by side objects, constraints are needed to prevent penetration during motion. To establish a good contact between side by side objects, the gaps between their boundaries have to be within some distance limit over the whole surface and the surfaces need to follow similar geometry. The contact "Tied surface to surface" is used for two contacts, between the Femur sutures and rigid suture.

4.11 Finite Element Modelling (FEM)

The previous study (Keyak, 2001) demonstrated that matched pairs of fresh-frozen human cadaveric proximal femora, obtained from ten female and eight male Caucasian donors aged from 52 to 92 (mean, 70.3year), were used for mechanical testing. The force was directed in the coronal plane at an angle of 20° to the shaft while the shaft was restrained. The proximal femora were mechanically tested to failure at 0.5 mm/s using a servo hydraulic testing machine. Force and displacement data were recorded at 200 Hz. Measured fracture load was defined a priori as the maximum load achieved (see Figure 4.10).

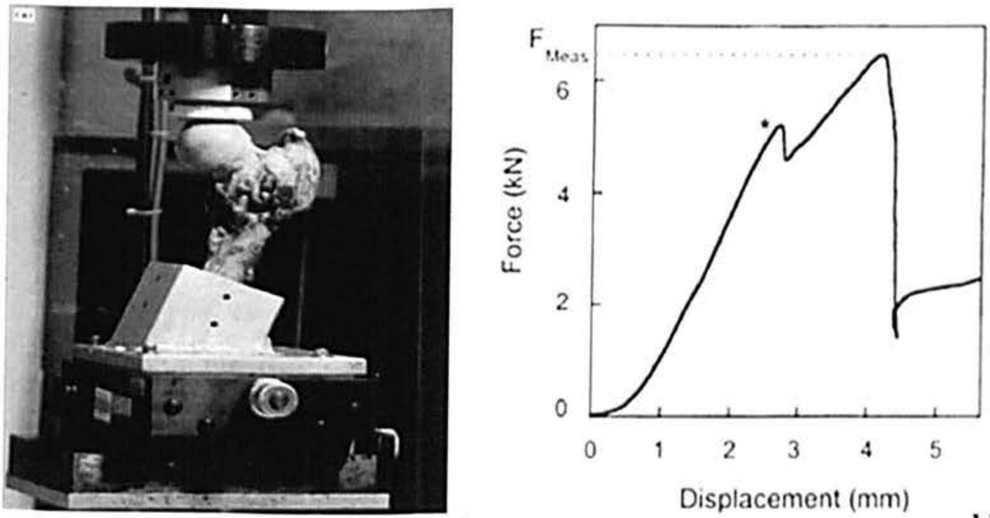

a) b)

Figure 4.10: a) Mechanical testing of a proximal femur. The force was directed in the coronal plane at an angle of 20° to the shaft and b) force–displacement curve obtained during mechanical testing (Keyak, 2001).

The hip was modelled using SHELL 163 which is a 4-node element with both bending and membrane capabilities. SHELL163 is a 4-noded element with both bending and membrane capabilities when used for the 3-D modelling of solid structures. It permits the use of in-plane and normal loads. Twelve degrees of freedom are available at each node-translations, accelerations, and velocities in the nodal x, y, and z directions and rotations about the nodal x, y, and z axes. The SHELL163 element offers the availability of 12 different formulations. The number of integration points per element directly impacts CPU time - as is the case with solid elements. So the reduced integration shell formulations are recommended for general analyses (see Figure 4.11).

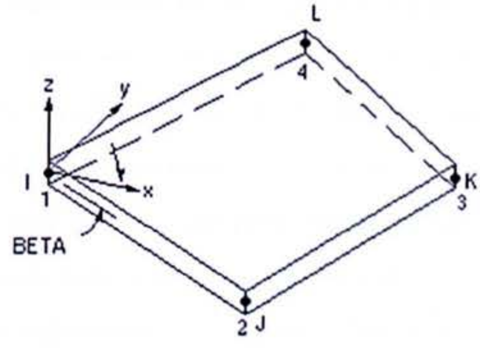

Figure 4.11: *Shell 163* Geometry in LS-DYNA.

The Belytschko-Lin-Tsay quadrilateral element formulation is the fastest of the explicit dynamics shells. This element formulation, which is also based on the Mindlin-Reissner assumption (Ghasemnejad *et al.,* 2009) to include the transverse shear, was chosen for FE analysis (see Figure 4.12).

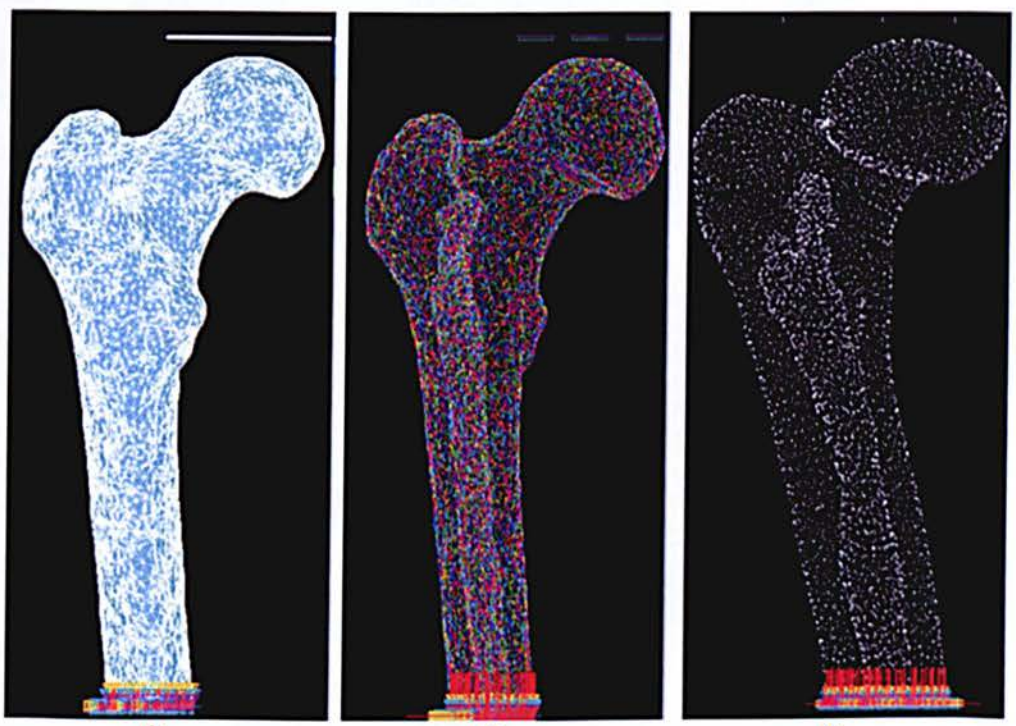

a) **b)** **c)**

Figure 4.12: Finite element model (FEM) in LSYNA. All DOF are restricted at the bottom edge, a) areas of hip, b) lines to make areas and c) key point distribution.

All surfaces of the model were meshed using quadratic shell element with the free mesh size (see Figure 4.13). In this work the two parts of bone, cortical and cancellous, were modelled with the integration point (IP) through the thickness of the element, with regard to allocated material ID and thickness of each section. The striker was modelled as a rigid block using a solid element. The contact between the rigid plate and the specimens was modelled using a nodes impacting surface with a friction coefficient of 0.35 which was measured experimentally to avoid lateral movements. To prevent the penetration of the crushed box boundary by its own nodes, a single surface contact algorithm without friction was used.

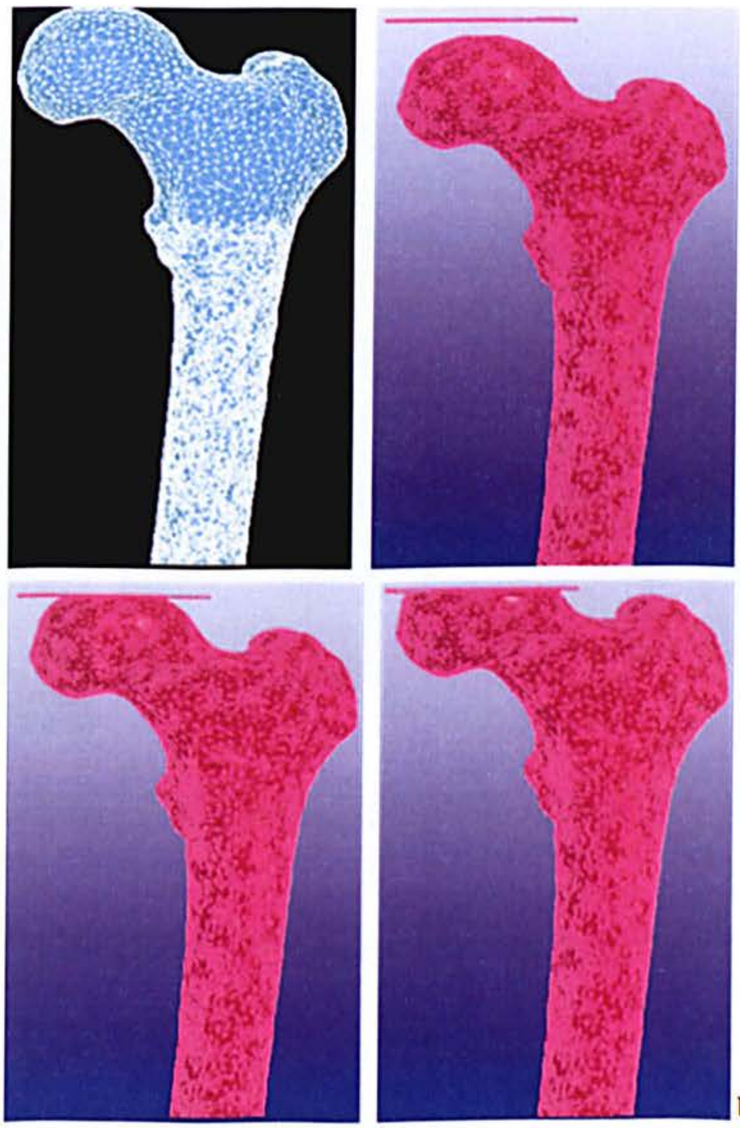

a)

b)

Figure 4.13: Finite Element Model of hip a) Pre-processing (mesh generation) and b) Post-processing (element deformation) in LSDYNA.

To simulate the quasi-static condition, the loading velocity of 1 m/s was applied to the rigid striker. However, the real loading speed was too slow for the numerical simulation. The explicit time integration method is only conditionally stable, and therefore by using real crushing speed, very small time increment is required. In this case the response of internal energy is very similar with one another and the kinetic energy is negligible in comparison to internal energy. For satisfying quasi-static conditions not only the total kinetic energy has to be very small compared to the total internal energy over the period of the quasi-static process, but also the force-displacement response must be independent from the applied velocity (see Figure 4.14).

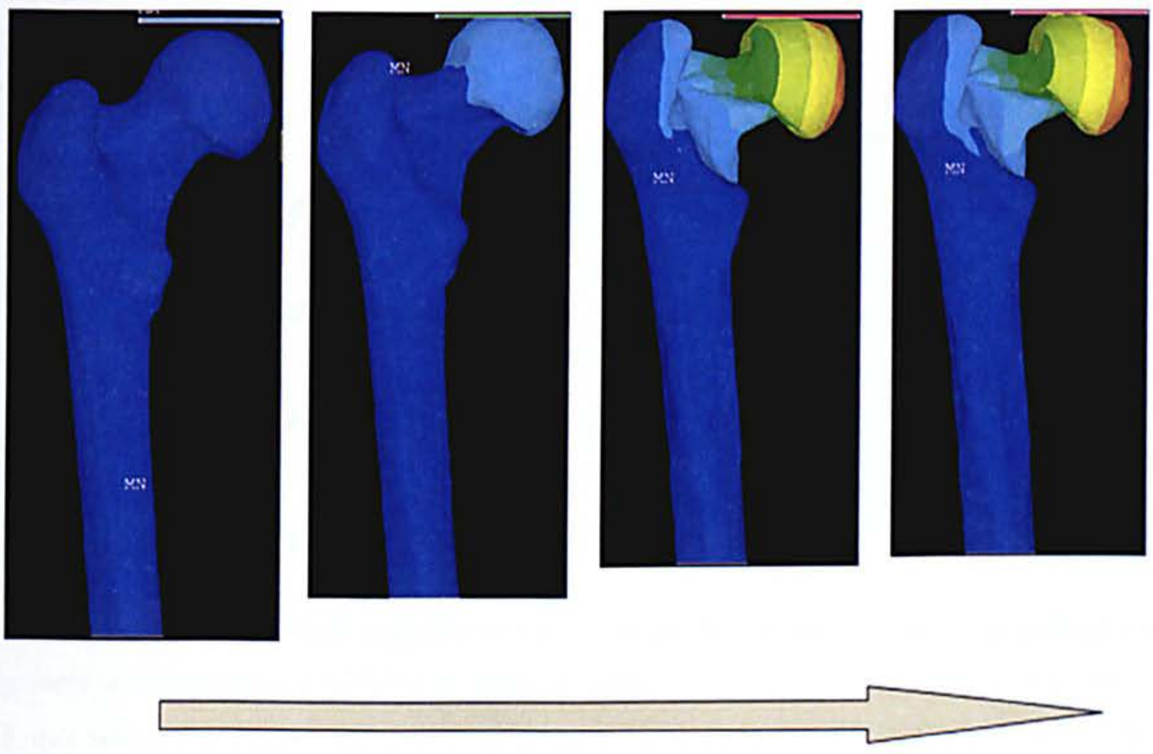

Figure 4.14: Finite Element Analysis (FEA) in axial deformation of hip at various stages in LSDYNA.

In Figure 4.15 the force-crush distance of all off-axis loading angles which were extracted from the FEA model is compared with the experimental results. The difference in maximum force and energy absorption between the FEA model and experiment is less than 5%.

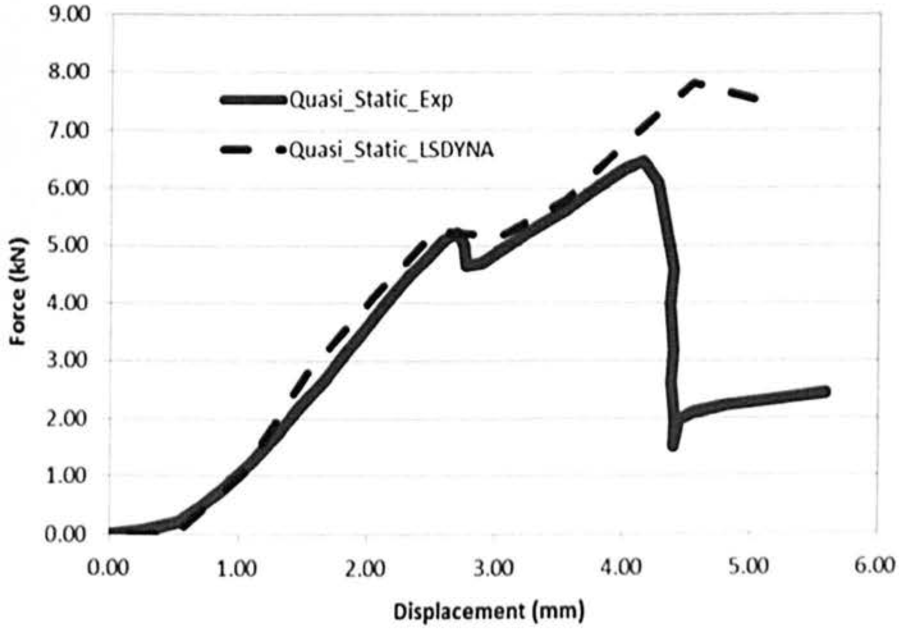

Figure 4.15: Comparison of Experimental data (Keyak, 2001) and FE modelling.

4.12 Effect of Various Impact Velocities

The effects of hip impact velocity, V, variations on the damage process of an osteoporosis hip were investigated in LSDYNA®. Various impact velocities of 1.9, 2.3, 2.6, 3.1, 4.0 and 4.5 m/s which have been reported in literature (Hambli *et al.*, 2012; Gomez *et al.*, 2005; Kroonenberg *et al.*, 1995) were chosen in this study. The cortical thickness was kept constant as 3.7 mm which represents a real sideways. The body weight of this person was set as 77.74 kg. In this case, the applied kinetic energy during the sideways fall was quantified according to various impact velocities. The solver was set for 70 ms fall duration. A time step increment of 4.32×10^{-4} ms solved the problem. The mass-scaling option was also applied to reduce the CPU time which led to average 20 h (see Figure 4.16).

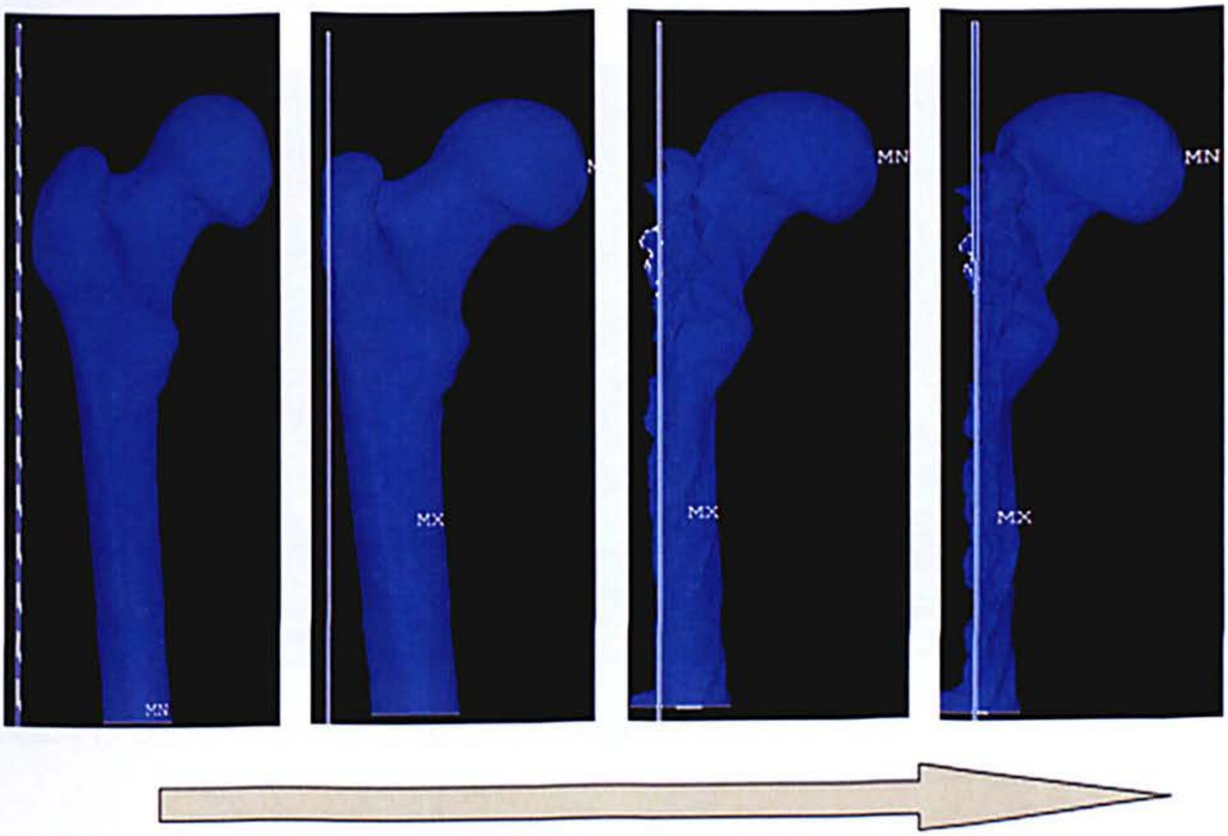

Figure 4.16: Various stages of sideways fall impact in LSDYNA.

4.13 Effect of Various Cortical Thicknesses

In the second part, effects of cortical thickness on the impact resistance of osteoporosis hip are studied. Different values of cortical thicknesses in the range of 3.4, 3.7 and 4mm were chosen in this study. Other parameters such as mass (77.74 kg) and velocity (1.9 m/s) were kept constant. In FE modelling, instead of dropping the whole body from standing position with zero initial velocity, the proximal femur solid model was placed laterally just 5 mm above the rigid floor. This technique led to reduce the CPU time. The rigid floor was also defined as non-translational and non-rotational in the FE model (see Figure 4.17).

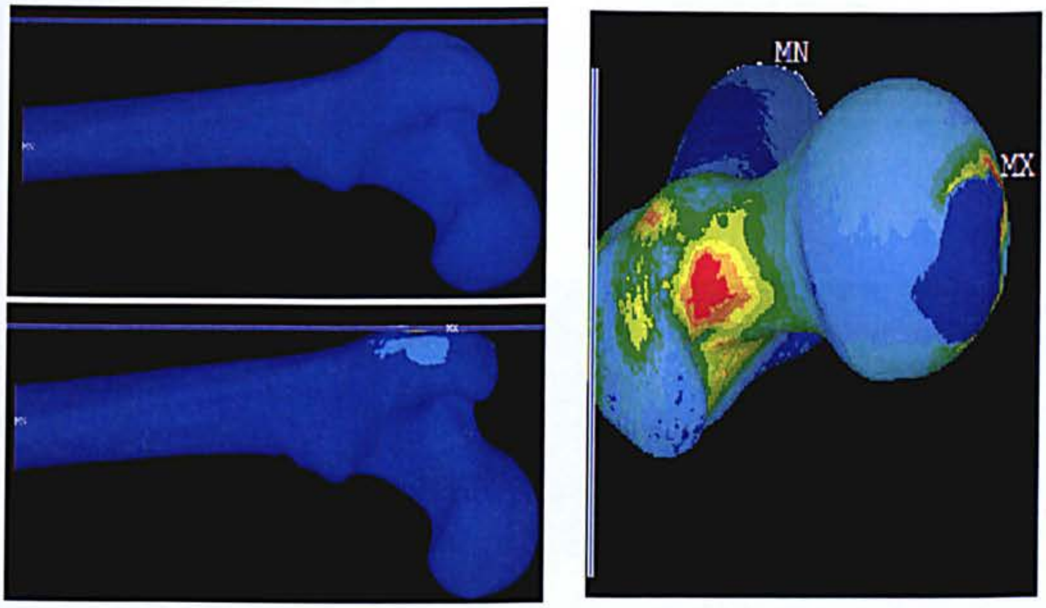

Figure 4.17: Effect of various cortical thicknesses and impact velocities in LSDYNA.

4.14 Effect of Cortical and Impact Velocity on Neck and Intertrochanteric Crack in Sideways Fall

From the previous studies which were mentioned in the literature review, in general, most femoral fractures are caused by side falls. Nevertheless, spontaneous fractures account for a significant amount of hip fractures. Consequently, both cases are commonly investigated using FE by simulating the side fall and the single-legged stance. The numerical example presented here follows closely the experimental investigation discussed by Keyak, 2001, where a left proximal of a male (age 61) was loaded until failure under one-leg stance.

Simulation, cracks were formed and initiated at around neck and intertrochanteric into the FEA model, virtually in straight line with thickness of 3 mm and propagated under an angle of $43.8^0 \pm 6.70^0$ with horizontal. Boundary and loading conditions are chosen according to the literature review reported in the previous chapter. The cortical thickness was kept constant as 3.7 mm which can reconstruct a real sideways fall for a person. The body weight of this person was set as 77.74 kg. In this case, the applied kinetic energy during the sideways fall was quantified according to various impact velocities (see Figure 4.18).

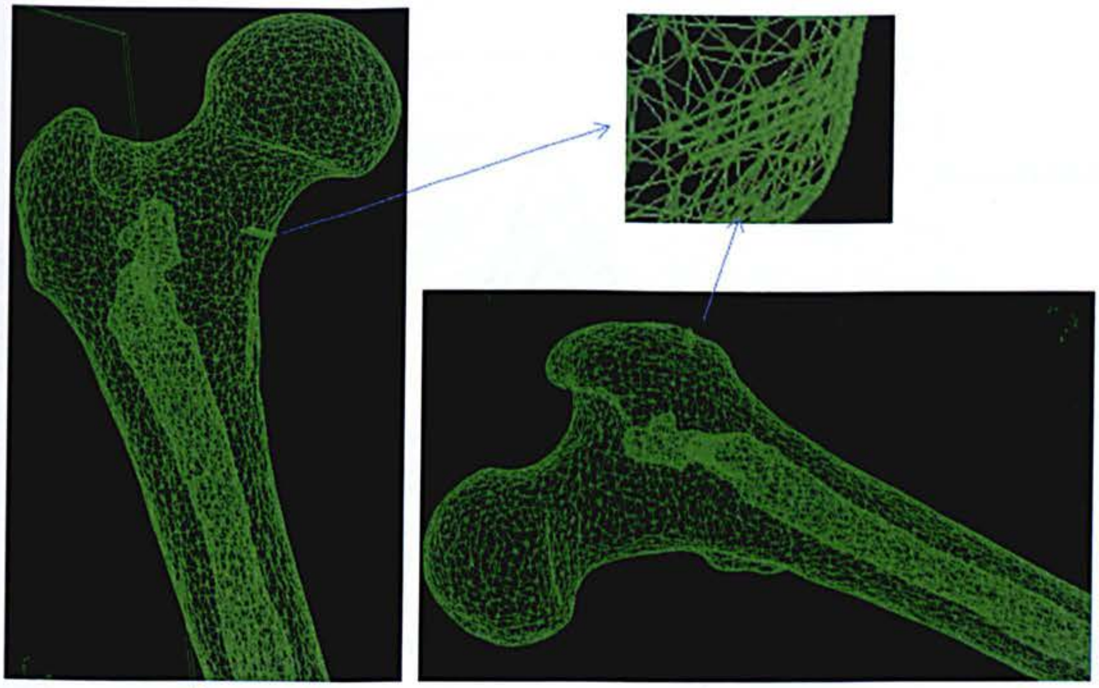

a) b)

Figure 4.18: a) Neck crack and b) Interochanteric crack.

4.15 Discussions and Results

In this work, the effects of various impact velocities and cortical thickness were studied on the impact damage of femur-hip. First, the impact velocity was kept constant as 1.9 m/s and the cortical thickness variables were set to 3.4, 3.7 and 4 mm. The results indicated that high acceleration can be experienced by the bone as the cortical thickness increases (see Figure 4.22). The force-displacement history was also extracted for the effect of change of thickness on the impact damage process of hip bone (see Figure 2.21). As it can be seen in Figure 4.23, an increase of cortical thickness causes higher energy absorption capability within bone structure. Second case studies were allocated to a change of impact velocity (1.9, 2.3, 2.6, 3.1, 4, and 4.5 m/s) with a constant cortical thickness of 3.4mm. Due to an increase of impact velocity, the experienced acceleration by the bone increased to higher values which causes raising the acceleration-time curve (see Figure 4.22a). The absorbed impact energy at different thicknesses of 3.4 and 3.7 mm cortical thicknesses has been compared in Figure 4.23; it is shown that increasing the impact velocity significantly increases the energy absorption capability of bone structures.

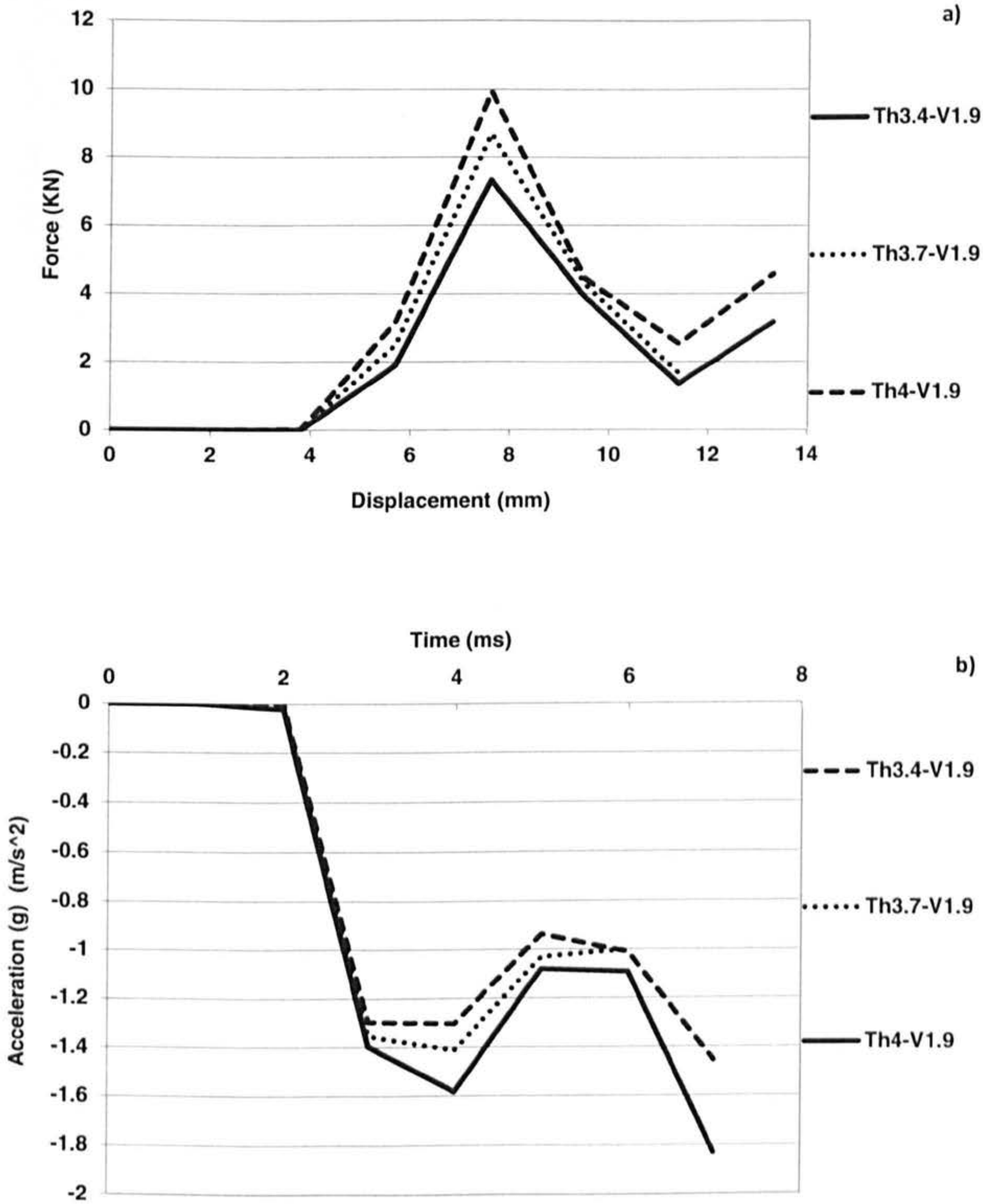

Figure 4.19: a) force-displacement histories for variation of cortical thickness and b) Force-time.

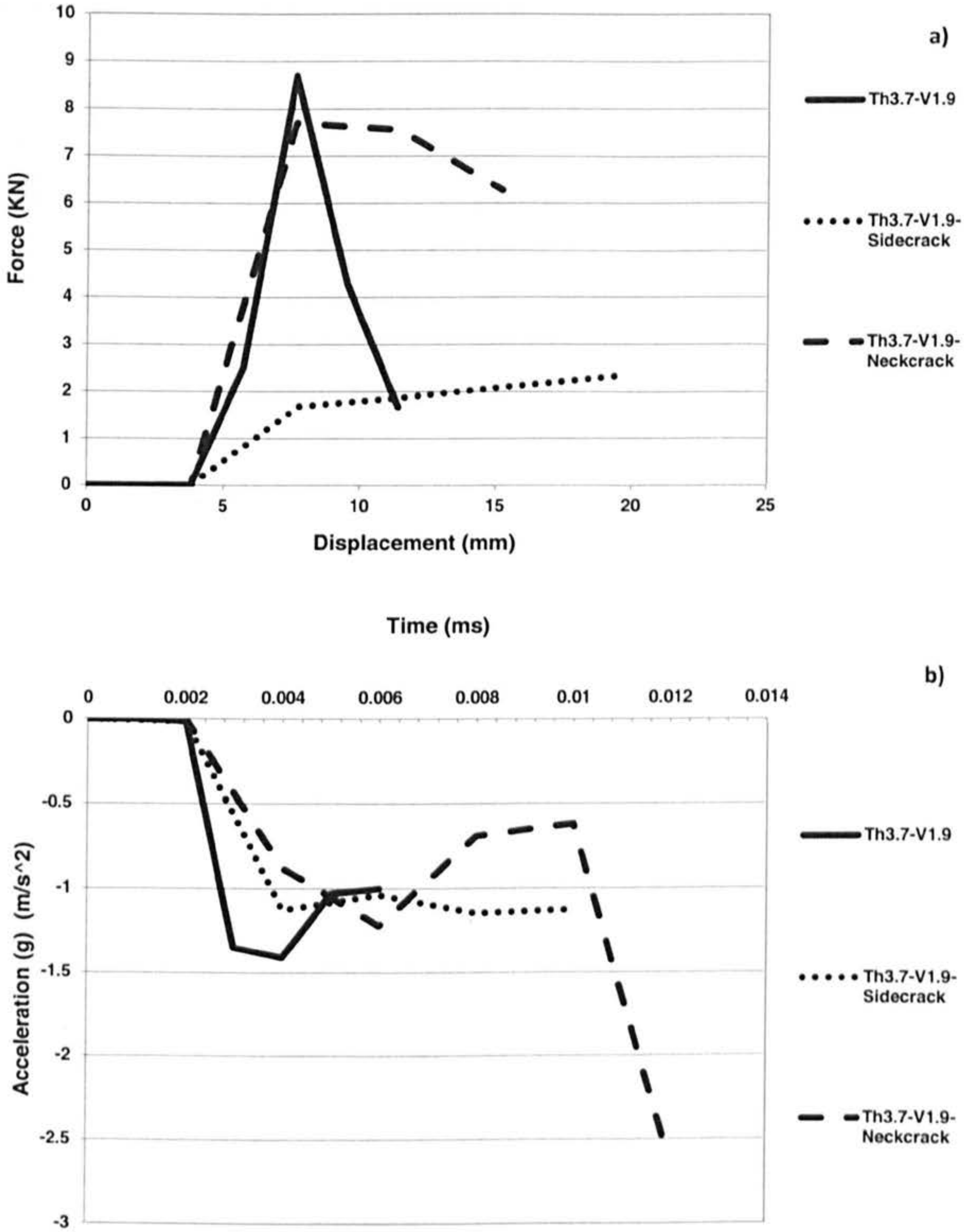

Figure 4.20: a) force-displacement and b) Acceleration-time histories of cortical and impact velocity on Neck and Intertrochanteric crack in sideways fall.

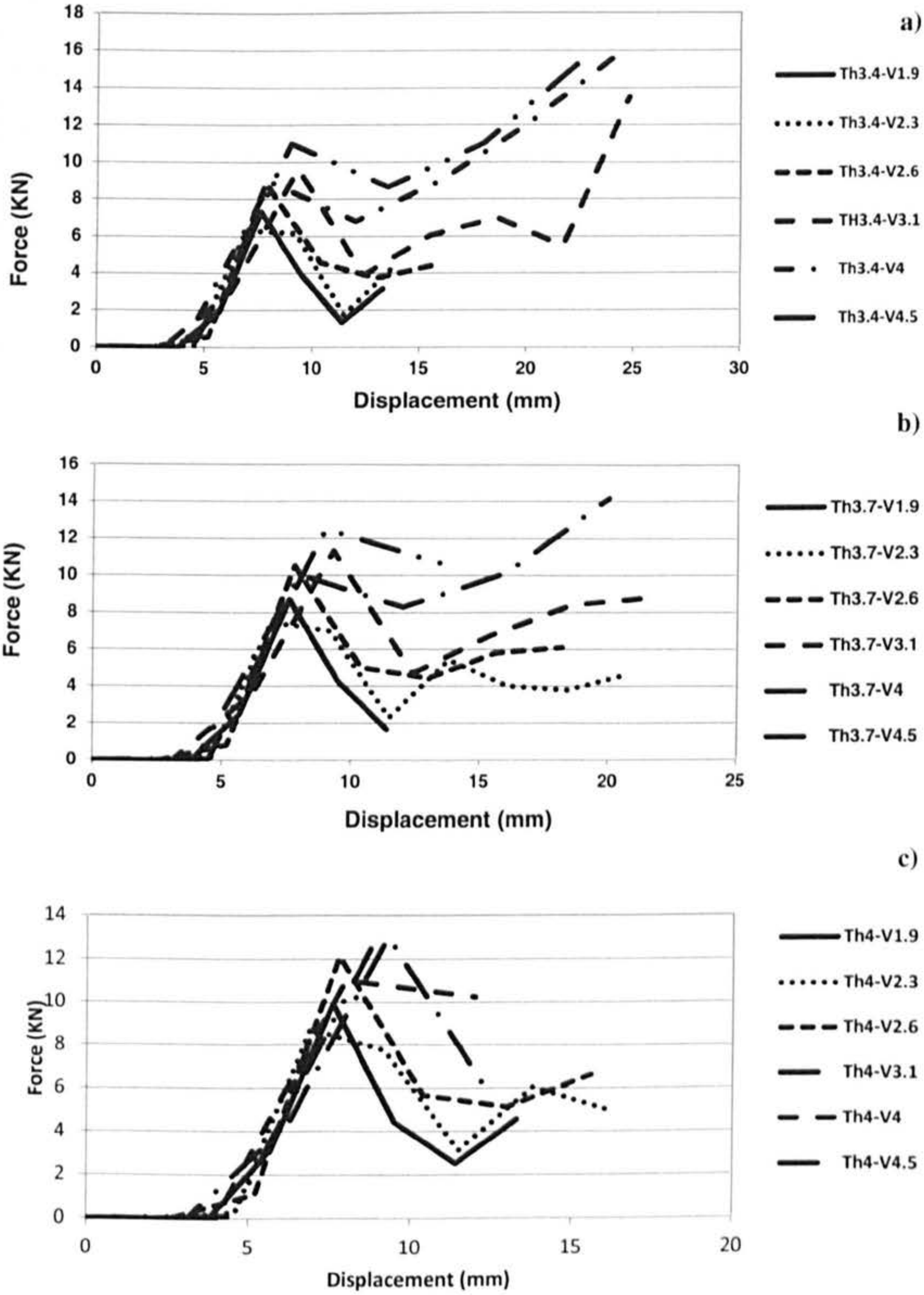

Figure 4.21: Force-displacement results for various cortical thicknesses; a) 3.4 mm, b) 3.7 mm, c) 4mm and impact velocities.

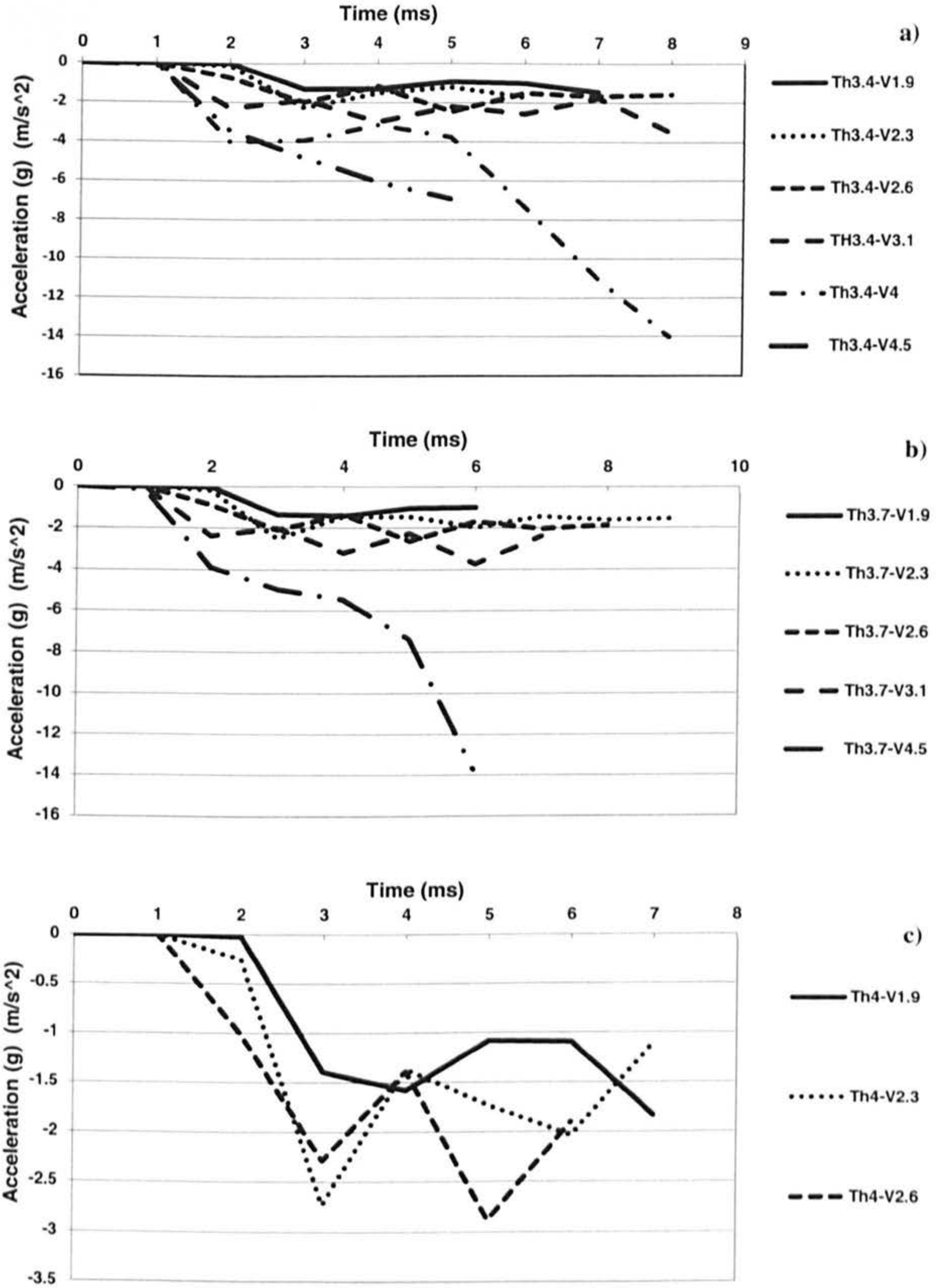

Figure 4.22: Acceleration-time history of cortical thicknesses of a) 3.4, b) 3.7 and c) 4mm and various impact velocities.

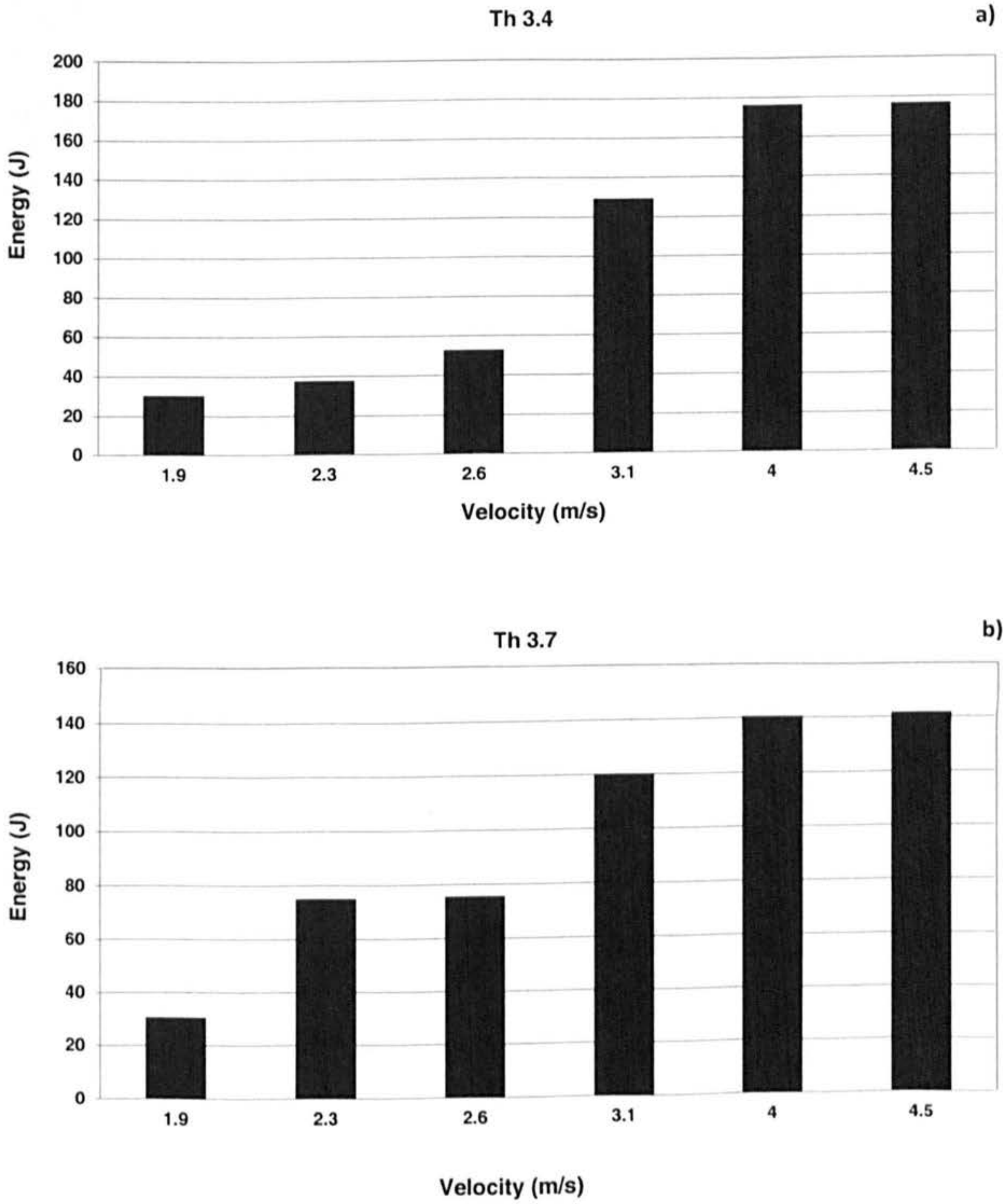

Figure 4.23: Kinetic Energy-time history of cortical thicknesses of a) 3.4 and b) 3.7 mm, various impact velocities.

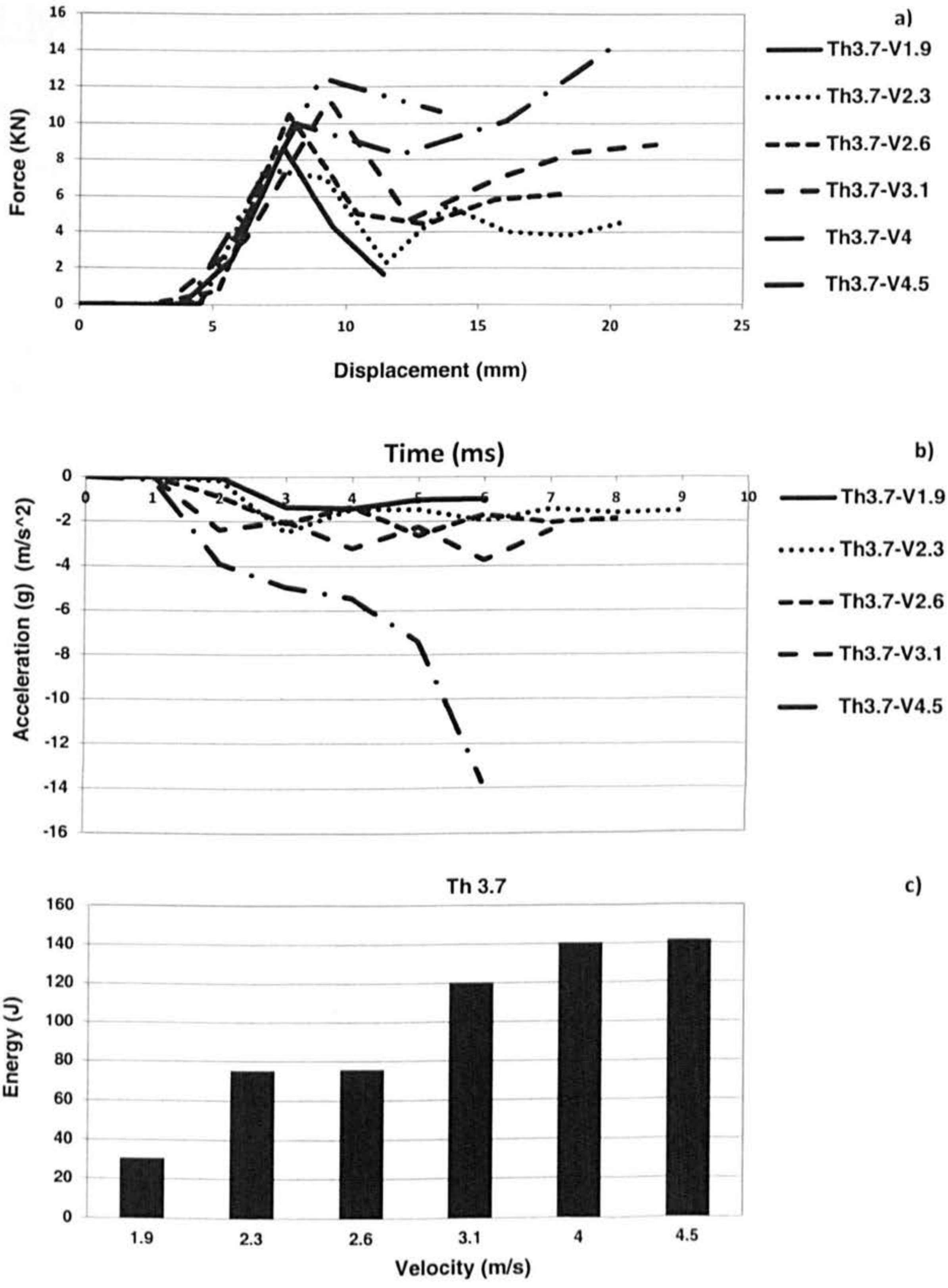

Figure 4.24: a) Force-displacement, b)Acceleration-time history and c) Kinetic energy vs time histories affecting of various impact velocities on cortical thickness of 3.7.

Chapter 5 - A Practical Approach

5.1 Introduction

The interest in assessing the mechanical properties of human bones which discover their behaviour and the traumatic injury patterns has been an interest for clinicians and engineers. Biomechanical analysis includes two methods frequently, first of all the experiment is carried out in-vivo and in-vitro. Human subjects are used for in vivo experimental studies which as a result have provided an accurate picture of what is clinically relevant. As a result, for almost a century mechanical in-vitro tests have been carried out on human cadaveric bones and long bone implants (Roesler, 1987).

Physiologic loading has been observed by researchers to be an intricate interaction of soft and hard tissue which has been found difficult in replicating real-world physiological conditions experimentally. Therefore researchers have created and implemented simple approaches to biomechanical testing by carrying out axial compression, lateral bending, torsion, 3-point bending and 4-point bending tests independent of each other (Zdero *et al.*, 2008). Cadaveric bones have many disadvantages in experimental testing. In order to acquire bones from cadavers, the requirement of consent from the family of deceased has to be considered as well as ethical approvals. Secondly if studies last several weeks, they can change the mechanical properties as seen in experimental investigations by McConnell *et al.*, (2008) where axial stiffness decreased by 30% over several months.

Cadaver bones which have been embalmed seem to have succeeded in preventing change in mechanical properties only after several months of the specimen being embalmed (Wainer 1990). The inter-specimen variability in material and geometric properties is the most essential aspect that faces both cadaver and embalmed bones. The studies carried out by Zdero *et al.*, (2007), showed that torsional and axial stiffness for human femurs intact varied by 3.3 and 3.2 times. Due to this inconsistency between specimens results in a large discrepancy in measured results. Synthetic long bones have advantages over cadaveric specimens and as a result are becoming more popular. These bones are easy to manufacture and have a geometry that is consistent which is 20-200 times more uniform than cadaveric bones. These bones do not decay over time, they are easy to store, non-toxic and are available commercially and relatively cheap to acquire.

This in turn includes the FEA modelling software which has enabled the development of more accurate models that behave similarly to actual human bone (Cheung *et al.*, 2004; Van Rietbergen *et al.*, 1995). Studies show that FEA provides a close approximation for comparing the performances of several implants. However for absolute predictions, clinical conditions would need to be replicated. Although FEA cuts down costs and time, it is still limited as models get more complicated such as introducing fracture fixation devices and the modelling of forces. These become difficult to model on FEA requiring assumptions to be made which may not be valid (which in turn may not give accurate results). For example, boundary conditions in FEA at the interfacial contact regions could affect the distribution of loads between bone and implant.

The assumption of bonded contact between the two surfaces in order to achieve perfect Osseo integration is considered in FE models i.e. bony growth around the implant. In reality this may not affect results. This investigation focuses on the assessment of the mechanical behaviour of the femur bone compared to the fresh-frozen specimens experiment carried out by Keyak, (2001) and the developed FEA model. FE models usually treat bone as a continuum as opposed to focusing on its microstructural details. This approach is enough for implant design when relative rather than absolute results are used in comparison between devices with respect to performance. It is essential that clinical conditions are replicated should the absolute quantitative performance of an implant be predicted. Even though many researchers persevere to legitimately carry out experimentation and FEA separately from one another, combining the two has advantages. Experimentation would be able to assess on what degree an FE model can successfully replicate more real-world conditions.

FEA on the other hand, has the ability to mimic loading conditions and extend data analysis far more than what is possible to perform in a laboratory setting. Two caveats must be kept in mind; firstly experimental setups should be able to simulate real-world physiological conditions as much as possible even though their inevitable limitations are recognized. Secondly, accurate and proper verification, validation and sensitivity of the FEA analysis should be run to ensure that the models are working properly.

Therefore the aim of this section will be to present practical tools for engineers and clinicians who combine mechanical experiments and FEA to successfully carry out orthopaedic biomechanics research. A specific overview will be given of the purpose, principles and data assessment when performing mechanical testing and FEA as independent research modalities. This will be followed by a practical and computational analysis which will be used in combination to generate results which assess a practical case study of a real world orthopaedic biomechanics problem.

5.2 Background to the Composite Bone

Composite bones replicate femurs (Sawbones, Pacific Research Laboratories, Inc., Vashon, WA) are widely used in orthopaedic research, and have undergone several design changes since their introduction in 1987. The second generation of composite bones with a fiberglass fabric reinforced epoxy for the cortical bone analogue was introduced in 1991, and the structural properties of these bones have been reported in (Cristofolini *et al.*, 1996; Cristofolini and Viceconti, 2000; Heiner and Brown, 2001). The third generation of composite bones, with a short glass fibre reinforced epoxy for the cortical bone analogue, was designed in 1998 to improve uniformity of mechanical properties and anatomic detail on the bones (Pacific Research Laboratories, Inc., 1998). This generation had similar inter specimen variability in structural properties when compared to the second generation bones under bending and torsional loading.

They also have significantly less variability under axial loading and they reasonably approximated the structural stiffness's of natural human bones (Heiner and Brown, 2001). Fourth generation composite bones are now available and they have the same geometries as the third generation bones. The cortical bone analogue material which is still a short glass fibre reinforced epoxy has been changed in order to provide better fracture and fatigue resistance, and to increase tensile and compressive strengths, thermal stability and moisture resistance (Pacific Research Laboratories, Inc., 2007). This fourth-generation cortical bone analogue material was shown to have better fatigue behaviour (higher fracture toughness, higher threshold stress intensity to propagate a crack, and a lower fatigue crack propagation rate) compared to the third generation cortical bone analogue material (Chong *et al.*, 2007b).

Additionally, the fourth-generation material's tensile yield modulus, ultimate tensile strength, fracture toughness, and fatigue crack propagation behaviour were closer to the values for fresh-frozen human cortical bone than were the values for the third-generation material (Chong *et al.*, 2007b). In a different study, third- and fourth-generation femurs were implanted with total hip femoral stems, immersed in an environmental chamber (isotonic saline solution at body temperature), and their fatigue performances were compared (Chong *et al.*, 2007a). In a cycled compression between 267N and 2670N at 5Hz in a simulated one-legged stance, the fourth-generation femurs had much better fatigue performance; the third-generation femurs experienced complete structural failure at an average of 3.16 million cycles, while the fourth-generation femurs survived to 10 million cycles without any structural failure, noticeable external crack formation or substantial change in actuator deflection (indicative of internal crack formation).

In-house testing by the company (Pacific Research Laboratories, Inc., 2007) demonstrated that the tensile and compressive strength and modulus values of the Table 5.1 Tensile and compressive properties of third-generation composite (3rd gen.), fourth-generation composite (4th gen.) and natural human cortical bone (Pacific Research Laboratories, Inc., 2007; data used with permission).

Table 5.1: Comparison of 3rd generation and 4th generation composite (Pacific Research Laboratories, Inc., 2007; data used with permission).

	Natural	3rd generation	4th generation
Compressive elastic modulus (GPa)	**17**	**7.6**	**16.6**
Compressive strength (MPa)	**170**	**120**	**154**
Tensile elastic modulus (GPa)	**17**	**12.4**	**16.0**
Tensile Strength (MPa)	**130**	**90**	**107**

Additionally, it was shown that the mechanical properties of the fourth-generation composite bones have been improved with increased fracture toughness, fatigue crack resistance and threshold, as well as increased tensile without any change in anatomical features (Pacific Research Laboratories, Inc., 2007). In this regard, the purpose of the present study was to measure the structural properties of the fourth-generation composite femurs and tibias under quasi-static loading conditions. The fourth-generation composite femur modelled natural cortical bone using a mixture of glass fibres and epoxy resin pressure injected around a foam core. The mid shaft area had an intramedullary canal of 16mm diameter. The cancellous core material comprised of cellular rigid polyurethane foam. The material's characteristics were obtained from the manufacturer and are summarised in Table 5.2.

Table 5.2: Material properties of composite femur specimens (Pacific Research Laboratories, Inc., 2011; data used with permission).

Material Properties of 4th generation composite femur						
		Tensile			**Compressive**	
Layer	**Material**	**Density (g/cm^3)**	**Strength (MPa)**	**Modulus (GPa)**	**Strength (MPa)**	**Modulus (GPa)**
Cortical	**Short glass fibre filled epoxy**	**1.64**	**106**	**16**	**157**	**16.7**
cancellous	**Cellular rigid polyurethane**	**0.2**	**-**	**-**	**3.9**	**0.0475**

The Fourth generation composite femur specimens were designed with a larger canal diameter of 16mm, in order to replicate osteoporotic cortices. This new composite femur also limits the number of screws that can be applied to the femoral shaft and is meant to simulate a worst-case clinical scenario. The detailed geometry of the specimen is shown in Figure 5.1.

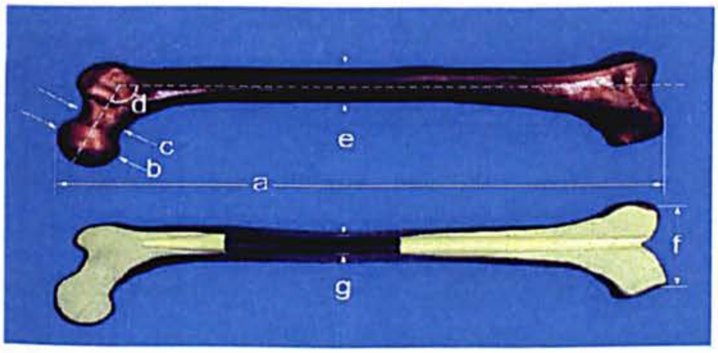

Dimension	
a	485mm
b	52mm
c	37mm
d	120°
e	32mm
f	93mm
g	16mm canal

Figure 5.1: Large left Fourth Generation Composite Femur ((Pacific Research Laboratories, Inc., 2011).

5.3 Anatomy and the Loading Conditions of the Force on Hip

This section describes the methodology used for both the experimental and computational studies. The two forces acting on the bone are $\mathbf{F}_{pelvis}$ and $\mathbf{F}_{tibia}$ in two different axes which are the mechanical axis and the femoral axis (see Figure 5.2).

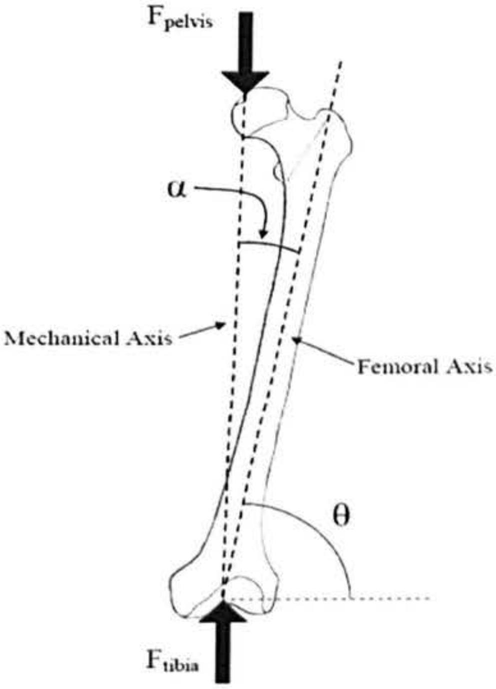

Figure 5.2: A free body diagram of the loading conditions of each femur test.

The mechanical axis is defined as the line between the two forces acting on the femur in its anatomical position. The femoral axis is the line that is parallel to the shaft of the femur. The angle between the femoral axis and the transverse plane is θ. The angle between the mechanical axis and the femoral axis is α which was set around $11°$ in this study.

5.4 Specimen Preparation

Three medium-size of fourth generation medium-sized composite bones (model number: 3403) from Sawbones (Pacific Research Laboratories, Inc., Vashon Island, WA, USA) were examined in this study. Each composite femur was fixed by a clamp then; the femur was subsequently sectioned at two-thirds of its length below the femoral head, and about 250 mm distal to the lesser trochanter and then cut (see Figures 5.3 and 5.4).

Figure 5.3: Sawbones rigidly fixed by a clamp.

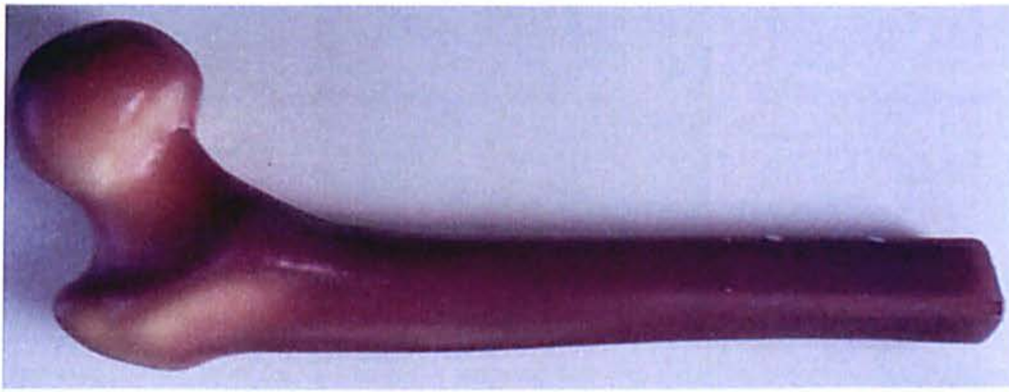

Figure 5.4: A sample of Sawbones' femur bone after cutting.

The femur composite bone was inserted in a jig with the depth being 100mm and secured inside the pot with 8 pointed screws to provide mechanical restraint as well as the jig was mounted rigidly onto the baseplate of the test machine. The femur composite bone was aligned at 20° adduction as shown in Figure 5.5.

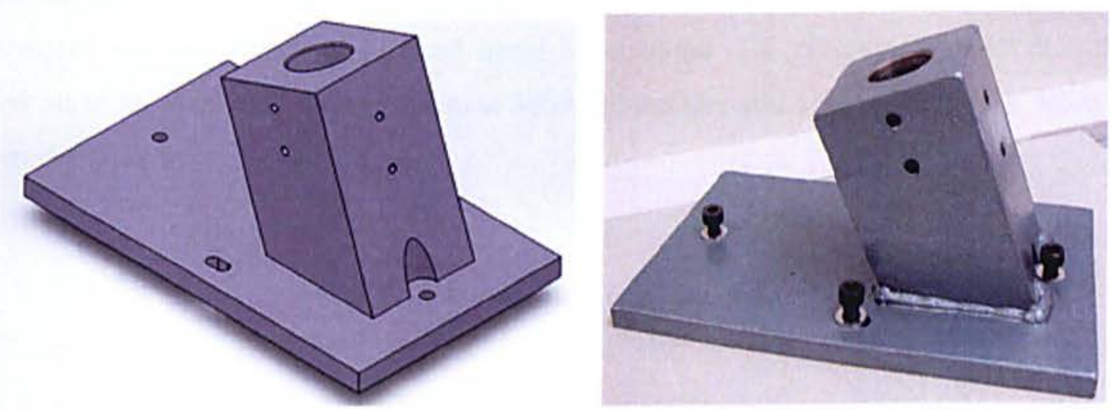

Figure 5.5: Design of fixtures for the experimental studies.

After analyzing the function of the bone support jig created, a slight motion of the bone was observed under test conditions which shown in Figure 5.6. To prevent that motion and to hold the bone firmly during the tests, two additional Tap Holes were drilled. For the screws to be tightened properly, chamfers were made to gain clearance.

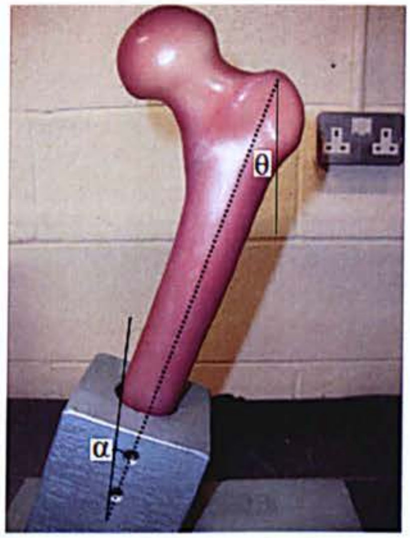

Figure 5.6: The axial loading setup for the composite proximal femurs.

The vertical and horizontal edges of this jig fixture base were also served as a coordinate system that was fixed relative to the femur to facilitate accurate vector derivation and modelling of the applied load. In this study the positioning of the femur bone at the given angle of $\theta = 20°$ was necessary in order to try and replicate the way a natural femur head is distally referenced in the two legged-stance of a human being.

In this case, values close to those acquired from the simulations of tensile stress loadings experienced on the natural femur head could be obtained. The composite model was then loaded on to an axial load testing machine between a platen and a jig secured to a datum as shown in Figure 5.7.

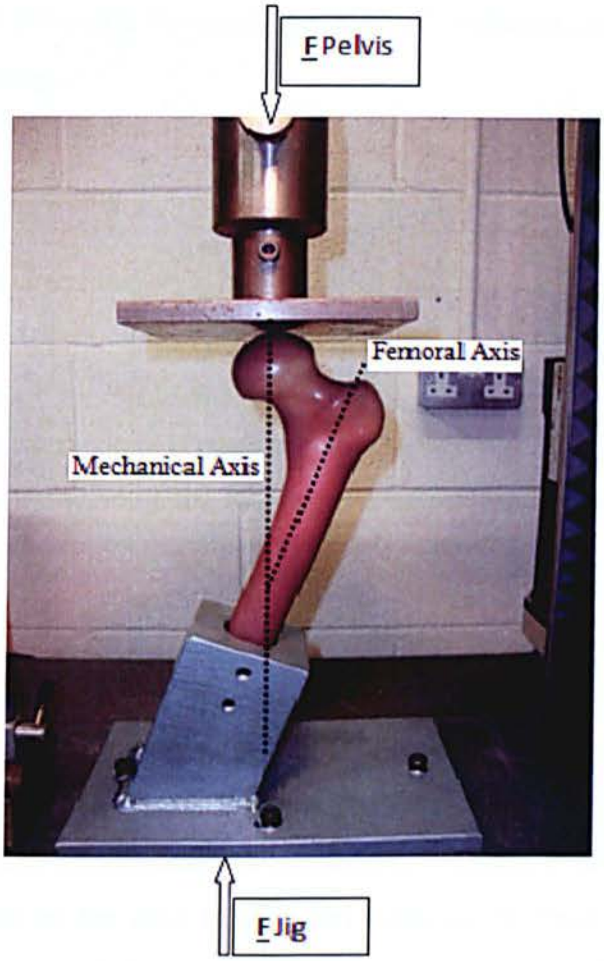

Figure 5.7: For the stance configuration, force was applied to the femoral head over a 3cm diameter region within the coronal plane and directed at 20° to the shaft axis while the shaft was restrained.

5.5 In-vitro Biomechanical Testing

The purpose of in vitro biomechanical testing is to create and obtain valuable pre-clinical data to the researchers and clinicians. It allows the intact human joints, long bones and soft tissue to be mechanically characterized. The experiment assesses the performance of joint prostheses and bone-implant fracture fixation constructs. It provides the ability for engineers and surgeons to improve the design of a potential new implant or surgical technique under controlled laboratory conditions. It helps researchers decide upon the feasibility to expand on time, energy resources and finances on subsequent clinical studies in live animal or human subjects. It prevents the need for unnecessary introductions of new orthopaedic devices into the market and their implantation into patient populations. As a result, there has been a recent consideration of the need for an evidence-based approach which brings new orthopaedic devices to market. This follows a hierarchy sequence of evaluation approaches, starting with basic biomechanical testing.

5.6 Quasi-Static Axial Loading

Experiments were carried out on a Zwick/ Roell machine included load cell capacity of ±25KN, a resolution of 0.1 N, and accuracy of ±0.5%. The loading frame was at an axial stiffness of 8 KN/ 50mm, joins withstanding a force of up to 7 KN / 50 mm which is 150-250 times stiffer than intact synthetic and human cadaveric femurs. A vertical compressive load was applied on the femoral head of the bone with a displacement control of max = 0.5mm, rate = 100 mm/sec.

There was no slippage of the femoral head observed at the applicator head interface. The load vs displacement curve's slope was defined as axial stiffness. Force and displacement data were recorded at 200 Hz. The loading frame was at an axial stiffness of 260 KN/mm. Therefore no compensation was needed for the intron tester compliance. The test regimes described above have been implemented in previous investigations such as Keyak, 2001. A vertical load was applied on the apex of the head using displacement control method. The force-displacement curve's gradient was also used to calculate the axial stiffness.

5.7 Results

Experimental data with respect to the mechanical behaviour of the femur was carried out to validate numerical methods which are used to assess femoral strength and bone quality. The discrepancy between force-displacement curves from mechanical testing of the cadaver and computational was minimum in comparison with the previous models. In all bones, the fracture was represented as a brittle crack and occurred at the same place which was in the neck-trochanter junction in all. The fracture started initially in a small region on the superior surface and then suddenly progressed through the neck region where low strains were measured earlier (see Figure 5.8).

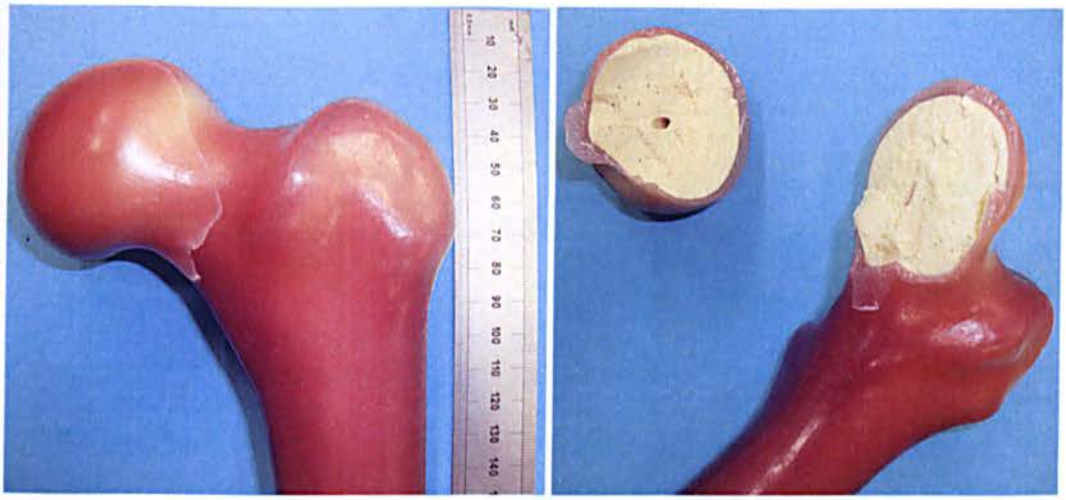

Figure 5.8: shows a Subcapital neck fracture caused due to fatigue under the loading conditions. It is seen that the fracture occurs at the superior surface of the femoral neck and travels down to the inferior surface at the junction between the femoral head and the femoral neck.

The patterns due to fracture at the neck-trochanter junction looked the same, but slightly more lateral to those reported for human cadaver femora during stance load in previous work (Kayak et al., 2001). The force-displacement results showed similar behaviour in the linear region for all bones (see Figure 5.9). This excludes the bone in test 3 which had a lower stiffness and ultimate strength in comparison with the other bones. Hence, the fracture loads for composite bones were as expected and the variability of fracture load was smaller in composite bones than in the cadaver bones. The femur experienced high peak stresses along the neck region, and surface stresses increase as the loads increased particularly in the proximal region. The peak stresses are to be concentrated in the superior region of the femoral neck especially in the posterior region. It seems that micro-damaged has been caused as a result of loading and this could lead to sub capital fracture.

In Figure 5.10, the force-crush distance of all off-axis loading angles which were extracted from the composite bones are compared with experimental data (Keyak, 2001) and FE modelling results. The difference in maximum force and energy absorption between the composite bones and FEA model and experiment are less than 5% in terms of stiffness.

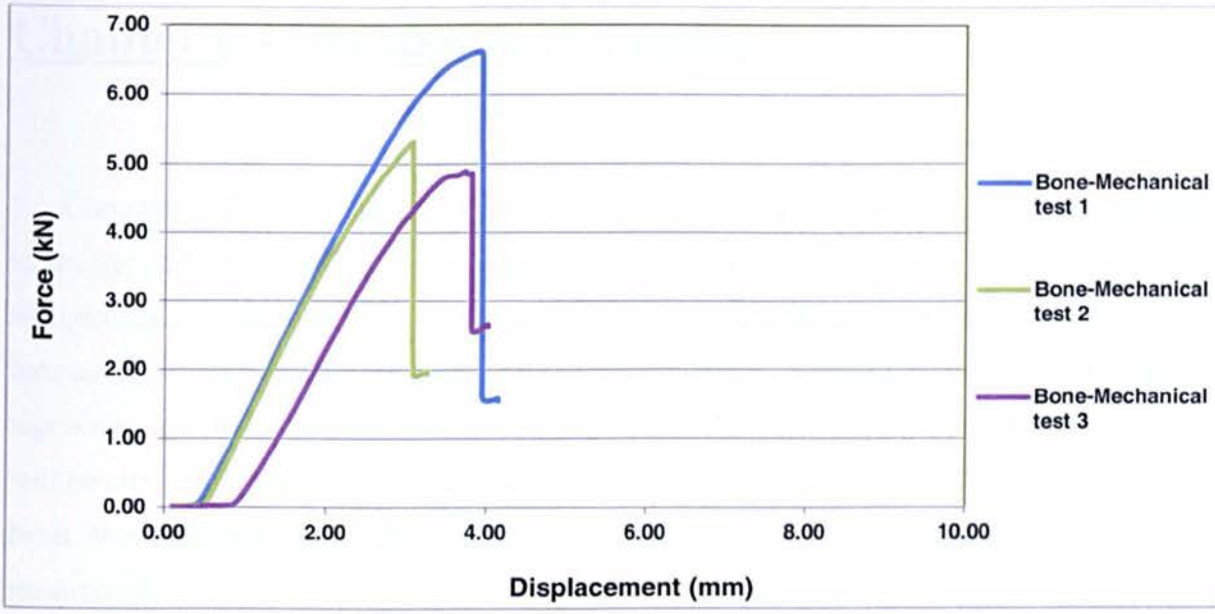

Figure 5.9: Force–displacement curves under axial compression for all three composite bones.

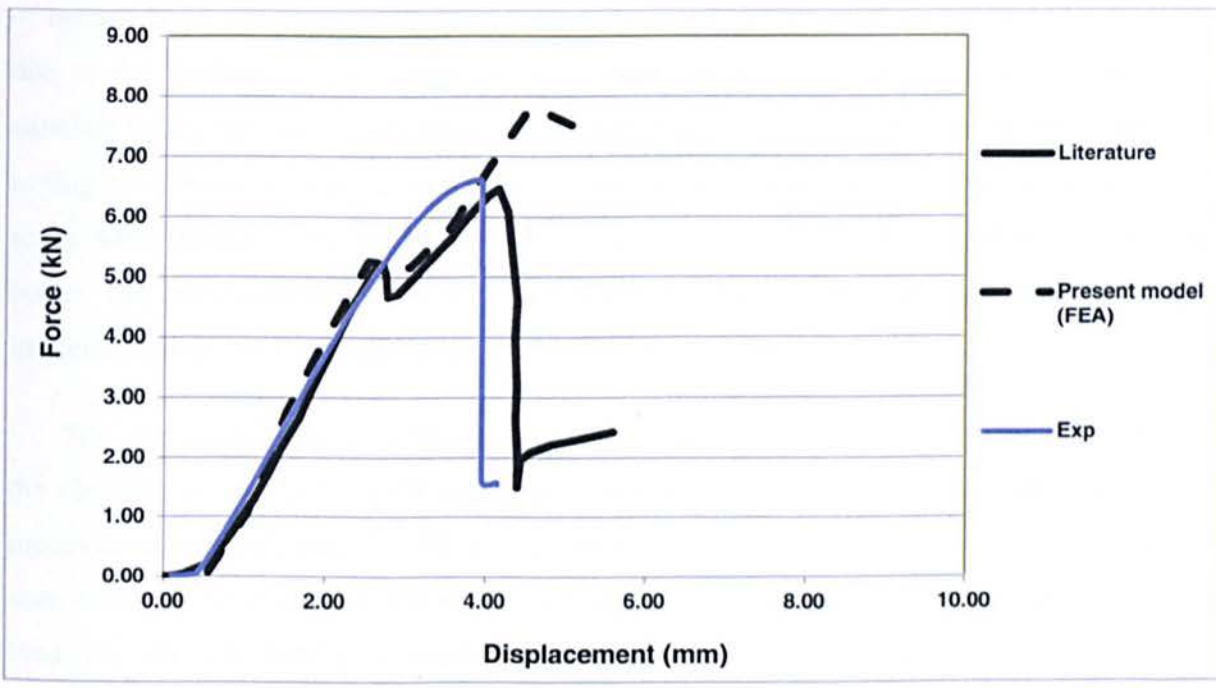

Figure 5.10: Comparison of experimental data, literature (Keyak, 2001) and FE modelling.

In general, there was reasonable agreement between experimental data obtained from mechanical tests and FE analysis, thereby validating the FE model. In orthopaedic biomechanics, an assessment of the mechanical properties of human bones and implants can be done using the proposed FE model in this research.

Chapter 6 - Discussion of results

Computed Tomography based Finite Element simulation is a developing research technique, which is offering the opportunities to test and simulate a wide range of biomechanical situations with increasing complexity and accuracy. The use of medical data increases geometrical accuracy of the simulation which provides a true patient specific representation. It is said that the development of the patient specific simulation techniques will be clinically implemented to assist in the determination of fracture risk on a case by case basis. It is essential that all FE results are simulated with the correct and extensive physical geometries.

The physical testing of human bone samples is a general rule of thumb for the validation of human bone simulation. The increase in number of studies with respect to older adults is due to the increased fracture risk in this cohort. However, studies may also be likely to simulate within this age group due to the increased accessibility of bone samples for physical testing as a result of death from natural causes. In this study, FEA simulation based on CT scans were used to simulate fracture load and compressive fracture of adult porcine long bones. The experimental studies were analysed to validate the geometry and material models implemented within the simulations.

The analysis of measured load-displacement curves in experimental testing showed that the obtained geometry from CT scan data and also the proposed material models in the FE model have been efficient. The FEA simulation was carried out well, illustrating that the CT scan based FE process is capable of performing on different elements and simulating different loads on different cortical thickness. Linear regression and mean error calculation showed accurate readings between predicted (simulated) and observed (tested) results with comparable accuracy to those observed for human samples in cited thesis papers. The relevance of the validated simulation process was confirmed through predicted failure loads of a number of composite femoral samples that were physically tested to fracture axial loads. The accuracy of the thesis can be compared directly with published research, since the original aims (Chapter 1) were selected to investigate the gaps shown in the existing research and also to provide a validated platform for the numerical simulations. The outputs and limitations of this work are detailed in the following section:

In order to predict fracture location and type of fracture for stance and fall-type loading conditions, the ability of automatically produced, CT scan-based FE models of the proximal femur were evaluated in this study. The outcome of new nonlinear FE model is remarkably better than others for the former nonlinear FE models in the stance configuration and models with accuracy parallel to that of current density-based techniques of fracture risk assessment.

The results indicated that high acceleration can be experienced by the bone as the cortical thickness increases (see Figure 4.22). The force-displacement history was also extracted for the effect of change of thickness on the impact damage process of hip bone. As it can be seen in Figure 4.23, increase of cortical thickness causes higher energy absorption capability within bone structure. Due to increase of impact velocity the experienced acceleration by the bone increased to higher values which causes rising the acceleration-time curve. This investigation was also carried out for the effect of change of velocity on the force-displacement history and consequently the energy absorption capabilities of bone structures at different thicknesses and also from the comparative acceleration–time histories (see Figure 4.23).

The absorbed impact energy for various cortical thicknesses has been compared in Figure 4.23. It is shown that increasing of impact velocity significantly increases the energy absorption capability of bone structures. Our results indicated that by increasing cortical thickness and impact velocities, the acceleration experienced during aside fall impact will increase as well as the energy absorption capabilities of bone (see Figure 4.22). Our nonlinear FE models examined here provide an acceptable level of precision for predicting proximal femoral fracture-loads in the stance configuration.

However, fracture loads and applied forces may need to be determined for additional loading conditions, and forces due to muscular action may also need to be considered. Current model is capable of correctly identifying stiffness, failure loads and energy absorption with a reasonable reliability in comparison with the other researches. The difference in fracture load is mainly related to toppling and fracture of specimens during the test while this behaviour wouldn't be modelled in numerical simulations (see Tables 6.1 and

6.2). These investigations would benefit those with the lowest fracture loads who are likely to be at greatest risk of fracture. It would also offer significant scope for clinical practice and implications for early identification of those at risk and prevention measures.

Table 6.1: St= Quasi-Static Axial Loading; Sw= sideways fall configuration; H: skeletally healthy bone specimens, P: bone specimens with clearly reported skeletal pathology, SP: bone specimens containing simulated pathology such as drilled holes representing metastatic lesions.

Study	n	Loading condition	Bone	Material model	Failure criterion	Reference
Present study	6	St + Sw	H, P	Material_ Piecewise_Linear_Plasticity Damage Model	Chang-Chang	-
Dall'Arra et al., 2013	72	St + Sw	H	Heterogeneous isotropic, elastic-damage constitutive law (Garcia et al., 2009), post-yield	Damage model (Garcia et al., 2009)	(Dall'Ara et al., 2013)
Derikx et al., 2011	4	St	H, SP	Heterogeneous non-linear isotropic post-yield*	Comparison of DPYC and VM.	(Derikx et al., 2011)

Table 6.2: The comparison between fracture load of present studies and previous researches: St= Quasi-Static axial loading.

Study	Loading condition	Fracture load data		Percentage error
		F_{FE} (N)	F_{Exp} (N)	
Present study	St	7830	6621(±722)	**18%**
Dall'Arra et al., 2013	St	4868	8684 (±2916)	**45%**
Derikx et al., 2011	St	5203	6378 (±2965)	**19%**

Chapter 7 - Conclusions and recommendation for future work

7.1 Conclusions

This chapter brings the PhD research to close by drawing some conclusions and making some recommendations for future works by providing some suggestion on how the future research can be undertaken.

In order to predict fracture location and type of fracture for stance and fall-type loading conditions, the ability of automatically produced, CT scan-based FE models of the proximal femur were evaluated in this study. It has been demonstrated, in this study, that this non-linear FE modelling method has the ability to yield accurate estimates of proximal femoral fracture load in the stance configuration. The outcome of new nonlinear FE model is remarkably better than that for the former nonlinear FE models by Dall'Areea *et al.*, (2013), in the stance configuration, models with accuracy parallel to that of current density-based techniques of fracture risk assessment. Nevertheless, around 50% of pathological hip fractures caused by tumours and osteoporosis arise unexpectedly, without a fall. Hence, assessing fracture risk for both stance and fall loading can be essential, mainly for patients with osteoporosis or tumours.

FE modelling of femora with tumours offers extra encounters that were not studied in the current study. While fracture loads calculated by FE models can be applied as direct guide of hip fracture risk, a more challenging, engineering-based methodology may offer an even more accurate indicator of hip fracture risk. Contrary to existing approaches that reflect only indicators of fracture load, including bone density, this method would also contemplate "the other side of the equation", specifically, the applied force. However, the above approach might be hard to apply since loading conditions in vivo can be highly complex and unstable. The outcomes of this study can be correlated with those of J.H. Keyak, 2001, who applied CT scan-based nonlinear FE models to calculate proximal femoral stiffness and then associated stiffness to measured fracture load. Through this method, they also compared their data with those of mechanical testing of the real bone.

Comparing the data obtained from the CT scan-based non-linear FE model which was carried out in Keyak, Derikx *et al.*, (2011) and Dall'sArra *et al.*, (2013) studied, our methodology can be considered more realistic. This is because the method applied in their study featured lest elements and the bone was treated as an isotropic material, whereas, our model had 26,071 nodes, 50,762 elements and treated bone as a piecewise_linear_plasticity material that has a close characteristics to real bone which is anisotropic material. The important development in accuracy established here is probably because of the capability of the nonlinear models to express mechanical performance past the inception of local material failure, while linear models are effective only up to the onset of failure.

Through applying nonlinear models, the course of proximal femoral fracture was simulated, from primary non-destructive loading, to the start of local bone failure, to spread of the failure area and, eventually, to final failure (the point of maximum load). Nevertheless, a weakness of these models is that the calculated force–displacement curves does not display the sharp fall in force seen during mechanical testing (see figure 4.15). The results indicated that high acceleration can be experienced by the bone as the cortical thickness increases (see Figure 4.19). The force-displacement history was also extracted for the effect of change of thickness on the impact damage process of hip bone. As it can be seen in Figure 4.24, increase of cortical thickness causes higher energy absorption capability within bone structure.

Due to increase of impact velocity the experienced acceleration by the bone increased to higher values which causes rising the acceleration-time curve (see Figure 4.24). This investigation was also carried out for the effect of change of velocity on the force-displacement history and consequently the energy absorption capabilities of bone structures at different thicknesses and also from the comparative acceleration–time histories, also observed that as Velocity decreased as well as Acceleration decreased (see Figure 4.24). The absorbed impact energy for various cortical thicknesses has been compared in Figure 4.24.

It is shown that increasing of impact velocity significantly increases the energy absorption capability of bone structures also the effect of cortical thickness and impact velocities on the damage process of the hip bone was studied. Our results indicated that by increasing cortical thickness and impact velocities, the acceleration experienced during aside fall impact will increase as will the energy absorption capabilities of bone. Our nonlinear FE models examined here provide an acceptable level of precision for predicting proximal femoral fracture-loads in the stance configuration. However, fracture loads and applied forces may need to be determined for additional loading conditions, and forces due to muscular action may also need to be considered.

Our nonlinear FE models examined here provide an acceptable level of precision for predicting proximal femoral fracture load in the stance configuration. These models are capable of correctly identifying failure loads and energy absorption with at a reasonable reliability. These investigations would benefit those with the lowest fracture loads and who are likely to be at greatest risk of fracture. It would also offer significant scope for clinical practice and implications for early identification of those at risk and prevention measures.

7.2 Recommendations for future work

The recommendation on future work is suggested to focus on Photometric Stereo in order to provide a high definition reconstruction in real time using real time data. BRDF models for semi-transparent objects will be developed. Furthermore, methodologies to extract material strength or structure information (i.e. micro-cracks, density, etc.) using sub-pixel motion estimation techniques operating in the frequency domain utilising both X-ray and ultrasound data will be introduced.

The first suggestion would be to investigate the modelling of the 3D geometry and detecting the micro-crack positions in the bone structures. Furthermore, the impact response of cracked bone structure at different body sections will also be examined subsequently.

The second suggestion would be to investigate the prediction of the novel FE methods for crack initiation and propagation in the human bone structure containing single and multi-cracks with different shapes and orientations (see Figure 7.1) under dynamic transient loading condition. This will be introduced using singular elements and cohesive zone modelling (CZM). For material modelling of cortical (compact) and cancellous (spongy) bones (which shape the lower leg bones) the inelastic foam materials model including viscosity will be applied to model the materials properties in the bone structures. Consequently, through understanding of real damage behaviour in the bone structure, designers will be able to propose and outline appropriate safety instruments to protect wide range of human bone structures during daily incidents.

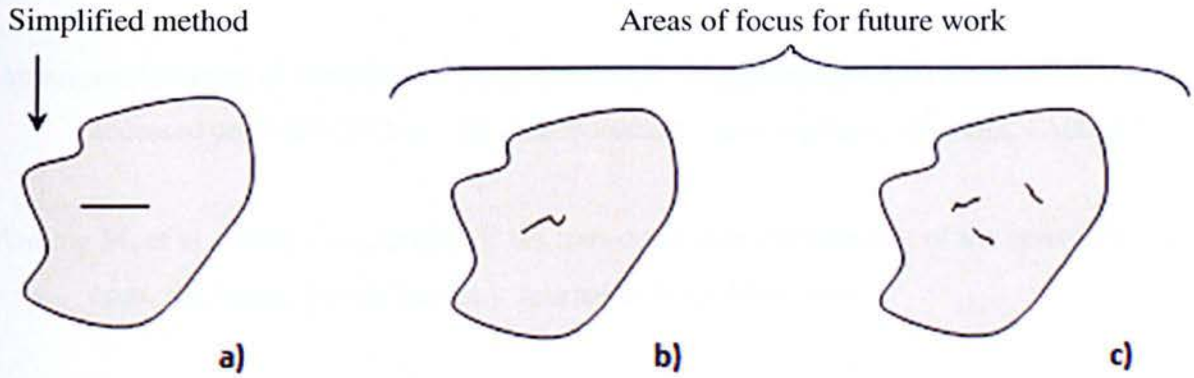

Figure7.1: a) Simplified cracked geometry, b) geometry with single crack & c) geometry with multiple cracks.

References:

American Heart Association. Heart and Stroke Facts, 1996. Statistical Supplement. Dallas,Texas: American Heart Association; 1996:1.

American Academy of Orthopaedic Surgeons, 2013. 'Thighbone (Femur) Fracture,' [Online], accessed on 09/10/2013 at URL:http://orthoinfo.aaos.org/topic.cfm?topic=A00364.

Amling M, et al., 1996. Comparison of the trabecular microarchitecture of the spine, the iliac crest, the femur. [Book Section]: Journal of Bone Miner Res.

Ashman, R. B., Cowin, S. C., Van Buskirk, W. C., and Rice, J. C., 1984. Continuous wave technique for measurement of elastic properties of cortical bone. Journal of biomechanics. 17(5), 349-361.

Ashman, R. B., and Rho, J.Y., 1988. Elastic modulus of trabecular bone material. Journal of biomechanics, 21(3), 177-181.

Bayraktar HH, Morgan EF, Niebur GL, Morris GE, Wong EK & Keaveny TM., 2004. Comparison of the elastic and yield properties of human femoral trabecular and cortical bone tissue. Journal of Biomech 37(1): 27–35.

Bertram, J. E. and Swartz, S. M.,1991. The 'law of bone transformation': a case of crying wolff? Biol Rev Camb Philos Soc, 66(3):245–273.

Boyce, W. J. and Vessey, M. P., 1988. Habitual physical inertia and other factors in relation to risk of fracture of the proximal femur. Age Ageing, 17:317-327.

British Orthopaedic Association, 2007. The care of patients with fragility fractures. Guideline Ref ID: BOA.

Burr DB, Forwood MR, Schaffler MB, Fyhrie DP, Martin RB, Turner CH., 1997. "Bone microdamage and skeletal fragility in osteoporotic and stress fractures" Journal of Bone, 12:6–15.

Campbell, A. J., Reinken, J., Allan, B. C., and Martinez, G. S., 1981. Falls in old age: a study of frequency and related clinical factors. Age Ageing, 10:264-270.

Carter, DR., Hayes, W., 1977. The compressive behavior of bone as a two-phase porous structure. Journal of Bone and Joint Surgery, 59A:954–62.

Carter, DR., Spengler, DM., 2002. Biomechanics of fracture, Bone in clinical orthopedics, 2nd edition. New York: AO Publishing, 8: 261-285.

Charpail, E., 2006. Analyse du comportement mecanique des côtes humaines en dynamique. Thèse à l'École Nationale Supérieure d'Arts et Métiers, Paris.

Cheung, G., Zalzal, P., Bhandari, M., Spelt, J.K and Papini, M., 2004. "Finite element analysis of a femoral retrograde intramedullary nail subject to gait loading." Journal of Med Eng Phys, vol. 26, issue. 2, pp. 93-108.

Chong, A.C., Friis, E.A., Ballard, G.P., Czuwala, P.J., Cooke, F.W., 2007a. Fatigue performance of composite analogue femur constructs under high activity loading. Annals of Biomedical Engineering 35, 1196–1205.

Chong, A.C., Miller, F., Buxton, M., Friis, E.A., 2007b. Fracture toughness and fatigue crack propagation rate of short fiber reinforced epoxy composites for analogue cortical bone. Journal of Biomechanical Engineering 129, 487–493.

Chopra, Anil K., 2001. Dynamics of structure, 2nd ed., Prentice Hall, New Jersey.

Clinical Gait Analysis, University of Vienna. History of the Study of Locomotion, [Online document], 2006. [cited July 15, 2009], Available HTTP:www.univie.ac.at/cga/history/modern.html

Colopy, S. A., Benz-Dean, J., Barrett, J. G., Sample, S. J., Lu, Y., Danova, N. A., Kalscheur, V. L., Vanderby, R., Markel, M. D., and Muir, P., 2004. Response of the osteocyte syncytium adjacent to and distant from linear microcracks during adaptation to cyclic fatigue loading. Bone, 35(4):881–891.

Cook, Robert D., 2002. Concepts and applications of finite element analysis, 4th ed, Wiley. Engineering Research AB, (2005). LS-DYNA introductory course.

Cooper, C., Campion, G., and Melton, L. J., 1992. Hip fractures in the elderly: a worldwide projection. Osteopor Int 2:285-289.

Cooper D.M. Thomas CD, Clement JG, Turinsky AL, Sensen CW, Hallgrímsson B., 2007. Age-dependent change in the 3D structure of cortical porosity at the human femoral.

Copper, C., Barker, D. J. P., Wickham, C., 1988. Physical activity, muscle strength, and calcium intake in fracture of the proximal femur in Britain. Br Med J, 297:1443-1446.

Coupland, C., Wood, D., Cooper, C., 1993. Physical inactivity is an independent risk factor for hip fracture in the elderly. Journal of Epidemiol Community Health 47(6): 441–443.

Cowin, S. (1997). The false premise of wolff's law. Forma, 12:247–262. 9

Cowin, S. C. and Boca Raton., 2001. Bone Mechanics Handbook [Book]: CRC Press, (2nd edition).

Cristofolini, L., Viceconti, M., Cappello, A., Toni, A., 1996. Mechanical validation of whole bone composite femur models. Journal of Biomechanics 29, 525–535.

Cristofolini, L., Viceconti, M., 2000. Mechanical validation of whole bone composite tibia models. Journal of Biomechanics 33, 279–288.

Cullinance, D.M. and Einhorn, T.A., 2002. 'Biomechanics of Bone',' Principles of Bone Biology', 2nd edition. San Diego: Academic Press, Vol 1, p17-32

Cummings, R. Klineberg, R., 1994. Fall frequency and characteristics and the risk of hip fractures. Journal of Am Geriatr Soc 42(7): 774–778.

Cummings, S. R. Nevitt, M. C., 1989. A hypothesis: the causes of hip fractures. J Gerontol, 44:M107-111.

Cummings SR, Nevitt MC, Browner WS, Stone K, Fox KM, Ensrud KE, Cauley J, Black D & Vogt TM., 1995. Risk factors for hip fracture in white women. Study of Osteoporotic Fractures Research Group. Journal of Med 332(12): 767–773.

Currey, JD., Brear, K., Zioupos, P., 1996. The effects of ageing and changes in mineral content in degrading the toughness of human femora. Journal of Biomechanics, 29:257–60.

Dall'Ara, E., Luisier, B., Schmidt, R., Kainberger, F., Zysset, P., Pahr, D., 2013. A nonlinear QCT-based finite element model validation study for the human femur tested in two configurations in vitro. Bone 52, 27–38.

Dave Thompson's lecture notes. Conventions for naming parts of the gait cycle, University of Oklahoma Health Sciences Centre. [Online document], 2002. [cited March 10, 2011], Available HTTP: http://moon.ouhsc.edu/dthompso/gait/terms.htm

David, K., Hakkarinen, MD., Kenny, VB., Hendey, GW., 2012. Magnetic resonance imaging identifies occult hip fractures missed by 64 slice computed tomography.

Dempster, DW., 2003. Bone microarchitecture and strength. Osteoporos Int 14 (5): S54–56.

Derikx, L.C., Vis, R., Meinders, T., Verdonschot, N., Tanck, E., 2011. Implementation of asymmetric yielding in case-specific finite element models improves the prediction of femoral fractures. Comput. Methods Biomech. Biomed. Eng. 14, 183–193.

Duan, Y., Wang XF, Evans A, Seeman E., 2005. Structural and biomechanical basis of racial and sex differences. Bone.

Eckstein, F., Wunderer, C., Boehm, H., Kuhn, V., Priemel, M., Link, TM., Lochmüller, EM., 2007. Reproducibility and side differences of mechanical tests for determining the structural strength of the proximal femur. Journal of Bone Miner Res 19(3): 379–385.

Einhorn, TA., 1998. The cell and molecular biology of fracture healing. Journal of Clinical Orthop Rel Res, 355:S7–S21.

Engineering Research AB. (2005). LS-DYNA introductory course.

Enlow, DH., 1963. Principles of bone remodeling. Springfield, IL: Charles C Thomas.

Enlow, DH., 1968. The human face. An account of the postnatal growth and development of the craniofacial skeleton. NewYork: Harper and Row.

Enoka, R., (2002). Neuromechanics of human movement. Champaign, IL, Human Kinetics.

Forman, J., Lessley, D., Kent, R. (2009). NHTSA:Rear sear sled test report covering test 1386,1387,1389. Center for applied Biomechanics, University of Virginia. USA.

Frost, H. M., 1973. Bone remodelling and its relation to metabolic bone diseases. Springfield, IL.

Garner, E., Lakes, R., Lee, T., Swan, C., and Brand, R., 2000. Viscoelastic dissipation in compact bone: implications for stress-induced fluid flow in bone. Journal of biomechanics, 122(2), 166-172.

Georgetown University Medical Center, 2011. Gallery, Dahlgren Memorial Library. Types of Hip Fracture. [Online image], [cited March 13, 2011], Available HTTP: http://www8.georgetown.edu/dml/facs/graphics/images/Basic%20Hip%20Fractures.jpg

Ghasemnejad, H., Hadavinia, H., Marchant, D and Aboutorabi, A., 2009. Energy Absorption of Thin-walled Corrugated Crash Box in Axial Crushing, SDHM, 98(1):1-17.

Gibson, LJ., 1985. The mechanical behavior of cancellous bone. Journal of Biomechanics, 18:317–28.

Gomez, M.J., Garcia, J.M, Doblare, M., 2005. Finite element prediction of proximal femoral fracture pattern under different loads. Journal of Biomechanical Engineering, 127:9–14.

Gray, H., 1918. Anatomy, Descriptive and Surgical. New York: Bounty Books.

Grisso, J. A., Kelsey, J. L., Strom, B. L., Chin, G. Y., Maislin, G., O'Brien, L. A., 1991. Risk factors for falls as a cause of hip fracture in women. Journal of Med, 324:1326-1331.

Grodin, J. M., Siitiri, P. K., and MacDonald, P.C., 1983. Source of estrogen production in postmenopausal women. Journal of Clin Endocrinol Metab, 36:207-214.

Gullberg, B., John, O. Kanis, J.A.,1997. Aestablished as result of cooperation between the European Foundation" World-wide projections for hip fracture. 407–13.

Gupta, HS., Stachewicz, U., Wagermaier, W., Roschger, P., Wagner, HD., Fratzl, P., 2006. Mechanical modulation at the lamellar level in osteonal bone. Journal of Materials Research, 21:1913–21.

Hallquist, JO., 2003. LS-DYNA 970 theoretical manual, Livermore Software Technology Corporation, Livermore.

Hambli, R.,Bettamer, A and Allaoui, S., 2012. Finite element prediction of proximal femur fracture pattern based on orthotropic behaviour law coupled to quasi-brittle damage. Medical Engineering & Physics, 34(2): p. 202-210.

Hancox, N., 1972. Biology of Bone. University Press, Cambridge. 6, 7

Havers, C., 1691. Osteologia Nova or some new observations of the bones. Cartilage, S. Smith, London.

Heath, Michael T., 2002. Scientific computing, An introductory survey, 2nd ed., Mc Graw Hill.

Heiner, A.D., Brown, T.D., 2001. Structural properties of a new design of composite replicate femurs and tibias. Journal of Biomechanics 34, 773–782.

Hordon, L.D, Raisi M, Aaron JE, Paxton SK, Beneton M, Kanis JA., 2000. Trabecular architecture in women and men of similar bone mass Bone.

Human gait cycle: http://www.orthopaedicsurgeries.co.uk/aims/ [Accessed: 9th May, 2011].

Iwamoto, J., Sato, Y., Takeda, T., Matsumoto, H., 2009. Role of sport and exercise in the maintenance of female bone health. Journal of Bone Miner Metab, 27(5): 530–537.

Jackson, AP., Vincent, JFV., Turner, RM., 1989. A physical model of nacre. Journal of Composites Science and Technology, 36, 255–66.

Jee, W. S. S., 2001. Integrated Bone Tissue Physiology: Anatomy and Physiology. In: Cowin S.C. ed. Bone Mechanics Handbook. CRC Press, Boca Raton.

Jensen, J. S., Tondevold, E., Sirensen, P. H., 1980. Costs of treatment of hip fractures. Acta Orthop Scand, 51:289-296.

Kabel. J, Van Rietbergen, B., Dalstra, M., Odgaard, A., Huiskes, R., 1999.The role of an effective isotropic tissue modulus in the elastic properties of cancellous bone. Journal Biomechanical Engineering, 32:673–80.

Kanis JA, Melton LJ, Christiansen, C., Johnston, CC. Khaltaev, N J., 1994. The diagnosis of osteoporosis. Bone Miner Res, 9(8): 1137–1141.

Kanis, JA., Johnell, O., Oden, A., Jonsson, B., De Laet, C., Dawson, A., 2000. Risk of hip fracture according to the World Health Organization criteria for osteopenia and osteoporosis. Journal of Bone, 27(5): 585–590.

Kaneko, TS., Pejcic, MR., Tehranzadeh, J. Keyak, JH., 2003. Relationships between material properties and CT scan data of cortical bone with and without metastatic lesions. Journal of Med Eng Phys, 25(6): 445–454.

Katsmanis, F., and Raftopoulos, D.D., 1990. Determination of mechanical peroperties of human femoral cortical bone by the Hopkinson bar stress technique. Journal of biomechanics, 23(11), 1173-1184.

Keyak, J., 2001. Improved prediction of proximal femoral fracture load using nonlinear finite element models. Med. Eng. Phys. 23, 165–173.

Kroonenberg van den, AJ., Hayes, W.C., McMahon, T.A., 1995. Dynamic models for sideways falls from standing height. Journal of Biomechanical Engineering, 117:309–318.

Kruzic JJ, Scott JA, Nalla RK, Ritchie RO., 2006. Propagation of surface fatigue cracks in human cortical bone. Journal of Biomechanics; 39:968–72.

Lanritzen, J. B. and Lund, B., 1993. Risk of hip fracture after osteoporosis fractures. Acta Orthop Scand, 64:297-300.

Lanritzen, J. B., McNair, P., Lund, B., 1993. Risk factors for hip fracture. A review. Danish Med Bull 40:479-485.

Lappi, V.G., King, M.S., and Le may, I., 1979. Determination of elastic constants for human femuurs. Journal of biomechanics, 101, 193-197.

Lau, E., Donnan, S., Barker, D.J.P., and Cooper, C., 1988. Physical activity and calcium intake of the proximal femur in Hong Kong. Br Med J 297:1441-1443.

Lau, KH., Baylink, DJ., 1999. Vitamin D therapy of osteoporosis: plain vitamin D therapy versus active vitamin D analog (D-hormone) therapy. Calcif Tissue Int, 65(4): 295–306.

Lauritzen, J. B., Petersen, M. M., Jensen, P. K., Hejgaard, L., and Lund, B., 1992. Body fat distribution and hip fractures. Acta Orthop Scand, 63 (248):89.

Launey, ME., Buehler, MJ., Ritchie, RO., 2010. On the mechanistic origins of toughness in bone. Ann Rev Mater Res; 40: (9) 1.

Lauritzen, J. B., Petersen, M. M., Lund, B., 1993. Effect of external hip protectors on hip fractures. Lancet, 341:11-13.

Lindsay, R., 1994. Prevention of osteoporosis. Prev Med. 23(5): 722–726.

Livermore Software Technology Corporation., 2012. 'LS-DYNA 970 keyword user's manual'.

Lochmüller, EM., Groll, O., Kuhn, V. Eckstein, F., 2002. chanical strength of the proximal femur as predicted from geometric and densitometric bone properties at the lower limb versus the distal radius. Bone, 30(1): 207–216.

Lotz, JC., Hayes, WC., 1990. The use of quantitative computed tomography to estimate risk of fracture of the hip from falls. Journal of Bone Joint Surgical, 72a, 689–700.

Lu-yao, GL., Baron, JA., Barrett, JA., Fisher, ES., 1994. Treatment and survival among elderly Americans with hip fractures: a population-based study. Journal of Pub Health, 84:1287–1291: 10.2105/AJPH.84.8.1287.

Manatomy, (2013) 'upper end of femure' [online], accessed on 14/10/2013 at URL: http://www.mananatomy.com/body-systems/skeletal-system/femur.

Marcus, R., 1989. Understanding and preventing osteoporosis. Hosp Pract, 24(4): 189–204, 209–11, 215.

Martini, F.H., 2001. "Osseous tissue and skeletal structure." Fundamentals of Anatomy and Physiology, P.F. Corey, ed., Prentice Hall, 168-170.

Martin, R. B. and Burr, D. B., 1989. Structure, function, and adaptation of compact bone. Raven Press, New York.

Martin, R.B., 1998. Skeletal tissue mechanics. Springer, New York.

McConnell, A., Zdero, K. Syed, R., Peskun, C. and Schemitsch, E., 2008. "The biomechanics of ipsilateral intertrochanteric and femoral shaft fractures: A comparison of 5 fracture fixation techniques". Journal of Orthop Trauma, vol. 22, issue. 8, pp. 517-524.

Medial andlateral trabeculae system of the femoral neck: [Accessed: 9th May, 2011]. http://orthopedicsurgeons.blogspot.com/2010_05_02_archive.html

Melton, L. J., Wahner, H. W., Richelson, L. S., O'Fallon, W. M., and Riggs, B. L., 1986. Osteoporosis and the risk of hip fracture. Am J Epidemiol, 124:254-261.

Melton, L. J., Chrischilles, E. A., Cooper, C., Lane, A. W., and Riggs, B.L.,1992. Perspective: How many women have osteoporosis? Journal of Bone Miner Res, 7:1005-1010.

Mercer, C., He, M.Y., Evans, A.G., 2006. Mechanisms governing the inelastic deformation of cortical bone and application to trabecular bone. Acta Biomaterialia, 59 – 68.

Mirzaei, M., 2011). Fracture Mechanics Theory and Applications. www.geotechlinks.com/Links/Mirzaei-FractureMechanicsLecture.pdf

Moore, K. L., 2007. Essential clinical anatomy. Baltimore, MD : Lippincott Williams & Wilkins. 12, 13, 14, 16, 220.

Morgan, D.B., Newton, H. M. V., Schorah, C.J., Jewitt, M.A., Hancock, M. R., and Hullin, R. P., 1986. Abnormal indices of nutrition in the elderly: a study of different clinical groups. Age Ageing, 15:65-76.

Mosekilde, L., 2000. Age-related changes in bone mass, structure, and strength - effects of loading. Zeitschrift Fur Rheumatologie.

Mueller T.L, 2009. Regional age and gender differences in architectural measures of bone quality and their correlation to bone mechanical competence in the human radius of an elderly population. Journal of Bone.

Nalla, RK., Kinney, JH., Ritchie, RO., 2003. Mechanistic fracture criteria for the failure of human cortical bone. Nature Materials, 2: 164–8.

Nalla, RK., Kruzic, JJ., Kinney, JH., Ritchie, RO., 2004. Effect of aging on the toughness of human cortical bone: evaluation by R-curves. Journal of Bone, 35:1240–6.

Nalla, RK., Kruzic, JJ., Kinney, JH., Ritchie, RO., 2005. Mechanistic aspects of fracture and R-curve behavior in human cortical bone. Biomaterials, 26:217–31.

Nalla, RK., Stolken, JS., Kinney, JH., Ritchie, RO., 2005. Fracture in human cortical bone: local fracture criteria and toughening mechanisms. Journal of Biomech, 38:1517.

Netter, F.H. and J.T Hansen, Atlas of Human Anatomy., 2002.3rd edition, Elsevier Health Sciences, 632.

Nordin, M. and Frankel, V., 2001. "Basic Biomechanics of the Musculoskeletal System." (3rd ed.) Lippincott Williams and Wilkins, Philadelphia, PA, USA.

Norman, TL., Nivargikar, SV., Burr, DB., 1996. Resistance to crack growth in human cortical bone is greater in shear than in tension. Journal of Biomech, 29:1023.

Norkin, C., L. P., 1992. Joint Structure and Function. F.A. Davis, Philadelphia., 2nd edition.

Peacock, M., 1998. Effects of calcium and vitamin D insufficiency on the skeleton. Osteoporos Int, 2: S45–51.

Pacific Research Laboratories Inc. http://www.sawbones.com/ [Accessed: 9th May, 2011].

Pacific Research Laboratories, Inc., 2007. 4th generation composite bones have improved fracture and fatigue properties. Informational handout.

Pacific Research Laboratories, Inc., 1998. Personal communication.

Patient, (2013) 'who is at risk of osteoporosis?',[online] ,accessed on 09/10/2013 at URL: http://www.patient.co.uk/health/osteoporosis-leaflet

Pankovich, A.M., Davenport, K.A., 2006. Fractures of the Femoral Shaft, Handbook of Fractures, 3rd edition. New York, McGraw-Hill, 19: 293-303.

Peterlik, H., Roschger, P., Klaushofer, K., Fratzl, P., 2006. From brittle to ductile fracture of bone. Nature Materials, 5:52–5.

Raftopoulos, D., Katsamanis, E., Sual, F., Liu, W., and saddemi,S., 1993. An intermediate loading rate technique for the determination of mechanical Properties of human femoral cortical bone. Journal of biomechanics, 15, 60-66.

Rho, JY., Kuhn-Spearing, L., Zioupos, P., 1998. Mechanical properties and the hierarchical structure of bone. Journal of Medical Engineering & Physics, 20:92-102.

Richelson, LS., Wahner, HW., Melton, LJ., Riggs, BL., 1984. Relative contributions of aging and estrogen deficiency to postmenopausal bone loss. Journal of Med 311(20): 1273–1275.

Riggs, BL., Melton, LJ., 1995. The worldwide problem of osteoporosis: insights afforded by epidemiology. Journal of Bone, 17:505S–511S

Ritchie, RO., Buehler, MJ., Hansma, PK., 2009. Plasticity and toughness in bone. Phys Today, 62:41.

Rizzoli, R., Bruyere, O., Cannata-Andia, JB., Devogelaer, JP., Lyritis, G., Ringe, JD., Vellas, B. Reginster, JY., 2009. Management of osteoporosis in the elderly. Curr Med Res Opin, 25(10): 2373–2387.

Roesler, H., 1987. "The history of some fundamental concepts in bone biomechanics." J Biomech, vol. 20, issue. 11-12, pp. 1025-1034.

Sanders. R., 2008. Trauma: Core knowledge in orthopaedics. Philadelphia, Mosby, Inc., an affiliate of Elsevier Inc., 253-296.

Schindler, A. E., Ebert, A., Friedrich, E., 1972. Conversion of androstendione to estrone by human fat tissue. J Endocrinol Metab, 35:627-630.

Schiessl, H., Frost, HM. Jee, WS., 1998. Estrogen and bone-muscle strength and mass relationships. Bone 22(1): 1–6.

Singh, D., Shetty, DK., 1989. Fracture toughness of polycrystalline ceramics in combined mode I and mode II loading. Journal of Am Ceram Soc, 72:78.

Sloan J, Holloway G., 1981.The cause of the fall and injury. Journal of Fractured neck of femur, pp. 13:230–2.

Stolk, J., Verdonschot, N., Murphy, B.P., Prendergast, P.J., Huiskes, R., 2002. Finite element simulation of anisotropic damage accumulation and creep in acrylic bone cement. Engineering Fracture Mechanics, in press.

Stott, S. and Gray, D. H., 1980. A prospective study of hip fracture patients. N Z Med J, 91:165-169.

Taylor, D., Hazenberg, J. G., and Lee, T. C., 2007. Living with cracks: Damage and repair in human bone. Nat Mater, 6(4):263–268.

Thakur, A.J, 2007. 'The Elements of Fracture Fixation', 2nd edition. New Delhi: Reed Elsevier India Private Limited.

Tortora, G. J, 2002. Principles of Human Anatomy. Wiley, New York.

Tscuchikane, A., Nakatsuchi, Y., and Normura, A, 1995. The influence of joints and soft tissue on the natural frequency of the human tibia using the impulse response method. Proceeding of institution of Mechanical Engineers part H, 209,149-155.

Turner, CH., Takano, Y., Tsui, T. Y., Pharr, GM, 1999. Elastic properties of trabecular and cortical bone tissues are similar: results from two microscopic measurement techniques. Journal of bio mechanics, 32(4), 437-441.

Turner, CH., 2005. The biomechanics of hip fracture. Lancent, 366 (9480): 98-9.

Turner, C. Burr, D, 2001. Experimental techniques for bone mechanics. In Cowin S. Bone mechanics handbook. New York, NY, Informa Healthcare.

Typical motion ranges of hip joint: [Accessed: 9th May, 2011]. http://people.emich.edu/pbogle/PHED_200/overheads/ch7_art/07_39.jpg

Van der perre, G., Cornelissen, P., 1983. On the mechanical resonance of a human tibia in vitro. Journal of biomechanics, 16(7), 549-552).

Van Rietbergen, B., Weinans, H., Huiskes, R and Odgaard, A.,1995. "A new method to determine trabecular bone elastic properties and loading using micromechanical finite-element models." J Biomech, vol. 28, issue. 1, pp. 69-81.

Van Rietbergen, B., Odgaard, A., Kabel, J., Huiskes, R., 1996. Direct mechanical assessment of elastic symmetries and properties of trabecular bone architecture. Journal Biomechanical Engineering, 29:1653–7.

Vashishth, D., Behiri, JC., Tanner, KE., Bonfield, W., 1996. Toughening mechanisms in cortical bone. 42nd Annual Meeting ORS, 19–22.

Wainer, R.A., Wright, P.H., Gilbert, J.A and Taylor, D.F., 1990. "Biomechanics of Ender rods, compression screw, and Zickel nail in the fixation of stable subtrochanteric femur osteotomies."J Orthop Trauma, vol. 4, issue. 1, pp. 58-63.

Wang, RZ., Wen, HB., Cui, FZ., Zhang, HB., Li, HD., 1995. Observations of damage morphologies in nacre during deformation and fracture. Journal of Materials Science, 30, 2299–304.

Wasnich, RD., 1997. Epidemiology of osteoporosis in the United States of America.Osteoporos Int, 7 (3): S68–72.

Wescott, DJ., 2005. Population Variation in Femur Subtrochanteric Shape. Journal of Forensic Science, 50: 286-293.

WHO, 1994. Assessment of fracture risk and its application to screening for postmenopausal osteoporosis. Report of a WHO Study Group. World Health Organ Tech Rep, 843: 1–129.

Wolff, J., 1892. Das, G. Transformation der Knochen. Translation by Maquet, P. Furlong, R. (1986). The law of bone remodelling. Springer-Verlag, Berlin.

Yeni, YN., Fyhrie, DP., 2003. A rate-dependent microcrack-bridging model that can explain the strain rate dependency of cortical bone apparent yield strength. Journal of Biomech, 36:1343.

Zdero, R., Rose, S., Schemitsch, E.H and Papini, M., 2007. "Cortical screw pullout strength and effective shear stress in synthetic third generation composite femurs." Journal of Biomech Eng, vol. 129, issue. 2, pp. 289-293.

Zdero, R., Walker, R., Waddell, J.P and Schemitsch, E.H., 2008. "Biomechanical evaluation of periprosthetic femoral fracture fixation." Journal of Bone Joint Surg Am, vol. 90, issue. 5, pp. 1068-1077.

Zebaze, RM., Jones, A., Welsh, F., Knackstedt, M., Seeman, E., 2005. Femoral neck shape and the spatial distribution of its mineral mass varies with its size: Clinical and biomechanical implications. Bone 37(2): 243–252.

Zimmermann, EA., Launey, ME., Barth, HB., Ritchie, RO., 2009. Mixed-mode fracture of human cortical bone. Biomaterials, 30:5877.

Zioupos, P., 1998. Recent developments in the study of failure of solid biomaterials and bone. 'fracture' and 'pre-fracture' toughness. Materials Science & Engineering C: Biomimetic Materials, Sensors & Systems, C6:33–40.

Zioupos, P., Currey, JD., 1998. Changes in the stiffness, strength, and toughness of human cortical bone with age. Journal of Biomechanics, 22(1):57–66.

Zysset, PK., Guo, XE., Hoffler, CE., Moore, KE., Goldstein, SA., 1999. Elastic modulus andhardness of cortical and trabecular bone lamellae measured by nanoindentation in the human femur. Journal of Biomechanics, 32(10): 1005–1012.

List of Publications

1. Razmkhah, O. and Ghasemnejad, H. (2014) Explicit finite element analysis to predict impact damage response of osteoporosis hip bone. Journal of Computer Methods in Biomechanics and Biomedical Engineering: Imaging & Visualization, ISSN (print) 2168-1163.

2. Razmkhah, O. and Ghasemnejad, H. (2014) Orthopaedic Biomechanics: A Practical Approach to Combining Mechanical Testing and CT scan-based linear FE model. In: 10th International Conference on APPLIED and THEORETICAL MECHANICS (MECHANICS '14) (to be published).

3. Razmkhah, O. and Ghasemnejad, H. (2013) Impact damage response of osteoporosis hip bone. In: 4th European Conference of Mechanical Engineering (ECME' 13); 29-31 Oct 2013, Paris, France. (Recent Advances in Mechanical Engineering Applications, no. 8) ISSN (print) 2227-4596 ISBN 9789604743452.

4. Razmkhah, O., Ghasemnejad, H., Argyriou, V. and Aboutorabi, A. (2013) Advanced finite element analysis to predict impact damage behaviour of fractured hip. In: 19th Congress of the European Society of Biomechanics (ESB 2013); Aug 25-28 2013, Patras, Greece.

5. Razmkhah, O. and Ghasemnejad, H. (2012) Green composites for advanced green structures. In: International Symposium on Environment Friendly Energies and Applications (EFEA 2012); 25-27 June 2012, Newcastle, UK.

PAGE/PAGES EXCLUDED UNDER INSTRUCTION FROM THE UNIVERSITY